Spiral phases from a systematic low-energy effective field theory for magnons and holes in an antiferromagnet on the honeycomb lattice

Masterarbeit

der
Philosophisch-naturwissenschaftlichen Fakultät
der Universität Bern

vorgelegt von

Bänz Bessire

2009

Leiter der Arbeit

Prof. Dr. Uwe-Jens Wiese
Institut für Theoretische Physik, Universität Bern

Abstract

Guided by baryon chiral perturbation theory, the effective field theory for pions and baryons in QCD, we construct the leading orders of a low-energy effective field theory for magnons and holes in an antiferromagnet on the honeycomb lattice. Based on a careful symmetry analysis of the underlying microscopic Hubbard Hamiltonian and the fact that doped holes reside in pockets centered around lattice momenta $(0, \pm 4\pi/(3\sqrt{3}a))$, we systematically derive the low-energy degrees of freedom and their transformation behaviour under the symmetries of the Hubbard model. In order to couple the magnons to the holes in the effective field theory, we use a non-linear realisation of the global spin symmetry. The leading order effective Lagrangian is then constructed by demanding that it must have the same symmetries as the Hubbard model. As an application of the effective field theory, we afterwards discuss possible spiral phases of the staggered magnetisation in an antiferromagnet on the honeycomb lattice containing a homogeneously distributed, small amount of doped holes. The effective field theory reveals that, depending on the values of the low-energy constants, the staggered magnetisation is either in a homogeneous or in a spiral phase where the spiral has no preferred spatial propagation direction.

As an intermediate step, we diagonalise the Hubbard Hamiltonian in the zero-coupling limit to derive the dispersion relation of free, massless Dirac fermions. Expanding the dispersion relation for small momenta allows us to determine an exact expression for the fermion velocity. The construction of the leading order effective Lagrangian for free fermions concludes this excursion.

Magnetes Geheimnis, erklär mir das!
Kein grösser Geheimnis als Lieb' und Hass.
Johann Wolfgang von Goethe, *Gott, Gemüt und die Welt*

Contents

Chapter 1

Introduction

The phenomenon of low-temperature superconductivity was discovered in the year 1911 by Heike Kammerlingh Onnes and Gilles Holst. While studying the resistance of solid mercury at low temperatures, Onnes and Holst observed that resistance suddenly disappears when the probe is cooled below 4.2 K. In 1957, John Bardeen, Leon N. Cooper, and John R. Schrieffer (BCS) proposed the microscopic theory of low-temperature superconductivity. According to BCS, superconductivity at low temperatures emerges from two-electron bound states in which the electron pairs feature opposite momenta close to the Fermi surface and zero total spin. These so-called Cooper pairs are bound by a long-ranged attractive force mediated by phonons which overcomes the short-ranged screened Coulomb repulsion. Low-temperature superconductors exhibit a critical temperature of a few Kelvin below which the Cooper pair formation is possible. Johannes G. Bednorz and Karl A. Müller, however, observed in 1986 that Lanthanum-Barium-Copperoxid ($La_{1,85}Ba_{0,15}CuO_4$) turns into the superconducting phase above 30 K [1]. This was the starting point for the still very rich research field of high-temperature superconductivity. Because it is assumed that the coupling due to phonons is too weak to completely explain bound fermion pairs in high-temperature superconductors (HTSC), the BCS theory can not be used to describe materials with a high critical temperature.

Most HTSC are hole- or electron-doped ceramic materials with layers of CuO_2 spaced by insulating layers of other atoms serving as a charge reservoir. Doping can be obtained by substituting ions in these insulating layers with the effect that the number of electrons in the copper-oxide layers changes. In an undoped system, a CuO_2 layer has on average one valence-electron per lattice site (half-filling). A material is called electron-doped when additional electrons enter the half-filled copper-oxide layers through doping. On the other hand, the charge reservoir in the insulating layers can pick up electrons from the crystal such that there is an electron vacancy or, equivalently, a hole in the CuO_2 plane. At zero or at least very low doping, the copper-oxide layers show, in a certain temperature range, the characteristic long-range order structure of an antiferromagnet. In real materials, these layers are weakly coupled. Therefore, the correlation length remains infinite also for non-zero temperature T and thus the antiferromagnetic phase is realised for $T > 0$. Fig. 1.1 shows a schematic phase diagram for $Nd_{2-x}Ce_xCuO_4$ and $La_{2-x}Sr_xCuO_4$, which both represents HTSC on a square lattice. However, as first suggested by Philip W. Anderson in [2], due to the weak coupling of the CuO_2 layers, the relevant physics of HTSC is reduced to a two-dimensional single

copper-oxide plane. It is thus legitimate to completely neglect the inter-layer coupling for a theoretical treatment of HTSC. However, one should keep in mind that Fig. 1.1 then no longer applies, since the correlation length of an exactly two-dimensional antiferromagnet gets finite as soon as $T > 0$, i.e. the antiferromagnetic phase exists only for $T = 0$. An antiferromagnet turns into the superconducting phase as soon as the doping concentration is high enough. The newest generation of HTSC are iron-based. Instead of the CuO_2 planes, these materials are based on layers consisting of iron and arsenic [3]. Although this thesis is ultimately motivated by high-temperature superconductivity, we assume that only a fundamental understanding of HTSC in the *antiferromagnetic* phase can be the key to access a correct theoretical description of high-temperature superconductivity.

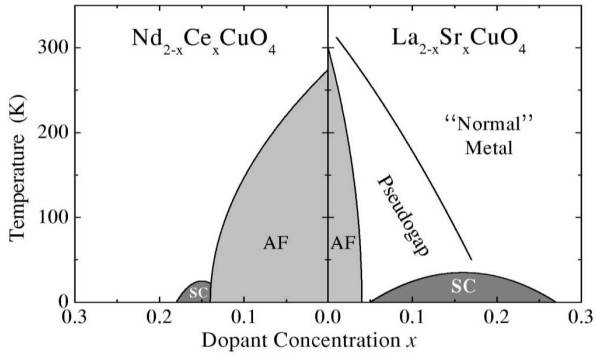

Figure 1.1: *Schematic phase diagram of electron- ($Nd_{2-x}Ce_xCuO_4$) and hole-doped ($La_{2-x}Sr_xCuO_4$) cuprates illustrating the antiferromagnetic (AF) and superconducting (SC) phase in dependence of temperature and doping concentration [4].*

In this thesis we focus on high-temperature superconductors with a honeycomb lattice in the antiferromagnetic phase. A HTSC on the honeycomb lattice is the dehydrated variant of $Na_xCoO_2{\cdot}yH_2O$ at $x = 1/3$. The relevant layers now consist of CoO_2 instead of CuO_2. Nevertheless, it is assumed that the underlying physics is similar to the copper oxides [5]. The structure of this material is depicted in Fig. 1.2. A further antiferromagnetic material on a honeycomb lattice is $InCu_{2/3}V_{1/3}O_3$. Because it seems that the important honeycomb lattice materials are hole-doped, we restrict all investigations in this thesis to lightly hole-doped antiferromagnets.

Appropriate models describing antiferromagnetism are the Hubbard or the t-J model. They are considered to be minimal models which contain the physics of itinerant spin-1/2 fermions on a two-dimensional lattice. These models further include on-site Coulomb repulsion (Hubbard model) and a nearest-neighbour spin-coupling (t-J model). Both of these models can be doped with fermions, but the t-J model allows only hole doping. However, because of their simplicity, the Hubbard as well as the t-J Hamiltonian neglect some physical aspects of real materials. Since the formation of a crystal lattice is not included in these microscopic descriptions, the phonons, as the Goldstone bosons of the spontaneously broken translation invariance, are not included in the Hubbard and the t-J model. Moreover, impurities due to doping and the already mentioned interlayer interaction are not captured by the two Hamiltonians. However, despite their various simplifications, these models are perfectly suited to

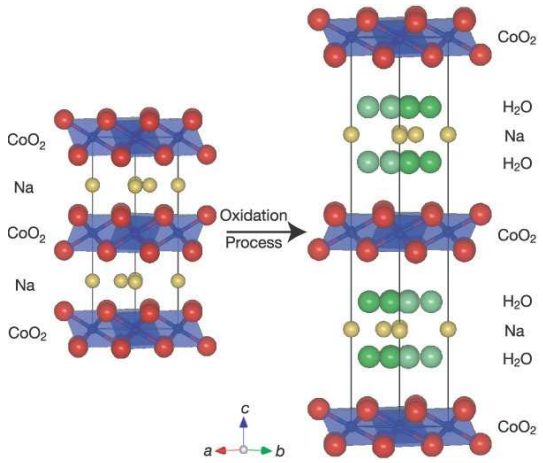

Figure 1.2: *Structural views of $Na_{0.7}CoO_2$ (left) and $Na_xCoO_2{\cdot}yH_2O$ (right), where Na and H_2O sites are partially occupied [5].*

describe a doped antiferromagnet in two dimensions. The main problem is that both models in general can not be solved analytically and numerical simulations, as soon as more than one doped hole or electron is included, suffer from a very severe fermion sign problem. Further, the exact antiferromagnetic ground state of these Hamiltonians is not known. This motivates the construction of a low-energy effective field theory for magnons and holes in an antiferromagnet on the honeycomb lattice. With this tool in our hand, we are then able to describe the low-energy physics of the Hubbard and the t-J model including a small amount of doped holes in a very efficient manner.

Let us first review some general facts about low-energy effective field theories. The basis of a low-energy effective field theory is a microscopic model (fundamental theory) describing the physics of a given system over a wide range in energy. In the majority of cases, these models are thus not solvable analytically. However, as long as one is interested only in the physics at *low* energies, there is a loophole. In this case one must identify *all* relevant degrees of freedom dominating the physics at low energies, i.e. low temperatures. Only these degrees of freedom are then used to construct a low-energy effective field theory (or simply effective field theory). As a consequence, the effective field theory describes the low-energy physics of the system in a much more economic or, in accordance with its name, effective manner than the fundamental theory, which at low energies also incorporates the degrees of freedom relevant for the high-energy regime. Let us now explain in detail how an effective field theory is constructed by considering the statement of Weinberg in [6] that once the effective degrees of freedom are identified, the most general effective Lagrangian, satisfying all fundamental principles of quantum field theory, has to be invariant under *all* symmetries of the underlying microscopic model. If one intends to construct an effective Lagrangian, one therefore first determines all the symmetries of the fundamental microscopic theory. As a second step, the low-energy degrees of freedom and their transformation behaviour under the symmetries of the underlying Hamiltonian are worked out. Finally, the low-energy effective Lagrangian is constructed as a systematic derivative expansion containing all terms of a certain order, expressed in the relevant effective degrees of freedom, which are invariant under all symmetries of

the microscopic model. Since derivatives in position space correspond to momenta in Fourier space, the low-energy behaviour of a system is suitably described by the leading order terms in the effective Lagrangian involving as few derivatives as possible. In the end, the (leading order) effective Lagrangian enters the path integral through a Euclidean action. It should be emphasised that the effective field theory is completely equivalent to the microscopic theory at low temperatures. Information about the high-energy regime of the fundamental theory is incorporated in the effective field theory through so-called low-energy constants. Each term in the effective Lagrangian is multiplied with a low-energy constant, which determines the coupling strength of the corresponding low-energy interaction process. However, within the scope of the effective field theory it is not possible to determine the numerical values of these constants. The values of the low-energy constants can be fixed by the use of a matching calculation. Such a procedure is realised by calculating a certain process, which includes the low-energy constant to be determined, in the framework of the effective field theory. On the other hand, the *same* process is investigated within the microscopic theory, e.g. with a Monte Carlo simulation. By comparing both predictions, one is then able to fix the value of the low-energy constant which itself depends on a parameter of the microscopic Hamiltonian. The effective field theory is insensitive to the details of the microscopic model and therefore is able to represent a whole class of microscopic theories as long as they share the same symmetries. However, the numerical values of the low-energy constants are model-dependent.

It is possible that a system at low temperature exhibits a spontaneously broken global symmetry. In this case, Goldstone's theorem predicts the existence of spin- and massless particles known as Goldstone bosons. Since these particles are massless, they govern the low-energy physics of the system and must therefore be considered a relevant low-energy degree of freedom although they do not appear as fundamental degrees of freedom in the microscopic model. The effective Lagrangian must thus include the description of the Goldstone bosons.

The most prominent example of a strongly coupled and thus hardly solvable fundamental theory is quantum chromodynamics (QCD), which describes the strong interaction between quarks and gluons. Assuming the quarks to be massless, QCD shows a spontaneous symmetry breakdown of the global $SU(2)_L \otimes SU(2)_R$ chiral symmetry to the isospin subgroup $SU(2)_{L=R}$ at low energies. The corresponding Goldstone bosons are the three pions π^+, π^0, and π^-, which are dominating the low-energy physics of QCD. [1] Chiral perturbation theory (χPT), a systematic low-energy effective field theory for the pionic sector of QCD, was formulated in [7] by Jürg Gasser and Heiri Leutwyler after preparatory work in [6, 8]. However, in addition to the pions, the particle spectrum of QCD also contains massive baryons. Baryon chiral perturbation theory (BχPT) is the corresponding low-energy effective field theory which describes pions as well as baryons [9–13]. Due to baryon number (B) conservation one can investigate the pion sector $B = 0$ and the baryon sector $B \neq 0$ independently. By the use of BχPT, the low-energy physics of QCD is by far more easily accessible than by solving the underlying strongly coupled microscopic theory.

Quantum antiferromagnets are systems in which the global $SU(2)_s$ spin symmetry is spon-

[1] To be exact: In reality the quarks are not exactly massless and therefore the pions pick up a small mass. However, since the pions are still the lightest particles in the spectrum, they dominate the low-energy physics anyhow.

taneously broken down to $U(1)_s$. The resulting Goldstone bosons are the magnons, which thus dominate the low-energy physics of an undoped antiferromagnet. In analogy to χPT, we formulate in this thesis a low-energy effective field theory for magnons in an antiferromagnet on the honeycomb lattice based on symmetry considerations. The leading order effective Lagrangian is constructed with the magnon field as the relevant degree of freedom and is completely defined by the two low-energy constants ρ_s (spin stiffness) and c (magnon velocity). However, since we are finally interested in the low-energy dynamics of a hole-doped antiferromagnet, the pure magnon theory must be extended by also including holes in the effective description. The guideline for this extension is given by BχPT, particularly with regard to the non-linear realisation of the global $SU(2)_s$ symmetry as a local symmetry in the unbroken subgroup $U(1)_s$ which allows us to couple the magnons to the holes in the effective Lagrangain. As baryon number is a conserved quantity in QCD, the fermion number Q is also conserved in the antiferromagnetic phase. We are therefore led to investigate the low-energy physics in each fermion number sector independently. The pure magnon sector ($Q = 0$) then corresponds to the pure pion sector in the QCD framework and, as soon as one hole is included ($Q = -1$), we enter the analogue of the baryon sector of QCD. An effective field theory for magnons and doped holes (electrons) in an antiferromagnet on the square lattice has been worked out in [14] ([15]).

The microscopic starting point for the effective field theory including magnons and doped holes is the strongly coupled Hubbard model, which we assume to be a valid model describing antiferromagnetism. By the use of numerical simulations it has been shown that the Hubbard Hamiltonian indeed reveals spontaneous $SU(2)_s \to U(1)_s$ breaking. The Hubbard model is invariant under the discrete symmetries of the honeycomb lattice as well as under the global spin symmetry $SU(2)_s$ and the fermion number symmetry $U(1)_Q$. As the construction of a low-energy effective field theory demands, the final effective Lagrangian for magnons and holes is invariant under *all* symmetries of the Hubbard model. The transformation behaviour of the effective fields under the various symmetries, and thus the final form of the effective Lagrangian, depends on where in momentum space doped holes occur. Numerical simulations in [16] have shown that holes reside in pockets centered around lattice momenta $(0, \pm 4\pi/(3\sqrt{3}a))$ where a denotes a lattice spacing. In fact, the locations of the pockets must be taken into account while identifying the effective degrees of freedom for holes. The energy scale of the Hubbard model is determined by the parameters t and U. The energy scale of the effective field theory, however, is set by the low-energy constants, which itself depend on the parameters of the Hubbard model. Therefore, the effective field theory is only valid for energies which are small compared to a low-energy constant like ρ_s.

It is an interesting question to ask whether the low-energy effective field theory for magnons and holes can also be used to describe materials in the high-temperature superconducting phase. In this phase, antiferromagnetism ceases to exist and thus $SU(2)_s$ is no longer spontaneously broken. The $SU(2)_s \to U(1)_s$ breakdown, however, is a key ingredient for the construction of the effective field theory. Therefore, a systematic construction according to this thesis is no longer possible. On the other hand, as long as the magnons, now with a finite correlation length, and the holes, with the index structure of the antiferromagnetic phase, still remain the relevant degrees of freedom, the effective field theory can be applied to the high-temperature superconducting phase.

Once the effective field theory is constructed, it is applicable to various low-energy phenomena hardly accessible in the framework of the microscopic theory. In this thesis, as an example, we investigate possible spiral phases of the staggered magnetisation in an antiferromagnet on the honeycomb lattice with a small amount of homogeneously doped holes. The corresponding results are obtained by the use of a variational calculation and are published in [17]. Shraiman and Siggia first introduced the idea that a spiral phase can be a potential ground state of a doped antiferromagnet even at arbitrarily small doping [18]. There are various theoretical descriptions showing that the spiral phase is indeed a stable configuration for low-doped antiferromagnets [19–35]. Spiral phases for doped antiferromagnets on the square lattice were first investigated within the framework of an effective field theory in [36, 37]. In [38], the influence of a periodic and piecewise constant potential on possible spiral configurations was worked out.

This thesis emerged from a close collaboration with Marcel Wirz. Besides the same construction of the effective field theory for magnons and holes, the thesis of Marcel Wirz contains, as a further application of the effective field theory, a detailed discussion of magnon induced two-hole bound states [39]. Two-hole bound states from an effective field theory for magnons and holes in an antiferromagnet on the square lattice have been investigated in [14, 40].

Part I

Systematic low-energy effective field theory for magnons and holes in an antiferromagnet on the honeycomb lattice

Chapter 2

Properties of the honeycomb lattice

Before discussing concrete microscopic models for antiferromagnetism, we first of all will present the symmetry properties of the underlying lattice. On this level of investigation we consider the honeycomb lattice as an infinite extended empty lattice without any physical objects on its sites. In chapter 3 we will then show that the microscopic models are indeed invariant under the discrete symmetries of the honeycomb lattice.

2.1 A bipartite non-Bravais lattice

To show that the honeycomb lattice features a two-dimensional non-Bravais lattice structure, let us first review a definition of a Bravais lattice. According to [41] *a Bravais lattice is an infinite array of discrete points with an arrangement and orientation that appears exactly the same, from whichever of the points the array is viewed.* This is not the case for the adjacent points A and B in Fig. 2.1. The orientation of the nearest neighbour sites from point B with respect to the nearest neighbour sites of point A is rotated by 180 degrees. In fact, the honeycomb lattice is a superposition of two triangular Bravais sub-lattices A and B, where we choose the primitive lattice vectors

$$a_1 = \left(\tfrac{3}{2}a, \tfrac{\sqrt{3}}{2}a\right), \qquad a_2 = \left(0, \sqrt{3}a\right), \tag{2.1}$$

with a denoting the distance between two neighbouring sites, as basis vectors of sub-lattice A and B. Since the honeycomb lattice can be decomposed into a disjoint union of two sub-lattices A and B, where each lattice site on A has only nearest neighbours on sublattice B and vice versa, it belongs to the class of bipartite lattices. Obviously, the coordination number z of the honeycomb lattice is three.[1]

Since the honeycomb lattice itself is not a Bravais lattice, we are led to derive its Brillouin zone by constructing the Brillouin zones of the underlying triangular sublattices A and B. These two Brillouin zones are identical since the sublattices are spanned by the same primitive vectors of Eq. (2.1). We calculate the basis vectors g_i of the reciprocal lattice by means of Eq. (2.1) and the Laue condition

[1] Due to the fact that on the honeycomb lattice z is smaller than the coordination number on the square lattice ($z = 4$), deviations in numerical results for various low-energy constants between these two lattices can be explained. This will be discussed in section 5.1.

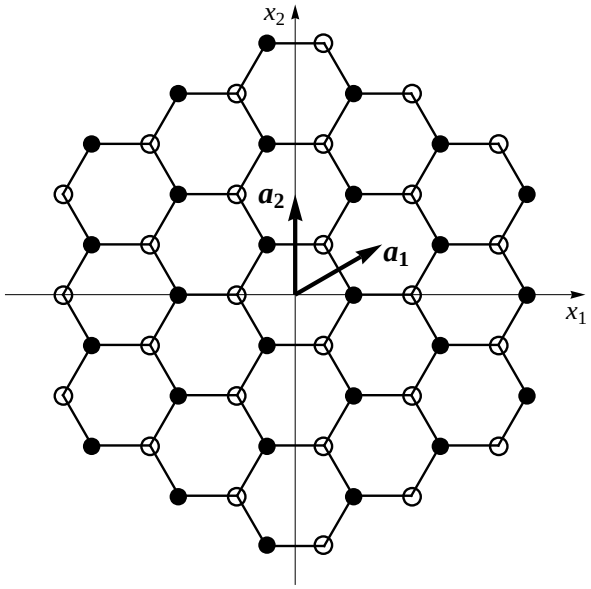

Figure 2.1: *The honeycomb lattice with its two sublattices A (•), B (∘), and the corresponding primitive lattice vectors* a_1, a_2.

$$a_i \cdot g_j = 2\pi\delta_{ij}, \qquad i,j \in \{1,2\}. \tag{2.2}$$

This implies

$$g_1 = \left(\tfrac{4\pi}{3a}, 0\right), \qquad g_2 = \left(-\tfrac{2\pi}{3a}, \tfrac{2\pi}{\sqrt{3}a}\right). \tag{2.3}$$

Fig. 2.2 shows that the first Brillouin zone of the honeycomb lattice is again a hexagon, however, rotated by an angle of 30 degrees with respect to the hexagon in coordinate space. Note, that the resulting Brillouin zone is a superposition of the Brillouin zones of sublattice A and sublattice B and is therefore doubly covered. A state in the Brillouin zone can therefore be occupied by two fermions with the same spin direction under the constraint that one of the two fermions is located on A and the other fermion on B. Thus, beside spin orientation and momentum, the sublattice indices A and B become additional quantum numbers.

An electron or a hole with a certain momentum k behaves exactly like an electron (hole) with momentum k' as long as the difference between k and k' is equal to a reciprocal lattice vector. For all momentum dependent quantities it is therefore sufficient to consider only the momenta in the first Brillouin zone. The six corners of the first Brillouin zone from the honeycomb lattice are given by the coordinates

$$\begin{aligned} k_1 &= \left(\tfrac{2\pi}{3a}, \tfrac{2\pi}{3\sqrt{3}a}\right), & k_2 &= \left(0, \tfrac{4\pi}{3\sqrt{3}a}\right), & k_3 &= \left(-\tfrac{2\pi}{3a}, \tfrac{2\pi}{3\sqrt{3}a}\right), \\ k_4 &= \left(-\tfrac{2\pi}{3a}, -\tfrac{2\pi}{3\sqrt{3}a}\right), & k_5 &= \left(0, -\tfrac{4\pi}{3\sqrt{3}a}\right), & k_6 &= \left(\tfrac{2\pi}{3a}, -\tfrac{2\pi}{3\sqrt{3}a}\right). \end{aligned} \tag{2.4}$$

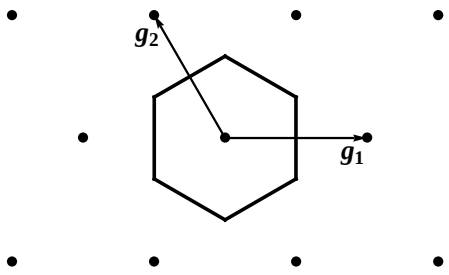

Figure 2.2: *The reciprocal lattice of the honeycomb lattice and the corresponding first Brillouin zone.*

From these six corners, only two points form a set of inequivalent points (Fig. 2.3). All the other sites of the reciprocal lattice are then periodic copies of these two inequivalent points. The area of the first Brillouin zone is given by

$$A_{BZ} = \frac{8\sqrt{3}\pi^2}{9a^2}. \tag{2.5}$$

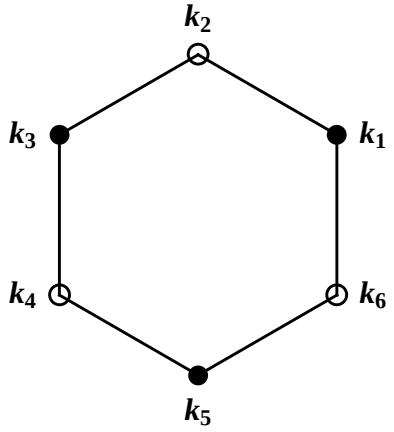

Figure 2.3: *The six corners of the first Brillouin zone. Each pair of* $\{\bullet,\circ\}$ *represents a set of inequivalent points.*

2.2 Symmetries of the honeycomb lattice

To cover all symmetries of the honeycomb lattice we need a minimal set of symmetry transformations, which generates all transformations leaving the lattice invariant. Such a set consists of a shift symmetry and the generating elements of the dihedral group D_6, which are a rotation of 60 degrees and a reflexion at the x_1-axis. For further investigations, it will turn out to be essential to distinguish between symmetry transformations under which the two sublattices map onto themselves ($A \to A$, $B \to B$), respectively sublattice A is mapped on B and vice versa ($A \leftrightarrow B$).

2.2.0.1 Shift symmetry D_i

The honeycomb lattice remains invariant under a displacement along the two primitive lattice vectors introduced in Eq. (2.1). Such a shift maps $A \to A$ and $B \to B$.

2.2.0.2 Rotation symmetry O

D_6 predicts a symmetry under a 60 degrees spatial rotation around an axis located in the center of a hexagon. This leads to $A \leftrightarrow B$ and O turns a lattice point $x = (x_1, x_2)$ into $Ox = (\frac{1}{2}x_1 - \frac{\sqrt{3}}{2}x_2, \frac{\sqrt{3}}{2}x_1 + \frac{1}{2}x_2)$.

We will now emphasise a characteristic difference between the honeycomb lattice and a square lattice with primitive vectors $e_1 = (a, 0)$, $e_2 = (0, a)$. For the square lattice, the rotation center is conventionally located at a certain lattice point. Compared to the honeycomb lattice, a shift along one of the vectors e_i now maps $A \leftrightarrow B$. On the other hand, a rotation around 90 degrees maps $A \to A$ and $B \to B$.

2.2.0.3 Reflexion symmetry R

The honeycomb lattice exhibits in total six reflexion symmetry axes. Three of them are perpendicular to the sides of the hexagon and the remaining three symmetry axes run through its edges. We only consider reflexions with respect to the x_1-axis (Fig. 2.1). Reflexions with respect to an arbitrary symmetry axis can then be obtained by first rotating the hexagon and then performing the reflexion at the x_1-axis. The reflexion symmetry maps $A \to A$ and $B \to B$. R acts on x as $Rx = (x_1, -x_2)$.

Chapter 3

Microscopic models for quantum antiferromagnets and their symmetries

QCD is the underlying theory of BχPT. We assume that the Hubbard model is a reliable model describing, in general, a doped quantum antiferromagnet, and therefore is valid as a concrete microscopic model for the low-energy effective field theory for magnons and holes to be constructed in this thesis. After introducing the Hamiltonian, we investigate the strong coupling regime of the Hubbard model to discuss briefly its two limiting cases namely the t-J model and the Heisenberg model. Furthermore, due to the fact that the effective Lagrangian must inherit all symmetries of the underlying microscopic system, a careful symmetry analysis of the Hubbard model is presented. Note, that whenever we speak about up ($\uparrow$) or down ($\downarrow$) spins in the framework of the microscopic theory, we mean the projection of the spin onto a global quantisation axis in the 3-direction.

3.1 The Hubbard model

Let $c_{xs}^\dagger$ denote the operator which creates a fermion with spin $s \in \{\uparrow, \downarrow\}$ on a lattice site $x = (x_1, x_2)$. The corresponding annihilation operator is c_{xs}. These fermion operators obey the canonical anticommutation relations

$$\{{c_{xs}}^\dagger, c_{ys'}\} = \delta_{xy}\delta_{ss'}, \tag{3.1}$$

and

$$\{c_{xs}, c_{ys'}\} = \{c_{xs}^\dagger, c_{ys'}^\dagger\} = 0. \tag{3.2}$$

By successively acting with the creation operator $c_{xs}^\dagger$ onto the vacuum state $|0\rangle$ for various x and s ($c_{xs}|0\rangle = 0$), one creates the Hilbert space of the model. Since we are considering fermions, the Pauli principle must be respected and therefore the anticommutation relations of Eq. (3.2) imply $(c_{xs}^\dagger)^2 = 0$. Thus, each lattice site can either be vacant, occupied by an $\uparrow$ spin or $\downarrow$ spin fermion, or occupied by two fermions with opposite spin.

According to [42], the Hubbard model is a minimal model, which takes into account quantum mechanical motion of electrons on a lattice and a short-ranged repulsive interaction between two electrons on the same lattice site. It was first introduced by Hubbard, Gutzwiler and Kanamori in [43]. The Hubbard model is simplified such that the inner structure of the atom is neglected and only electrons, hopping from site to site, are considered. This corresponds to the tight-binding picture of a solid. The second quantized Hubbard Hamiltonian is defined by

$$\mathcal{H} = -t \sum_{\substack{\langle x,y\rangle \\ s=\uparrow,\downarrow}} (c^\dagger_{xs} c_{ys} + c^\dagger_{ys} c_{xs}) + U \sum_x c^\dagger_{x\uparrow} c_{x\uparrow} c^\dagger_{x\downarrow} c_{x\downarrow} - \mu' \sum_{\substack{x \\ s=\uparrow,\downarrow}} c^\dagger_{xs} c_{xs}, \tag{3.3}$$

where $\langle x, y\rangle$ indicates summation over nearest neighbours. The parameter t is the probability amplitude for a fermion to tunnel from site x to site y. Remember, that in the case of the honeycomb lattice, the Hubbard model is formulated on a bipartite lattice. Therefore, only hopping between different sublattices is allowed. The parameter $U > 0$ fixes the strength of the Coulomb repulsion between two fermions located on the same lattice site. Note that, unlike in real materials, the Coulomb interaction in the framework of the Hubbard model is considered to be only short-ranged. In the terms proportional to U and μ' one can identify the fermion number-density operator $n_{xs} = c^\dagger_{xs} c_{xs}$. The parameter μ' denotes the chemical potential and controls a possible doping. The corresponding term counts the additional fermions relative to an empty lattice. For $\mu' = 0$, the system is said to be half-filled, which means that the number of fermions is equal to the number of lattice sites, i.e. on average the system has one fermion per lattice site.

The fermion creation and annihilation operators can be used to define the following $SU(2)_s$ (s for spin), Pauli spinor

$$c^\dagger_x = \left(c^\dagger_{x\uparrow}, c^\dagger_{x\downarrow}\right), \qquad c_x = \begin{pmatrix} c_{x\uparrow} \\ c_{x\downarrow} \end{pmatrix}. \tag{3.4}$$

To display the various symmetries of the Hubbard model in a manifest way, it is convenient to reformulate Eq. (3.3) in terms of $c^\dagger_x$ and c_x. This leads to

$$\mathcal{H} = -t \sum_{\langle x,y\rangle} (c^\dagger_x c_y + c^\dagger_y c_x) + \frac{U}{2} \sum_x (c^\dagger_x c_x - 1)^2 - \mu \sum_x (c^\dagger_x c_x - 1). \tag{3.5}$$

The parameter $\mu = \mu' - \frac{U}{2}$ controls a possible doping where the fermions, due to the subtraction of the constant 1, are now counted with respect to half-filling.

3.1.1 The strong coupling regime ($U \gg t$) of the Hubbard model

By investigating the strong coupling limit $U \gg t$ of the Hubbard model one finds two limiting cases depending on the doping parameter μ.

3.1.1.1 $U \gg t$ and $\mu \neq 0$: The t-J model

Away from half-filling and for $U \gg t$, second order perturbation theory applied to the Hubbard model leads to the t-J model, which in terms of Eq. (3.4) is described by

$$\mathcal{H} = \mathcal{P}\Big\{ -t \sum_{\langle x,y \rangle} (c_x^\dagger c_y + c_y^\dagger c_x) + J \sum_{\langle x,y \rangle} \vec{S}_x \cdot \vec{S}_y - \mu \sum_x (c_x^\dagger c_x - 1) \Big\} \mathcal{P}. \tag{3.6}$$

Also the t-J model is supposed to describe the dynamics of mobile and interacting fermions in an antiferromagnet. The exchange coupling J is related to the parameters of Eq. (3.3) by $J = \frac{2t^2}{U} > 0$. Again, t is the hopping amplitude and the chemical potential μ controlls the doping with respect to a half-filled system. The $SU(2)_s$ spin operator on a site x is given by

$$\vec{S}_x = c_x^\dagger \frac{\vec{\sigma}}{2} c_x, \tag{3.7}$$

where $\vec{\sigma}$ are the Pauli matrices.[1] The components of Eq. (3.7) obey $[S_x^l, S_y^m] = i\delta_{xy}\varepsilon^{lmn} S_x^n$.

Since for $U \gg t$ doubly occupied sites are energetically unfavourable, such states are projected out of the Hilbert space by the operator $\mathcal{P}$. We are then left with a restricted configuration space, only allowing empty and singly occupied lattice sites. Therefore, the t-J model can solely describe hole-doped systems. In [16], the single-hole sector of the t-J model was simulated on the honeycomb lattice by using an efficient loop-cluster algorithm.

Due to their strong coupling, the Hubbard model as well as the t-J model are inaccessible to a systematic analytic treatment. Moreover, numerical simulations for $\mu \neq 0$ are afflicted by a severe fermion sign problem.

3.1.1.2 $U \gg t$ and $\mu = 0$: The antiferromagnetic spin $\frac{1}{2}$ quantum Heisenberg model

As already mentioned, for $U \gg t$ doubly occupied sites are energetically very unfavorable and therefore, in a system at half-filling, each lattice site is occupied either by an $\uparrow$ or $\downarrow$ spin. Every such configuration is then a ground state of the interaction term in the Hubbard Hamiltonian with eigenvalue $E = 0$. Hence, we are left with an infinite degeneracy. Note, that this situation corresponds to $t = 0$ and thus represents the leading order in a perturbation theory in $\frac{t}{U}$. The first order in $\frac{t}{U}$ corresponds to a single hop of a fermion. However, there can be no correction at first order because one hop of a spin cannot again lead to a ground state of the Hubbard U-term. First corrections to the ground state occur at second order perturbation theory, i.e. $\frac{t^2}{U}$. Now a spin can virtually hop to a neighbouring site, occupied with a fermion of opposite spin, and then hop back or it can stay on the new site, while the other spin hops back to the empty site. In this case the new state differs from the old one by the exchange of two spins. Of course, the Pauli principle must always be respected and therefore a fermion cannot hop to a neighbouring site with an identically oriented spin on it. In the end, these virtual hopping processes then favour antiparallel spin alignment. Formally, this procedure results in the use of Brillouin-Wigner perturbation theory, where the Coulomb part of the Hubbard Hamiltonian is the unperturbed system and the kinetic part represents

[1] We use the standard representation

$$\sigma_1 = \begin{pmatrix} 0 & 1 \\ 1 & 0 \end{pmatrix}, \qquad \sigma_2 = \begin{pmatrix} 0 & -i \\ i & 0 \end{pmatrix}, \qquad \sigma_3 = \begin{pmatrix} 1 & 0 \\ 0 & -1 \end{pmatrix}, \tag{3.8}$$

of the Pauli matrices. Throughout this thesis we set $\hbar = 1$.

the perturbation. According to [44], the Hubbard Hamiltonian for $U \gg t$ and $\mu = 0$ can then be approximated by the spin $\frac{1}{2}$ quantum Heisenberg Hamiltonian

$$\mathcal{H} = J \sum_{\langle x,y \rangle} \vec{S}_x \cdot \vec{S}_y. \tag{3.9}$$

The exchange coupling constant J is related the Hubbard model parameters by $J = \frac{2t^2}{U} > 0$. $\vec{S}_x$ is the spin operator on lattice site x given by

$$\vec{S}_x = \frac{1}{2}\vec{\sigma}_x. \tag{3.10}$$

Note, that the Heisenberg model includes no fermion hopping. It only describes localised spins, interacting among nearest neighbours with coupling strength J. For $J < 0$, Eq. (3.9) describes ferromagnetism and the corresponding ground state can be derived analytically. This is not the case for the antiferromagnetic ground state of the Heisenberg model with $J > 0$. Intuitively it seems to be natural to assume the classical Néel state

$$|N\rangle = \prod_{x \in A} c^\dagger_{x\uparrow} \prod_{x \in B} c^\dagger_{x\downarrow} |0\rangle \tag{3.11}$$

to be the ground state of Eq. (3.9). Its characteristic antiparallel alignment of spins emanates from the bipartite structure of the honeycomb lattice.[2] A short calculation, however, shows that the state of Eq. (3.11) is not an eigenstate of Eq. (3.9). Moreover, Marshall's theorem in [45] states that the antiferromagnetic ground state of the Heisenberg Hamiltonian is a singlet, which the classical Néel state is not. Actually, the ground state of the Heisenberg Hamiltonian consists of Eq. (3.11) and additional spin fluctuations. Nevertheless, the classical Néel state induces an order parameter - the staggered magnetisation vector defined as[3]

$$\vec{M}_s = \sum_x (-1)^x \vec{S}_x. \tag{3.12}$$

We define $(-1)^x = 1$ for all $x \in A$ and $(-1)^x = -1$ for all $x \in B$, where A and B are the triangular sublattices of the honeycomb lattice introduced in section 2.1. The staggered magnetisation, as a Hermitean operator, shows a non-vanishing vacuum expectation value in the antiferromagnetic phase, which is maximised for the classical Néel state. In contrast to a ferromagnet, the total uniform magnetisation $\vec{M} = \sum_x \vec{S}_x$ vanishes for an antiferromagnet.

3.2 Symmetries of the Hubbard model

Since all terms in the effective Lagrangian must be invariant under all symmetries of the Hubbard model, a careful symmetry analysis of Eq. (3.5) is needed. Investigating symmetries will now essentially be reduced to determining the transformation properties of the Pauli spinor c_x. Let us divide the symmetries of the Hubbard model into two categories: Continuous symmetries ($SU(2)_s$, $U(1)_Q$ and $SU(2)_Q$), which are implicit symmetries of Eq. (3.5), and discrete symmetries (D_i, O and R), which are symmetry transformations of the underlying

[2] A non-bipartite lattice, e.g. a triangular lattice, cannot induce perfect antiparallel alignment of spins.

[3] The existence of a non-vanishing order parameter, i.e. $\langle 0|\vec{M}_s|0\rangle \neq 0$, indicates a spontaneously breakdown of a continuous, global symmetry. This will be discussed in section 5.1.

honeycomb lattice. There is also time reversal implemented by an anti-unitary operator T. This symmetry, however, will be discussed only in the framework of the effective field theory for magnons (section 5.1). Let us begin with the two basic continuous symmetries of the Hubbard model, namely the $SU(2)_s$ spin rotation symmetry and the $U(1)_Q$ charge (fermion number) symmetry. A detailed analysis of these two symmetries can be found in [46].

3.2.1 $SU(2)_s$ spin rotation symmetry

In order to construct the appropriate unitary transformation representing a global $SU(2)_s$ spin rotation, we first define the total $SU(2)_s$ spin operator by

$$\vec{S} = \sum_x \vec{S}_x = \sum_x c_x^\dagger \, \frac{\vec{\sigma}}{2} \, c_x. \tag{3.13}$$

The three generators of $SU(2)_s$ are then given by

$$S_1 = \frac{1}{2}\sum_x (c_{x\uparrow}^\dagger c_{x\downarrow} + c_{x\downarrow}^\dagger c_{x\uparrow}),\ S_2 = \frac{i}{2}\sum_x (c_{x\downarrow}^\dagger c_{x\uparrow} - c_{x\uparrow}^\dagger c_{x\downarrow}),\ S_3 = \frac{1}{2}\sum_x (c_{x\uparrow}^\dagger c_{x\uparrow} - c_{x\downarrow}^\dagger c_{x\downarrow}). \tag{3.14}$$

An $SU(2)_s$ symmetry is now implemented by the unitary operator

$$V = \exp(i\vec{\eta}\cdot\vec{S}), \tag{3.15}$$

which acts on c_x as

$$c_x' = V^\dagger c_x V = \exp\left(i\vec{\eta}\cdot\frac{\vec{\sigma}}{2}\right) c_x = g c_x, \qquad g \in SU(2)_s. \tag{3.16}$$

Due to the fact that $[\mathcal{H}, \vec{S}\,] = 0$, the total spin is conserved and by means of Eq. (3.16) it is straightforward to show that the Hubbard Hamiltonian is indeed invariant under global $SU(2)_s$ spin rotations.

3.2.2 $U(1)_Q$ charge symmetry

For the purpose of constructing the appropriate unitary transformation of a $U(1)_Q$ symmetry, we proceed in full analogy to the $SU(2)_s$ case by first defining the $U(1)_Q$ charge operator

$$Q = \sum_x Q_x = \sum_x (c_x^\dagger c_x - 1) = \sum_x (c_{x\uparrow}^\dagger c_{x\uparrow} + c_{x\downarrow}^\dagger c_{x\downarrow} - 1), \tag{3.17}$$

which counts the fermion number with respect to half-filling. The corresponding $U(1)_Q$ unitary operator is given by

$$W = \exp(i\omega Q), \tag{3.18}$$

and the fermion operators transform as

$${}^{Q}c_x = W^\dagger c_x W = \exp(i\omega) c_x, \qquad \exp(i\omega) \in U(1)_Q. \tag{3.19}$$

$[\mathcal{H}, Q] = 0$ and therefore charge is a conserved quantity of the Hubbard model. Instead of saying charge is conserved, it is equivalent to speak about fermion number conservation. It is easy to see that the Hubbard Hamiltonian is invariant under the $U(1)_Q$ fermion number symmetry.

3.2.3 Shift symmetry D_i

The Hubbard model shows invariance under shifts along the two primitive lattice vectors a_1 and a_2. These transformations are generated by the unitary operators D_i, which act on the spinor c_x as

$$^{D_i}c_x = D_i^\dagger c_x D_i = c_{x+a_i}. \tag{3.20}$$

By applying Eq. (3.20) on the Hubbard Hamiltonian of Eq. (3.5) and redefining the sum over lattice sites x, one can see that indeed $[\mathcal{H}, D_i] = 0$. Since the shift symmetry maps $A \to A$ and $B \to B$, this transformation does not affect the order parameter $\vec{M}_s$.

3.2.4 Rotation symmetry O

A spatial rotation of 60 degrees leaves Eq. (3.5) invariant. Since spin-orbit coupling is neglected in the Hubbard model, and therefore spin and angular momentum are separately conserved, spin becomes an internal quantum number. A global $SU(2)_s$ spin rotation can thus be performed independent of a rotation in coordinate space and vice versa. The rotation symmetry is implemented by the use of a unitary operator O, which acts on the fermion operators as

$$^{O}c_x = O^\dagger c_x O = c_{Ox}. \tag{3.21}$$

Rotation symmetry on the honeycomb lattice is spontaneously broken because O maps sublattice $A \leftrightarrow B$ and therefore the staggered magnetisation $\vec{M}_s$ gets flipped. This is, however, just the same as redefining the sign of $(-1)^x$ and should therefore not change the physics. In the construction of the effective field theory for magnons and holes, it will turn out to be useful to incorporate the combined symmetry O' consisting of a spatial rotation O and a global $SU(2)_s$ spin rotation $g = i\sigma_2$. O' transforms c_x as

$$^{O'}c_x = O'^\dagger c_x O' = (i\sigma_2)^{O}c_x = (i\sigma_2)c_{Ox}. \tag{3.22}$$

The specific $SU(2)_s$ element g corresponds to a global spin rotation of 180 degrees and thus flips back $\vec{M}_s$, such that, in fact, at the end the order parameter is not affected by O'. As opposed to the honeycomb lattice, $\vec{M}_s$ changes sign under the shift symmetry D_i on a bipartite square lattice. In this case, a combined shift symmetry D_i' is needed. Since on the square lattice O maps sublattice $A \to A$ and $B \to B$, the staggered magnetisation is not affected by under rotation by an angle of 90 degrees.

3.2.5 Reflexion symmetry R

The Hubbard Hamiltonian is invariant under reflexion of the lattice points x. Under this transformation, the fermion operators transform as

$$^{R}c_x = R^\dagger c_x R = c_{Rx}. \tag{3.23}$$

Since R maps the two sublattices onto themselves, $\vec{M}_s$ remains invariant.

3.2.6 $SU(2)_Q$ - A non-Abelian extension of the $U(1)_Q$ charge symmetry

In [47, 48], Yang and Zhang proved the existence of a non-Abelian extension for the $U(1)_Q$ fermion number symmetry in the half-filled Hubbard model. They call this symmetry a pseudospin symmetry, which contains $U(1)_Q$ as a subgroup. $SU(2)_Q$ is realised on the square as well as on the honeycomb lattice and is generated by the three operators

$$\begin{aligned} Q^+ &= \sum_x (-1)^x c^\dagger_{x\uparrow} c^\dagger_{x\downarrow}, \qquad Q^- = \sum_x (-1)^x c_{x\downarrow} c_{x\uparrow}, \\ Q^3 &= \sum_x \frac{1}{2}(c^\dagger_{x\uparrow} c_{x\uparrow} + c^\dagger_{x\downarrow} c_{x\downarrow} - 1) = \frac{1}{2} Q. \end{aligned} \tag{3.24}$$

The factor $(-1)^x$ again distinguishes between the two sublattices A and B of the honeycomb lattice. Defining $Q^\pm = Q^1 \pm iQ^2$, we can work out

$$Q^1 = \sum_x \frac{1}{2}(-1)^x (c^\dagger_{x\uparrow} c^\dagger_{x\downarrow} + c_{x\downarrow} c_{x\uparrow}), \qquad Q^2 = \sum_x \frac{1}{2i}(-1)^x (c^\dagger_{x\uparrow} c^\dagger_{x\downarrow} - c_{x\downarrow} c_{x\uparrow}), \tag{3.25}$$

to show that the $SU(2)_Q$ Lie-algebra $[Q^l, Q^m] = i\varepsilon^{lmn} Q^n$, with $l, m \in \{1, 2, 3\}$, indeed is satisfied. Moreover, it is straightforward to calculate $[\mathcal{H}, \vec{Q}] = 0$ with $\vec{Q} = (Q^1, Q^2, Q^3)$ for the Hubbard $\mathcal{H}$ with $\mu = 0$.

The Hubbard Hamiltonian in the form of Eq. (3.3) or Eq. (3.5) is not manifestly invariant under $SU(2)_s \otimes SU(2)_Q$. In order to find a manifestly $SU(2)_s \otimes SU(2)_Q$ invariant representation, we arrange the fermion operators in a 2×2 matrix-valued operator. How this is done in detail can be found in [46]. Here we simply state the new fermion representation by

$$C_x = \begin{pmatrix} c_{x\uparrow} & (-1)^x\, c^\dagger_{x\downarrow} \\ c_{x\downarrow} & -(-1)^x c^\dagger_{x\uparrow} \end{pmatrix}. \tag{3.26}$$

The $SU(2)_Q$ transformation behaviour of Eq. (3.26) can now be worked out by applying the unitary operator $W = \exp(i\vec{\omega} \cdot \vec{Q})$. One then finds

$$^{\vec{Q}} C_x = W^\dagger C_x W = C_x \Omega^T, \tag{3.27}$$

with

$$\Omega = \exp\left(i\vec{\omega} \cdot \frac{\vec{\sigma}}{2}\right) \in SU(2)_Q. \tag{3.28}$$

The Pauli matrices now belong to the $SU(2)_Q$ space. Under an $SU(2)_s$ spin rotation, C_x transforms exactly like c_x, i.e.

$$C'_x = g C_x, \qquad g \in SU(2)_s. \tag{3.29}$$

Applying an $SU(2)_s \otimes SU(2)_Q$ transformation to Eq. (3.26) then leads to

$$^{\vec{Q}} C'_x = g C_x \Omega^T. \tag{3.30}$$

Since the $SU(2)_s$ spin symmetry acts from the left and the $SU(2)_Q$ pseudospin symmetry acts from the right onto the fermion operator, it is now obvious that these two non-Abelian symmetries do commute. Under the discrete symmetries of the Hubbard model, C_x has the following transformation properties

$$\begin{aligned} D_i: &\quad {}^{D_i}C_x = C_{x+a_i}, \\ O: &\quad {}^{O}C_x = C_{Ox}\sigma_3, \\ O': &\quad {}^{O'}C_x = (i\sigma_2)\, C_{Ox}\sigma_3, \\ R: &\quad {}^{R}C_x = C_{Rx}, \end{aligned} \tag{3.31}$$

which can be worked out by using the already elaborated transformation laws of c_x. In terms of Eq. (3.26), we are now able to write down the Hubbard Hamiltonian in a manifestly $SU(2)_s$, $U(1)_Q$, D_i, O, O' and R invariant form

$$\mathcal{H} = -\frac{t}{2}\sum_{\langle x,y\rangle} \mathrm{Tr}[C_x^\dagger C_y + C_y^\dagger C_x] + \frac{U}{12}\sum_x \mathrm{Tr}[C_x^\dagger C_x C_x^\dagger C_x] - \frac{\mu}{2}\sum_x \mathrm{Tr}[C_x^\dagger C_x \sigma_3]. \tag{3.32}$$

Obviously, the σ_3 Pauli matrix in the chemical potential term prevents the Hubbard Hamiltonian from being invariant under $SU(2)_Q$ away from half-filling. For $\mu \neq 0$, $SU(2)_Q$ breaks down to its subgroup $U(1)_Q$. In addition, the pseudospin symmetry is realised in Eq. (3.32) only if nearest neighbour-hopping is included. As soon as the Hubbard model is modified such that it describes next-to-nearest-neighbour tunneling, the $SU(2)_Q$ invariance gets lost even for $\mu = 0$. $SU(2)_Q$ contains a particle-hole symmetry which physically implies a symmetry between the positive energy spectrum of a particle and the negative energy spectrum of a hole. Although this pseudospin symmetry is not present in real materials, it will play an important role in the construction of the effective field theory. The identification of the final effective fields for holes then leads us to explicitly break the $SU(2)_Q$ symmetry (section 6.5).

3.3 Symmetries of the t-J model

The symmetries of the the t-J model are identical to the ones of the Hubbard model up to the $SU(2)_Q$ symmetry. Remember, that the t-J model can only describe hole-doped systems. Since $SU(2)_Q$ relates the electron- and the hole-doped sectors in a symmetric way, this symmetry is not present in the t-J model. However, during the construction of the effective degrees of freedom for holes we will break $SU(2)_Q$ anyway and hence the t-J Hamiltonian as an underlying microscopic model for the effective theory is as reliable as the Hubbard model.

Chapter 4

Low-energy effective field theory for free fermions

A system on the honeycomb lattice, that is under thorough investigation, is graphene (see e.g. [49–51]). Neutral graphene is a two-dimensional graphite monolayer consisting of carbon atoms arranged on a honeycomb lattice, which shows semi-metallic behaviour. A peculiar interesting feature of graphene is that its low-energy excitations are free, massless and relativistic Dirac fermions moving with a speed v_F. Undoped graphene is well described by the Hubbard model at half-filling in the weak coupling limit ($U \ll t$). Monte Carlo simulations of the half-filled Hubbard model in [52] have shown that for sufficiently large repulsion U there exists a phase transition leading graphene from its weakly correlated unbroken phase into a strongly coupled antiferromagnetic phase, which is governed by a spontaneous breakdown of $SU(2)_s$ to $U(1)_s$. This kind of a phase transition does not occur on a square lattice since such a system already exhibits antiferromagnetic behaviour for arbitrarily small U and $t' = 0$.

In general, spontaneous symmetry breaking is not a necessary condition for the existence of an effective field theory. As long as the low-energy degrees of freedom are describing the lightest particles in the spectrum, the effective theory approach is valid. Therefore, one is allowed to describe the massless Dirac excitations of semi-metallic graphene by an effective Lagrangian since these particles are the only relevant low-energy degrees of freedom.

In this section, we first confirm the existence of massless Dirac fermions by diagonalising the Hubbard Hamiltonian in the weak coupling limit. Furthermore, this procedure allows us to determine an analytic expression for the fermion velocity v_F. Once the microscopic model is solved, we establish the correct degrees of freedom to construct an effective field theory for free Dirac fermions with zero mass only based on the symmetries of the underlying microscopic model. Note, that this theory is not yet a correct description of graphene's low energy excitations, since spin and contact interaction between fermions are not included. However, the corresponding Lagrangian $\mathcal{L}_2^{free}$ will indeed reveal the form of a Dirac Lagrangian without a mass term what proves the equivalence between our effective field theory approach and the corresponding microscopic model in the low-energy regime.

4.1 Massless, free Dirac fermions in the framework of the Hubbard model

In the weak coupling limit of the Hubbard model ($U \ll t$) the Coulomb interaction U can be treated as a small perturbation. In [44] it is assumed that states of weakly coupled fermions are equivalent to states of free fermions and therefore we completely neglect the interaction term in the Hubbard Hamiltonian. An undoped system ($\mu = 0$), consisting of weakly coupled fermions, is then described by

$$\mathcal{H} = \mathcal{H}_t + \mathcal{H}_{t'} = -t \sum_{\langle x,y \rangle} (c_x^\dagger c_y + c_y^\dagger c_x) - t' \sum_{\langle\langle x,y \rangle\rangle} (c_x^\dagger c_y + c_y^\dagger c_x), \tag{4.1}$$

where t' now allows next-to-nearest neighbour hopping with the corresponding summation indicated by $\langle\langle x, y\rangle\rangle$. Remember, that $t' = 0$ leads to a manifestly $SU(2)_Q$ variant Hubbard Hamiltonian. The $U = 0$ limit now allows us to derive the energy-momentum relation for free fermions by transforming Eq. (4.1) into momentum space. As a first step, we expand the Pauli spinor c_x on a 2-dimensional, infinite extended honeycomb lattice as

$$c_x^X = \frac{1}{A_{BZ}} \int\limits_{A_{BZ}} d^2k \ \exp(ikx) c_k^X, \qquad X \in \{A, B\}, \tag{4.2}$$

where $c_x^{A\dagger}$ (c_x^A) creates (annihilates) fermions on sublattice A and $c_x^{B\dagger}$ (c_x^B) creates (annihilates) fermions on sublattice B. A detailled derivation of Eq. (4.2) can be found in [44]. Note, that $c_{k\uparrow}^X$ and $c_{k\downarrow}^X$ still obey canonical anticommutation relations. To capture all nearest and next-to-nearest neighbours we introduce the vectors $\{j_i, j_i'\}$ with $i = 1, 2, 3$. Then Eq. (4.1) takes the form

$$\begin{aligned} \mathcal{H} \ = \ & -t \sum_{i=1}^{3} \sum_{x \in A} (c_x^{A\dagger} c_{x+j_i}^B + c_{x+j_i}^{B\dagger} c_x^A) \\ & -t' \sum_{i=1}^{3} \Big[\sum_{x \in A} (c_x^{A\dagger} c_{x+j_i'}^A + c_{x+j_i'}^{A\dagger} c_x^A) + \sum_{x \in B} (c_x^{B\dagger} c_{x+j_i'}^B + c_{x+j_i'}^{B\dagger} c_x^B) \Big], \end{aligned} \tag{4.3}$$

where

$$j_1 = (a, 0)\,, \qquad j_2 = \left(-\tfrac{1}{2}a, \tfrac{\sqrt{3}}{2}a\right), \qquad j_3 = \left(-\tfrac{1}{2}a, -\tfrac{\sqrt{3}}{2}a\right), \tag{4.4}$$

connect each $x \in A$ with its nearest neighbours on B, and

$$j_1' = \left(\tfrac{3}{2}a, \tfrac{\sqrt{3}}{2}a\right), \qquad j_2' = \left(0, \sqrt{3}a\right), \qquad j_3' = \left(\tfrac{3}{2}a, -\tfrac{\sqrt{3}}{2}a\right), \tag{4.5}$$

connect each $x \in A$ ($x \in B$) with its next-to-nearest neighbours which are located on the same sublattice A (B). Plugging Eq. (4.2) in Eq. (4.3) and using

$$\frac{1}{A_{BZ}} \sum_x \exp(i(k - k')x) = \delta^{(2)}(k - k'), \qquad \frac{1}{A_{BZ}} \int\limits_{A_{BZ}} d^2k \ \exp(ik(x - x')) = \delta_{x,x'}, \tag{4.6}$$

one obtains

$$\mathcal{H} = -\frac{1}{A_{BZ}} \int\limits_{A_{BZ}} d^2k \left(c_k^{A\dagger}, c_k^{B\dagger} \right) \mathcal{H}(k) \begin{pmatrix} c_k^A \\ c_k^B \end{pmatrix}, \tag{4.7}$$

with

$$\mathcal{H}(k) = \begin{pmatrix} t'f(k) & tg(k) \\ tg^*(k) & t'f(k) \end{pmatrix}, \tag{4.8}$$

and

$$f(k) = 4\cos\left(\frac{3}{2}k_1a\right)\cos\left(\frac{\sqrt{3}}{2}k_2a\right) + 2\cos\left(\sqrt{3}k_2a\right), \tag{4.9}$$

$$g(k) = \cos\left(k_1a\right) + i\sin\left(k_1a\right) + 2\cos\left(\frac{\sqrt{3}}{2}k_2a\right)\left[\cos\left(\frac{1}{2}k_1a\right) - i\sin\left(\frac{1}{2}k_1a\right)\right]. \tag{4.10}$$

The diagonalisation of the Hamiltonian in Eq. (4.8) yields the energy eigenvalues

$$\begin{aligned} E_\pm(k) &= t'f(k) \pm tg(k) \\ &= t'f(k) \pm t\sqrt{3 + f(k)} \\ &= t'\left[4\cos\left(\frac{3}{2}k_1a\right)\cos\left(\frac{\sqrt{3}}{2}k_2a\right) + 2\cos\left(\sqrt{3}k_2a\right)\right] \\ &\quad \pm t\sqrt{3 + 4\cos\left(\frac{3}{2}k_1a\right)\cos\left(\frac{\sqrt{3}}{2}k_2a\right) + 2\cos\left(\sqrt{3}k_2a\right)}, \end{aligned} \tag{4.11}$$

where the the plus sign applies to the upper (conduction) and the minus sign applies to the lower (valence) band. In the half-filled ground state, i.e. $T = 0$, all states with E_- are occupied, while the conduction band is completely empty. Let us first investigate the case $t' = 0$. As one can see in Fig. 4.1 (a), the Fermi energy lies at the *common* points of the two bands with $E_F = 0$. The Fermi surface therefore consists of the six points at the six Brillouin zone corners where the two bands are degenerated. These points are known as Dirac points. The contact of the valence and the conduction band indicates the semi-metallic phase of graphene. For $t' = 0$ the two bands are completely symmetric around zero energy, which illustrates the particle-hole symmetry of $SU(2)_Q$. The value of the energy for an electron occupying a state in the conduction band is equal to the absolute value of the energy from its corresponding hole in the valence band. Increasing (decreasing) the value of t raises (lowers) the energy scale but does not affect E_F or the topology of the two bands. The situation changes when we allow $t' \neq 0$ (Fig. 4.1 (b)). As we already discussed, $SU(2)_Q$ is now broken down to $U(1)_Q$ and therefore the valence and the conduction band become asymmetric. The presence of t' now shifts E_F and for some values of t and t' the two bands even cover the same energy region. In this case, the Fermi surface is no longer at the Dirac points (Fig. 4.1 (c)). However, we have calculated that the two bands touch each other at the Dirac points for all values of t and t'.

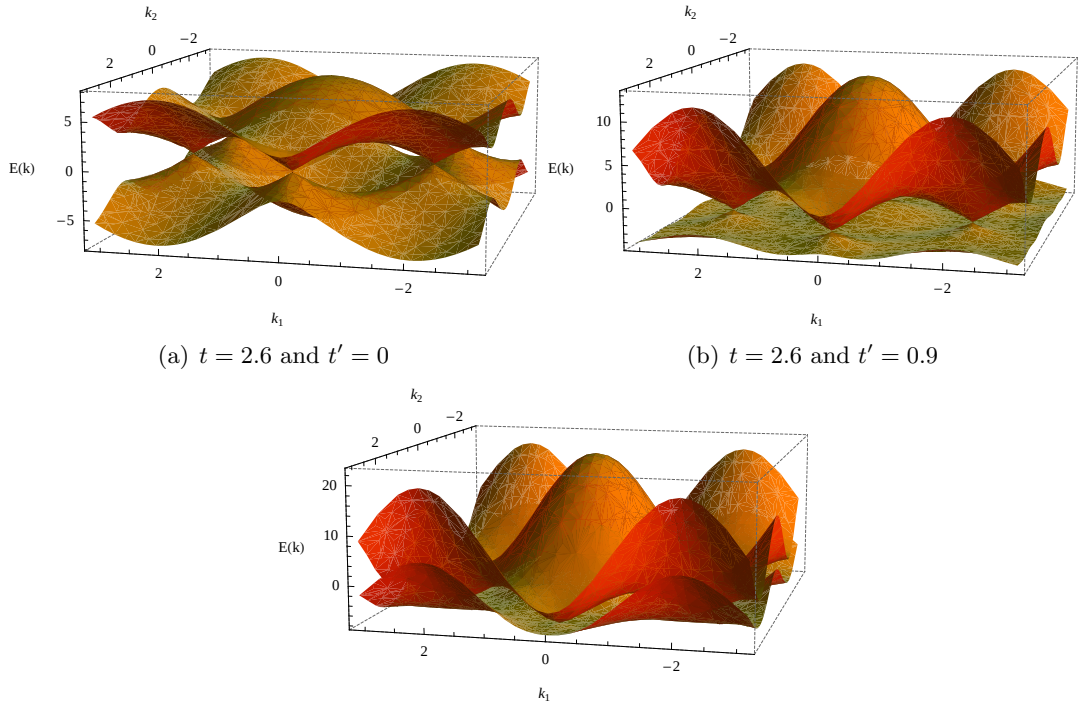

(a) $t = 2.6$ and $t' = 0$

(b) $t = 2.6$ and $t' = 0.9$

(c) $t = 2.6$ and $t' = 2.5$

Figure 4.1: $E(k)$ for a free fermion.

How can we now see that the low-energy physics of graphene is governed by massless relativistic Dirac fermions? Let us expand $E_{\pm}(k)$ in a Taylor series in $k = (k_1, k_2)$ at all the six Dirac points up to first order. This leads to

$$E_{+}(p) = -3t' + \frac{3ta}{2}\sqrt{p_1^2 + p_2^2} + \mathcal{O}(p^2), \tag{4.12}$$

and

$$E_{-}(p) = -3t' - \frac{3ta}{2}\sqrt{p_1^2 + p_2^2} + \mathcal{O}(p^2), \tag{4.13}$$

with momentum p=(p_1, p_2) now defined relative to the appropriate Dirac point. Neglecting the energy shift proportional to t', one indeed can recognise the relativistic energy-momentum relation for a massless, free particle with momentum p

$$E_{\pm}(p) = \pm c|p| = \pm c\sqrt{p_1^2 + p_2^2}, \tag{4.14}$$

and c in this case being the fermion velocity

$$v_F = \frac{3ta}{2}. \tag{4.15}$$

It is interesting to see that the fermion velocity v_F shows no momentum dependence and moreover solely depends on the hopping parameter t and the lattice spacing a.[1] Since the

[1]The value of the fermion velocity $v_F \simeq 1 \times 10^6 m/s$ was obtained by P. R. Wallace in [53].

dispersion relation $E_{\pm}(p)$ becomes isotropic and linear in the vicinity of E_F, so called Dirac cones arise. According to the above expansion such cones occur in every Dirac Point. Although we allow $t' \neq 0$, the Dirac fermions remain massless since for all t and t' the two bands are connected at the six Brillouin zone corners. Let us briefly summarize our findings. In the weak coupling limit we are able to diagonalise the Hubbard Hamiltonian for $U = 0$, including next-to-nearest neighbour hopping, analytically. Expanding the resulting dispersion relation around the six Dirac points indeed shows that the low-energy excitations are free, relativistic fermions with zero mass. By means of the lattice specific vectors $\{j_i, j_i'\}$, we incorporated the geometry of the honeycomb lattice to derive the dispersion relation of Eq. (4.11). We therefore conclude, that massless Dirac excitations are generated by the geometry of the underlying honeycomb lattice.

Free, relativistic fermions with zero mass in two space dimensions are described by the Dirac Hamiltonian

$$\mathcal{H}_D(p) = \alpha p c = (-\sigma_2 p_1 + \sigma_1 p_2)c, \tag{4.16}$$

where $\alpha_i = \gamma_0 \gamma_i$. We choose the corresponding γ^μ to be

$$\gamma_0 = \sigma_3, \qquad \gamma_1 = i\sigma_1, \qquad \gamma_2 = i\sigma_2, \tag{4.17}$$

satisfying

$$\{\gamma_\mu, \gamma_\nu\} = 2 g_{\mu\nu} \mathbb{1}_{2\times 2}, \qquad \mu, \nu \in \{0, 1, 2\}, \qquad \text{with} \qquad g_{\mu\nu} = \begin{pmatrix} 1 & 0 & 0 \\ 0 & -1 & 0 \\ 0 & 0 & -1 \end{pmatrix}. \tag{4.18}$$

Again, c denotes the fermion velocity and not the speed of light. To show that the Hamiltonian $\mathcal{H}(k)$ of Eq. (4.8) is equivalent to $\mathcal{H}_D(p)$ in the low-energy regime, we expand $\mathcal{H}(k)$, incorporating only $g(k)$ and $g^*(k)$ (we set $t' = 0$), for small momenta at the six Dirac points. The resulting Hamiltonians can then be decomposed according to Eq. (4.16). However, now the σ-matrices appear in a specific representation for each Dirac point, which may differ from the standard representation used in Eq. (4.17). To prove the equivalence of $\mathcal{H}(k)$ and $\mathcal{H}_D(p)$, it is sufficiently to show that for each Dirac point there exist some specific matrices $U \in U(2)$ such that the standard representation of the σ-matrices can be obtained by a unitary transformation. We have shown that indeed such matrices exist for each corner of the Brillouin zone and therefore $\mathcal{H}(k)$ is equal to $\mathcal{H}_D(p)$ near E_F.

It is an interesting question to ask whether a low-energy effective field theory for free fermions on the honeycomb lattice, only based on symmetry considerations, also prohibits mass terms.

4.2 Effective degrees of freedom for free fermions

Before we are able to construct the effective field theory for free fermions, we first have to identify the correct low-energy degrees of freedom and their transformation behaviour under all symmetries of the Hubbard Hamiltonian. In the following considerations we only allow nearest neighbour hopping, i.e. $t' = 0$, and we do not yet consider spin. To include spin would be a trivial step. One just has to add a corresponding spin index to the fermion fields.

4.2.1 Momentum space pockets for free fermions

Exact diagonalisation of the half-filled Hubbard Hamiltonian for $U = 0$ has revealed free, massless fermions occurring in the vicinity of the six Dirac points. A small, circular shaped neighbourhood of any of these points we define as a pocket. According to section 2.1, among these six points only two points form a set of inequivalent points. The transformation behaviour of the final fermion fields turns out to be remarkably simple when we choose

$$k_2 = k^\alpha = \left(0, \tfrac{4\pi}{3\sqrt{3}a}\right), \qquad k_5 = k^\beta = \left(0, -\tfrac{4\pi}{3\sqrt{3}a}\right), \tag{4.19}$$

to be the inequivalent points. Then α and β denote the corresponding pockets. All the other points of the reciprocal lattice are in fact periodic copies of k^α and k^β. Moreover, $\Gamma = (0, 0)$ must be included since it can be reached by adding k^α and k^β. In section 2.1 we emphasized that the Brillouin zone of a honeycomb lattice is doubly covered, dual to the two triangular sublattices A and B. Therefore, in coordinate space the $\{\Gamma, k^\alpha, k^\beta\}$ structure of the Brillouin zone induces a three sublattice structure for A and B. The resulting six sublattices $\{A_1, A_2, A_3\}$ and $\{B_1, B_2, B_3\}$ are then superimposed on the antiferromagnetic A-B bipartite lattice structure (Fig. 4.2).

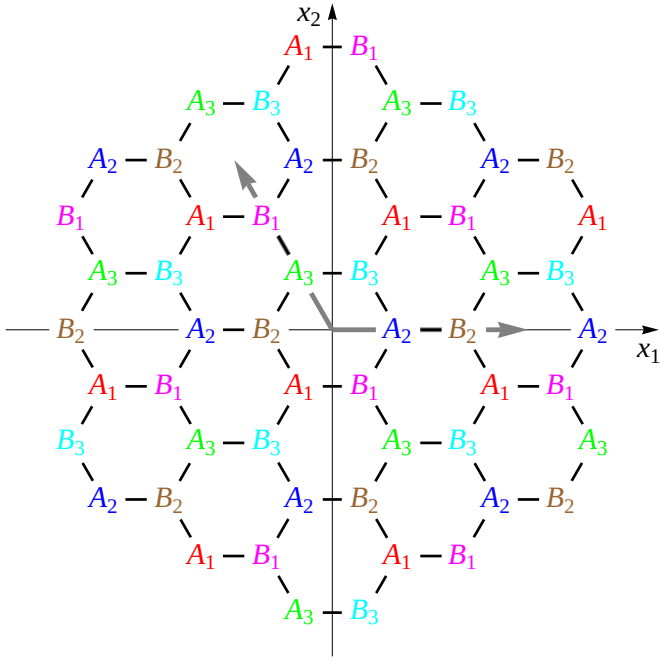

Figure 4.2: $\{A_1, A_2, A_3\}$ *and* $\{B_1, B_2, B_3\}$ *sublattice structure and the corresponding primitive lattice vectors.*

4.2.2 Free fermion fields with a sublattice and a momentum index

Since at the end, the low-energy effective Lagrangian for free fermions is constructed in a Euclidean path integral formalism, the appropriate fermion fields are represented by Grassmann numbers $\psi(x)$. Representing the fermion degrees of freedom by anticommuting numbers

on the level of the effective field theory, they inherit the anticommuting behaviour of the microscopic lattice operators. However, in contrast to these operators, the fermion fields are now defined in a space-time continuum. In coordinate space a fermion at space-time point $x = (x_1, x_2, t)$ is represented by the Grassmann field $\psi^{X_i}(x)$, with $i \in \{1, 2, 3\}$, and $X \in \{A, B\}$, where X_i denotes the corresponding sublattice introduced in section 4.2.1. It is important to point out that, opposed to the microscopic operators, the conjugated Grassmann fields $\psi^{X_i\dagger}(x)$ are independent of $\psi^{X_i}(x)$.

We now want to directly relate the fermion fields to the lattice momenta k^α and k^β, i.e. to the fermion pockets α and β. This can be achieved by introducing an additional index $f \in \{\alpha, \beta\}$, which indicates where in the Brillouin zone the Grassmann fields are located. The new degrees of freedom describing free fermions are then labelled with a sublattice index $X \in \{A, B\}$ *and* a "flavour" index $f \in \{\alpha, \beta\}$ addressing the corresponding lattice momenta in the Brillouin zone. These fields are derived through the following discrete Fourier transformations

$$\psi^{A,f}(x) = \frac{1}{\sqrt{3}} \sum_{n=1}^{3} \exp(-ik^f v_n)\psi^{A_n}(x), \qquad \text{and} \qquad \psi^{B,f}(x) = \frac{1}{\sqrt{3}} \sum_{n=1}^{3} \exp(-ik^f w_n)\psi^{B_n}(x), \tag{4.20}$$

where

$$\begin{aligned} v_1 &= \left(-\tfrac{1}{2}a, -\tfrac{\sqrt{3}}{2}a\right), & v_2 &= (a, 0), & v_3 &= \left(-\tfrac{1}{2}a, \tfrac{\sqrt{3}}{2}a\right), \\ w_1 &= \left(\tfrac{1}{2}a, -\tfrac{\sqrt{3}}{2}a\right), & w_2 &= (-a, 0), & w_3 &= \left(\tfrac{1}{2}a, \tfrac{\sqrt{3}}{2}a\right). \end{aligned} \tag{4.21}$$

The above vectors connect the discrete three-sublattice structure of A and B in position space with lattice momenta k^f in momentum space (Fig. 4.3).

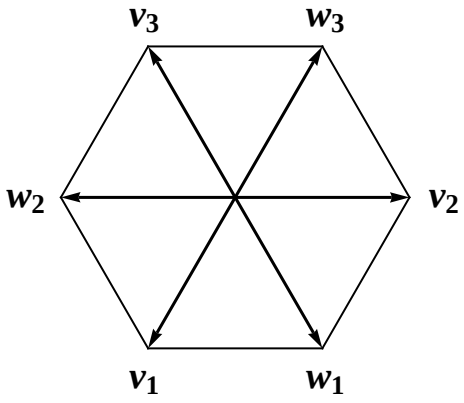

Figure 4.3: *Sublattice vectors from Eq. (4.21).*

We find

$$\begin{aligned}
\psi^{A,\alpha}(x) &= \frac{1}{\sqrt{3}}\Big[\exp(i\tfrac{2\pi}{3})\psi^{A_1}(x) + \psi^{A_2}(x) + \exp(-i\tfrac{2\pi}{3})\psi^{A_3}(x)\Big],\\
\psi^{A,\beta}(x) &= \frac{1}{\sqrt{3}}\Big[\exp(-i\tfrac{2\pi}{3})\psi^{A_1}(x) + \psi^{A_2}(x) + \exp(i\tfrac{2\pi}{3})\psi^{A_3}(x)\Big],\\
\psi^{B,\alpha}(x) &= \frac{1}{\sqrt{3}}\Big[\exp(i\tfrac{2\pi}{3})\psi^{B_1}(x) + \psi^{B_2}(x) + \exp(-i\tfrac{2\pi}{3})\psi^{B_3}(x)\Big],\\
\psi^{B,\beta}(x) &= \frac{1}{\sqrt{3}}\Big[\exp(-i\tfrac{2\pi}{3})\psi^{B_1}(x) + \psi^{B_2}(x) + \exp(i\tfrac{2\pi}{3})\psi^{B_3}(x)\Big],
\end{aligned} \tag{4.22}$$

and the independent conjugate fields

$$\begin{aligned}
\psi^{A,\alpha\dagger}(x) &= \frac{1}{\sqrt{3}}\Big[\exp\left(-i\tfrac{2\pi}{3}\right)\psi^{A_1\dagger}(x) + \psi^{A_2\dagger}(x) + \exp\left(i\tfrac{2\pi}{3}\right)\psi^{A_3\dagger}(x)\Big],\\
\psi^{A,\beta\dagger}(x) &= \frac{1}{\sqrt{3}}\Big[\exp\left(i\tfrac{2\pi}{3}\right)\psi^{A_1\dagger}(x) + \psi^{A_2\dagger}(x) + \exp\left(-i\tfrac{2\pi}{3}\right)\psi^{A_3\dagger}(x)\Big],\\
\psi^{B,\alpha\dagger}(x) &= \frac{1}{\sqrt{3}}\Big[\exp\left(-i\tfrac{2\pi}{3}\right)\psi^{B_1\dagger}(x) + \psi^{B_2\dagger}(x) + \exp\left(i\tfrac{2\pi}{3}\right)\psi^{B_3\dagger}(x)\Big],\\
\psi^{B,\beta\dagger}(x) &= \frac{1}{\sqrt{3}}\Big[\exp\left(i\tfrac{2\pi}{3}\right)\psi^{B_1\dagger}(x) + \psi^{B_2\dagger}(x) + \exp\left(-i\tfrac{2\pi}{3}\right)\psi^{B_3\dagger}(x)\Big].
\end{aligned} \tag{4.23}$$

Since we are solely interested in fermion fields located in the pockets α and β, we do not list the linear combinations of fields corresponding to $\Gamma = (0,0)$.

4.2.3 Transformation behaviour of free fermion fields with a sublattice and a momentum index

Within the scope of the effective theory for free fermions, we simply replace the microscopic operators $c_x^{X_i}$, now defined on the six sublattices and without a spin index, by the Grassmann-valued fields $\psi^{X_i}(x)$. The transformation properties under the different continuous and discrete symmetries of the microscopic operators were already worked out in section 3.2. We now just have to take into account how the additional sublattices X_i map onto each other under the various symmetries. It is then straightforward to determine the transformation properties of the linearly combined operators

$$c_x^{A,f} = \frac{1}{\sqrt{3}}\sum_{n=1}^{3}\exp(-ik^f v_n)c_x^{A_n}, \qquad \text{and} \qquad c_x^{B,f} = \frac{1}{\sqrt{3}}\sum_{n=1}^{3}\exp(-ik^f w_n)c_x^{B_n}, \tag{4.24}$$

where we perform a discrete Fourier transform analogue to Eq. (4.20) with $x = (x_1, x_2)$ now being a discrete lattice point. To evaluate the transformation laws of the fermion fields $\psi^{X,f}(x)$, we now postulate that these fields transform exactly like their microscopic counterparts in Eq. (4.24). With this postulate, we establish a connection between the microscopic and the effective theory. However, it is not possible to connect the microscopic and the effective theory in a mathematically more rigorous sense.

Since we do not yet consider spin, it is not possible to define the generators $\{Q_1, Q_2, Q_3\}$ of $SU(2)_Q$. However, the Hubbard Hamiltonian of Eq. (4.1) with $t' = 0$ is still invariant under the discrete subgroup $\mathbb{Z}(2) \subset SU(2)_Q$, where 2 symbolically indicates the fact that applying $\mathbb{Z}(2)$ twice, we end up with the original object. $\mathbb{Z}(2)$ is the particle-hole symmetry, which interchanges holes and electrons. The microscopic operators transform under $\mathbb{Z}(2)$, with $i \in \{1, 2, 3\}$, as

$$\begin{aligned} {}^{\mathbb{Z}(2)}c_x^{A_i} &= c_x^{A_i\dagger}, \\ {}^{\mathbb{Z}(2)}c_x^{B_i} &= -c_x^{B_i\dagger}. \end{aligned} \tag{4.25}$$

With Eq. (4.25), Eq. (4.24) and the above postulate, we can then derive the transformation behaviour of the fermion fields under $\mathbb{Z}(2)$.

Under the various symmetries the fermionic Grassmann fields $\psi^{X,f}(x)$ finally transform as

$$\begin{aligned} \mathbb{Z}(2): \quad {}^{\mathbb{Z}(2)}\psi^{A,f}(x) &= \psi^{A,f'\dagger}(x), \\ {}^{\mathbb{Z}(2)}\psi^{B,f}(x) &= -\psi^{B,f'\dagger}(x), \\ U(1)_Q: \quad {}^{Q}\psi^{X,f}(x) &= \exp(i\omega)\psi^{X,f}(x), \\ D_i: \quad {}^{D_i}\psi^{X,f}(x) &= \exp(ik^f a_i)\psi^{X,f}(x), \\ O: \quad {}^{O}\psi^{A,\alpha}(x) &= \exp(-i\tfrac{2\pi}{3})\psi^{B,\beta}(Ox), \\ {}^{O}\psi^{A,\beta}(x) &= \exp(i\tfrac{2\pi}{3})\psi^{B,\alpha}(Ox), \\ {}^{O}\psi^{B,\alpha}(x) &= \exp(i\tfrac{2\pi}{3})\psi^{A,\beta}(Ox), \\ {}^{O}\psi^{B,\beta}(x) &= \exp(-i\tfrac{2\pi}{3})\psi^{A,\alpha}(Ox), \\ R: \quad {}^{R}\psi^{X,f}(x) &= \psi^{X,f'}(Rx), \\ T: \quad {}^{T}\psi^{X,f}(x) &= -\psi^{X,f'\dagger}(Tx), \\ {}^{T}\psi^{X,f\dagger}(x) &= \psi^{X,f'}(Tx), \end{aligned} \tag{4.26}$$

with O, R, and T now acting on a space-time point x as

$$\begin{aligned} Ox &= (\tfrac{1}{2}x_1 - \tfrac{\sqrt{3}}{2}x_2, \tfrac{\sqrt{3}}{2}x_1 + \tfrac{1}{2}x_2, t), \\ Rx &= (x_1, -x_2, t), \\ Tx &= (x_1, x_2, -t). \end{aligned} \tag{4.27}$$

Here, f' indicates the other pocket than f. Since the fields are now defined in a space-time continuum, the arguments do not change from x to $x + a_i$ under the shift symmetry D_i. Moreover, applying D_i on a fermion field with a certain "flavour" index f leads to a phase factor indicating the corresponding lattice momentum k^f in the Brillouin zone. The transformation properties of the conjugated fields $\psi^{X,f\dagger}(x)$ can be obtained by applying a †-operation on the transformed fields in Eq. (4.26). However, one should keep in mind that these conjugated counterparts are independent fields. The time-reversal symmetry T is implemented on the fields in the standard way. We now have completed the necessary preparatory work

for the construction of the low-energy effective field theory for free relativistic fermions. We have identified the relevant degrees of freedom describing fermions without spin and we have determined their transformation properties under all symmetries of the underlying Hubbard Hamiltonian of Eq. (4.1) with $t' = 0$.

4.3 Effective field theory for free fermions

A low-energy effective Lagrangian is constructed as a derivative expansion, consisting of all terms, up to a certain order, that are invariant under all symmetries of the underlying microscopic Hamiltonian. We classify the terms in a Lagrangian $\mathcal{L}_{n_\psi}$ according to the number of fermion fields n_ψ and derivatives they include. Because the number of fields and derivatives are unaffected by symmetry transformations, we can investigate each class of terms separately. Since we are interested in the low-energy physics regime of a given system, the effective Lagrangian should contain as few derivatives as possible. We have shown for $t' = 0$ and $\mu = 0$ that massless Dirac fermions have a relativistic dispersion relation, i.e. $E \propto p$, for small energy values. Thus, when acting on a fermion field, a time derivative counts like a spatial derivative. In the leading order effective Lagrangian we therefore allow only one time and one spatial derivative. By considering the $U(1)_Q$ fermion number symmetry, it becomes obvious, that the terms must be combined with the same number of $\psi^{X,f\dagger}(x)$ and $\psi^{X,f}(x)$ fields. Otherwise, after applying a $U(1)_Q$ symmetry transformation, uncompensated phase factors $\exp(\pm i\omega)$ remain. Hence, n_ψ must be always even. Furthermore, terms of the form $\partial_t\psi^{X,f\dagger}(x)\psi^{X,f}(x)$ or $\partial_i\psi^{X,f\dagger}(x)\psi^{X,f}(x)$ can be partially integrated (assuming the fields to be zero at infinity) and are thus, up to an absorbable minus sign, equal to $\psi^{X,f\dagger}(x)\partial_t\psi^{X,f}(x)$ and $\psi^{X,f\dagger}(x)\partial_i\psi^{X,f}(x)$. One therefore has to be careful including only one of these expressions in the Lagrangian. The leading order Lagrangian with two fermion fields and up to one derivative is of order $\mathcal{O}(p)$ and describes the kinetic energy of a free, *massless* fermion

$$\mathcal{L}_2^{free} = \sum_{\substack{f=\alpha,\beta \\ X=A,B}} \Big[\psi^{X,f\dagger}\partial_t\psi^{X,f} + v_F(\sigma_X\psi^{X,f\dagger}\partial_1\psi^{X',f} + i\sigma_f\psi^{X,f\dagger}\partial_2\psi^{X',f})\Big], \tag{4.28}$$

with

$$\sigma_X = \begin{cases} 1 & X = A \\ -1 & X = B \end{cases}, \qquad \text{and} \qquad \sigma_f = \begin{cases} 1 & f = \alpha \\ -1 & f = \beta \end{cases}. \tag{4.29}$$

Here, X' denotes the other sublattice than X and the fermion velocity v_F in the framework of the effective field theory now plays the role of a low-energy constant. The above Lagrangian is valid only in an infinitesimal vicinity of the Dirac points and therefore describes electrons and holes simultaneously. $\mathcal{L}_2^{free}$ demonstrates the strength of the effective field theory approach: Just applying symmetry constraints, one concludes that the Lagrangian in Eq. (4.28) does not contain mass terms. This is in full agreement with the predictions from the exact diagonalisation procedure of the Hubbard model in the weak coupling limit.

At the beginning of section 4.1, we have assumed that weakly coupled fermions are similar to free fermions and thus completely neglected the Coulomb part of the Hubbard Hamiltonian. In real, semi-metallic graphene, however, the fermions are not free but weakly coupled. Thus, besides including spin, the leading order of a realistic description of graphene's low-energy

excitations additionally must contain contact interaction terms consisting of more than two fermion fields, e.g. 4-Fermi terms.

The Dirac Lagrangian in $(2+1)$-dimensions for a free and massless particle with Euclidean metric is given by

$$\mathcal{L}_D = c\bar{\Psi}\gamma_\mu\partial_\mu\Psi, \qquad \text{with} \qquad \bar{\Psi} = \Psi^\dagger\gamma_3, \tag{4.30}$$

and the γ-matrices are represented by

$$\gamma_j = i\sigma_j, \qquad j \in \{1,2,3\}, \tag{4.31}$$

such that

$$\{\gamma_k, \gamma_l\} = -2\delta_{kl}. \tag{4.32}$$

Again, c is considered to be a parameter for the fermion velocity. After some modifications, $\mathcal{L}_2^{free}$ has the same form as $\mathcal{L}_D$ in Eq. (4.30). As a first step, the fermion fields are combined to the spinors

$$\Psi^\alpha(x) = \begin{pmatrix} \psi^{A,\alpha}(x) \\ \psi^{B,\alpha}(x) \end{pmatrix}, \qquad \Psi^\beta(x) = \begin{pmatrix} \psi^{A,\beta}(x) \\ \psi^{B,\beta}(x) \end{pmatrix}. \tag{4.33}$$

Furthermore, we multiply $\mathcal{L}_2^{free}$ and $\mathcal{L}_D$ with $1/v_F$ and $1/c$, respectively. This allows the existence of a unitary transformation for the γ_j such that $\mathcal{L}_2^{free}$ takes the form of $\mathcal{L}_D$ under the condition $c = -v_F$. One should bear in mind, that the fermion velocity depends on the hopping parameter t through $v_F = \frac{3ta}{2}$. Therefore, $c = -v_F$ implies $t \to -t$ in the Hubbard Hamiltonian. This only interchanges particles and holes but does not affect the physics of the model. After these arrangements, the Lagrangian of Eq. (4.30) consists of two identically structured terms which are both indeed equivalent to $\mathcal{L}_D$

$$\mathcal{L}_2^{free} = v_F\left(\bar{\Psi}^\alpha\gamma_\mu\partial_\mu\Psi^\alpha + \bar{\Psi}^\beta\gamma_\mu\partial_\mu\Psi^\beta\right). \tag{4.34}$$

Chapter 5

Low-energy effective field theory for magnons

In this section we investigate the low-energy physics of an undoped quantum antiferromagnet. On the microscopic level such a system is described by the spin $\frac{1}{2}$ Heisenberg Hamiltonian with exchange coupling $J > 0$. We will first argue that quantum antiferromagnets are systems featuring a spontaneous $SU(2)_s \to U(1)_s$ symmetry breakdown, which induces two massless Goldstone bosons - the magnons. Since magnons are the lightest particles in the spectrum, one may describe their low-energy physics by an effective field theory. We therefore present the leading order effective action for the pure magnon sector of an antiferromagnet on the honeycomb lattice. In the framework of QCD this corresponds to χPT, the low-energy effective field theory for pions. Afterwards, as in BχPT, a non-linear realisation of the $SU(2)_s$ spin symmetry is constructed, disguising the global $SU(2)_s$ group to a *local* symmetry in the unbroken subgroup $U(1)_s$. It will later become clear that the procedure of a non-linear realisation is an unavoidable step to couple the magnons to the holes in the final effective theory.

5.1 Spontaneous symmetry breaking and the corresponding effective theory for magnons

Spontaneous symmetry breaking occurs if the Hamiltonian features a continuous global symmetry, which is not shared by the ground state of the system. We have derived the quantum Heisenberg model in Eq. (3.9) by investigating the $U \gg t$ limit of the Hubbard model. The corresponding Hamiltonian exhibits a global $SU(2)_s$ symmetry, which can be proved by evaluating the commutator of $\vec{S} = \frac{1}{2}\sum_x \vec{\sigma}_x$ and $\mathcal{H}$. This leads to

$$[\mathcal{H}, \vec{S}\,] = 0. \tag{5.1}$$

To illustrate the phenomenon of a spontaneous symmetry breakdown, let us naively assume the specific Néel state of Eq. (3.11), with its corresponding direction of $\vec{M}_s$, to be a ground state of the Heisenberg Hamiltonian. The system has spontaneously selected this state from the set of infinitely many ground states all related by an $SU(2)_s$ transformation. This specific Néel state, however, is not $SU(2)_s$ invariant. It only exhibits a $U(1)_s$ symmetry around the accidental direction of $\vec{M}_s$. We therefore conclude that quantum antiferromagnets are

systems in which the global $SU(2)_s$ spin symmetry is spontaneously broken down to $U(1)_s$ by the formation of a staggered magnetisation, i.e. $\langle 0|\vec{M}_s|0\rangle \neq 0$. As already mentioned in section 3.1.1.2, we do not know the analytic ground state of the antiferromagnetic Heisenberg Hamiltonian in Eq. (3.9) and hence the existence of a spontaneously broken symmetry is not evident. Numerical simulations, however, revealed the spontaneous $SU(2)_s \to U(1)_s$ breakdown. Because the Hubbard model leads to the Heisenberg model in the strong coupling limit, and thus features a spontaneous breakdown of a continuous global symmetry, we are allowed to describe the low-energy sector of the Hubbard Hamiltonian by the use of BχPT. On the other hand, the $U(1)_Q$ fermion number symmetry remains unbroken. This is also the case in real materials until the antiferromagnet turns into the superconducting phase.

Goldstone's theorem predicts for every spontaneously broken global and continuous symmetry G a number of particles with zero mass and spin known as Goldstone bosons [54]. Goldstone bosons are described by fields, which are elements of the coset space G/H. The number of Goldstone boson fields is given by the dimension of G/H, which corresponds to the number of generators of G that are not also generators of the unbroken subgroup H. In the case of a spontaneously $G = SU(2)_s \to H = U(1)_s$ symmetry breakdown, the coset space is given by the two-sphere

$$SU(2)_s/U(1)_s \equiv S^2. \tag{5.2}$$

There are

$$\dim(SU(2)_s) - \dim(U(1)_s) = 3 - 1 = 2 \tag{5.3}$$

massless Goldstone bosons known as antiferromagnetic spin waves or magnons described by the unit-vector field

$$\vec{e}(x) = \big(e_1(x), e_2(x), e_3(x)\big) \in S^2, \qquad \vec{e}(x)^2 = 1, \tag{5.4}$$

where $x = (x_1, x_2, t)$ denotes a point in Euclidean space-time. The two magnon degrees of freedom can be interpreted as two linearly independent spin wave fluctuation directions. Since short distances correspond to high momenta, the effective field theory is a theory for a macroscopic length scale and therefore does not account for behaviour at the lattice spacing scale. Hence, the representation of the local $\vec{M}_s$ through $\vec{e}(x)$ within the scope of the field theory only makes sense if $\vec{M}_s$ includes a large region of lattice sites x, e.g. at least 100 sites.

A global $SU(2)_s$ spin rotation is realised on the vector field $\vec{e}(x)$ by an ordinary $\mathcal{R} \in SO(3)_s$ rotation[1]

$$\vec{e}(x)' = \mathcal{R}\vec{e}(x). \tag{5.5}$$

Since we consider spin as an internal quantum number, a global spin rotation does not affect a space-time point x. The staggered magnetisation changes sign under a rotation O of 60 degrees. Since $\vec{e}(x)$ is the field theory representation of $\vec{M}_s$, we therefore have

[1]Note that in general $SO(3) \cong SU(2)/\mathbb{Z}(2)$ with $SU(2)$ being the universal covering group of $SO(3)$. Moreover, there exists a mapping between an element g of $SU(2)$ and a 3×3 matrix $\mathcal{R} \in SO(3)$ given by $\mathcal{R}_{kl} = \frac{1}{2}Tr[g^\dagger \sigma_k g \sigma_l]$ with $k, l \in \{1, 2, 3\}$ and σ_k,σ_l being Pauli matrices.

$$^{O}\vec{e}(x) = -\vec{e}(Ox), \tag{5.6}$$

and thus O as a discrete symmetry is also spontaneously broken. Under shift D_i and reflexion symmetry R, the $\vec{e}(x)$ field transforms as

$$\begin{aligned} ^{D_i}\vec{e}(x) &= \vec{e}(x), \\ ^{R}\vec{e}(x) &= \vec{e}(Rx). \end{aligned} \tag{5.7}$$

A space-time point $x = (x_1, x_2, t)$ transforms under time-reversal T to $Tx = (x_1, x_2, -t)$. On the level of the microscopic theory, T acts as an anti-unitary operator. How T transforms the microscopic fermion operators is investigated in [55]. In the framework of an Euclidean path integral, the staggered magnetisation vector $\vec{e}(x)$ represents the microscopic spin operators $\vec{S}_x$ as a classical field. Since spin obeys the same commutation relations as a classical angular momentum $\vec{L} = \vec{r} \times \vec{p}$, one is led to investigate how time-reversal acts on $\vec{L}$ and then deduce the correct transformation behaviour of $\vec{e}(x)$. Under T the momentum $\vec{p}$ changes sign and therefore $^{T}\vec{L} = -\vec{L}$. As a consequence, the staggered magnetisation behaves under time-reversal as

$$^{T}\vec{e}(x) = -\vec{e}(Tx). \tag{5.8}$$

Note, that also T is a spontaneously broken symmetry. Since the $\vec{e}(x)$ field describes bosons, it stays invariant under the fermion number symmetry $SU(2)_Q$ and its subgroup $U(1)_Q$. This holds for all magnon field representations in this chapter.

According to χPT we can write down an effective Lagrangian $\mathcal{L}_0$ for magnons, containing as few derivatives acting on the $\vec{e}(x)$ fields as possible. At low energy, the antiferromagnetic magnons show a relativistic dispersion relation ($E \propto p$).[2] Therefore, temporal and spatial derivatives are counted on an equal footing in the derivative expansion. Since $\vec{e}(x) \cdot \vec{e}(x) = 1$ and $\vec{e}(x) \cdot \partial_\mu \vec{e}(x) = 0$, the leading order terms of the pure magnon Lagrangian contain either two temporal or two spatial derivatives. Using the above transformation laws of $\vec{e}(x)$, we have constructed the leading order effective Euclidean action in the magnon sector for an antiferromagnet on the honeycomb lattice. It is given by

$$S[\vec{e}] = \int d^2x\, dt\ \mathcal{L}_0 = \int d^2x\, dt\ \frac{\rho_s}{2}\left(\partial_i \vec{e} \cdot \partial_i \vec{e} + \frac{1}{c^2}\partial_t \vec{e} \cdot \partial_t \vec{e}\right), \tag{5.9}$$

where we leave out the space-time argument x for notational simplification. The index $i \in \{1, 2\}$ indicates the two spatial directions. The Euclidean time direction is compactified to a circle S^1 of circumference $\beta = 1/T$. For a square lattice, the leading order effective Euclidean action was first derived in [56, 57] and is completely identical to Eq. (5.9). The above action is fully determined by the two low-energy constants ρ_s, standing for the spin stiffness, and c, denoting the spin wave (magnon) velocity. In fact, these two low-energy constants depend on the properties of a specific material. Moreover, the energy scale, below which the low-energy expansion is valid, is fixed by the spin stiffness. Since ρ_s and c contain information from the high-energy regime of the underlying theory, they can not be determined within the framework of the effective field theory. Rather experiments or numerical

[2] In the low-energy regime, the ferromagnetic magnons are non-relativistic.

simulations are used to fix ρ_s and c. Both low-energy constants are determined with high precision for the square lattice [58], as well as for the honecomb lattice [16] by fitting Monte Carlo data to the predictions of the effective theory.

Lattice	ρ_s	c
Square	$0.1808(4)J$	$1.6585(10)Ja$
Honeycomb	$0.102(2)J$	$1.297(16)Ja$

Table 5.1: Summary of the numerical results for ρ_s and c. J is the exchange coupling constant of the Heisenberg Model and a denotes the lattice spacing.

The reduction of ρ_s and c on the honeycomb lattice, compared to the square lattice, are due to larger spin fluctuations on the honeycomb lattice. This can be explained by the coordination number z, which is smaller for the honeycomb than for the square lattice. The numerical values for ρ_s and c are summarised in Tab. 5.1.

As a short interlude, let us briefly discuss the statement of Mermin, Wagner [59], Hohenberg [60], and Coleman [61] that there can be no spontaneous symmetry breaking for systems in less than three dimensions. Prima facie, this seems to refuse the existence of magnons on a two-space-dimensional lattice. At exactly zero temperature, however, Euclidean time, with an extent inversely proportional to the temperature T, serves as a third dimension. Therefore in fact, we deal with a $(2+1)$-dimensional system, in which spontaneously symmetry breaking is allowed. For $T > 0$, the extent of the time dimension is finite and the magnons pick up a mass, which is exponentially small in the inverse temperature [56]. The effective field theory approach is then still valid as long as the magnons are the lightest particles in the spectrum.

Once doped holes are included, instead of using the vector field $\vec{e}(x)$, it is more convenient to represent the magnon field by a 2×2 matrix defined by

$$P(x) = \frac{1}{2}\big(\mathbb{1} + \vec{e}(x) \cdot \vec{\sigma}\big) = \frac{1}{2}\begin{pmatrix} 1 + e_3(x) & e_1(x) - ie_2(x) \\ e_1(x) + ie_2(x) & 1 - e_3(x) \end{pmatrix}, \tag{5.10}$$

where $P(x) \in \mathbb{C}P(1) \cong S^2$ has the properties

$$P(x)^\dagger = P(x), \qquad \mathrm{Tr}P(x) = 1, \qquad P(x)^2 = P(x), \tag{5.11}$$

and therefore is a Hermitean projection matrix. In terms of $P(x)$ the lowest order action for magnons is formulated as

$$S[P] = \int d^2x\, dt\ \rho_s \mathrm{Tr}\left[\partial_i P \partial_i P + \frac{1}{c^2}\partial_t P \partial_t P\right]. \tag{5.12}$$

In contrast to the vector field $\vec{e}(x)$, a global $SU(2)_s$ spin rotation is realised on a $\mathbb{C}P(1)$ magnon field by a unitary transformation with a 2×2 matrix $g \in SU(2)_s$

$$P(x)' = gP(x)g^\dagger. \tag{5.13}$$

Under an $SU(2)_s$ transformation, $P(x)$ maintains its Hermitean projection properties ${P(x)'}^\dagger = P(x)'$, $\mathrm{Tr}P(x)' = 1$ and ${P(x)'}^2 = P(x)'$. Using the cyclicity of the trace, Eq. (5.12) is obviously invariant under a global $SU(2)_s$ spin rotation.

We have already worked out how the magnon field $\vec{e}(x)$ transforms under the discrete symmetries D_i, O, R, and T. These findings can then be used to determine the transformation behaviour of the $\mathbb{C}P(1)$ magnon representation under these symmetries. A shift D_i leaves the magnon field $P(x)$ invariant, i.e.

$$^{D_i}P(x) = P(x). \tag{5.14}$$

Under a rotation of 60 degrees the staggered magnetisation $\vec{M}_s$ changes sign and therefore

$$^{O}P(x) = \frac{1}{2}\big(\mathbb{1} - \vec{e}(Ox)\cdot\vec{\sigma}\big) = \mathbb{1} - P(Ox). \tag{5.15}$$

To ensure that $P(x) \in \mathbb{C}P(1)$ is a valid representation of $\vec{e}(x)$, $^{O}P(x)$ must be an element of $\mathbb{C}P(1)$ as well. This is obviously the case in an $SU(2)$ model where $\mathrm{Tr}\mathbb{1} = 2$. The transformation property of Eq. (5.15) simplifies under the composed symmetry O'.The magnon field then transforms under the unbroken symmetry O' as

$$^{O'}P(x) = (i\sigma_2)^{O}P(x)(i\sigma_2)^\dagger = P(Ox)^*. \tag{5.16}$$

Since on a square lattice a shift D_i along one lattice axis is a spontaneously broken symmetry, the combined symmetry D_i' is considered. Reflexion symmetry R solely acts on the argument of $P(x)$

$$^{R}P(x) = P(Rx). \tag{5.17}$$

We have already legitimised the transformation behaviour of $e(x)$ under time-reversal T. Except the change of the argument, $\vec{e}(x)$ shows exactly the same behaviour under T as under rotation O. Consequently, under time-reversal T the $\mathbb{C}P(1)$ magnon field representation transforms as

$$^{T}P(x) = \mathbb{1} - P(Tx) = {}^{O}P(O^{-1}Tx). \tag{5.18}$$

Since also T is a spontaneously broken symmetry, we will again encounter a composed transformation, consisting of a regular time-reversal symmetry T and the specific spin rotation $g = i\sigma_2 \in SU(2)_s$. This yields the unbroken, combined symmetry T'. Under T' the magnon field $P(x)$ transforms as

$$^{T'}P(x) = {}^{O'}P(O^{-1}Tx). \tag{5.19}$$

As the construction of an effective action demands, Eq. (5.15) is invariant under all these symmetries.

5.2 Non-linear realisation of $SU(2)_s$

How a general compact, connected, and semi-simple Lie group G is restricted by a non-linear realisation to a continuous subgroup H, is investigated in [8,62]. For the purpose of coupling

magnons to holes, one must construct a non-linear realisation of the spontaneously broken $G = SU(2)_s$ spin symmetry, which then manifests itself as a local symmetry in the unbroken subgroup $H = U(1)_s$. To construct this local $U(1)_s$ transformation, which will finally act on the hole fields, one first defines a local unitary transformation $u(x) \in SU(2)_s$, which diagonalises the $\mathbb{C}P(1)$ magnon field by a unitary transformation

$$u(x)P(x)u(x)^\dagger = \frac{1}{2}(\mathbb{1} + \sigma_3) = \begin{pmatrix} 1 & 0 \\ 0 & 0 \end{pmatrix}, \qquad u_{11}(x) \geq 0. \tag{5.20}$$

Eq. (5.20) demands that the local field $u(x)$ rotates an arbitrary magnon field configuration $P(x)$ into the specific configuration $P = \mathrm{diag}(1, 0)$. Using Eq. (5.10), it becomes clear that $P = \mathrm{diag}(1, 0)$ corresponds to a constant vacuum field configuration $\vec{e}(x) = (0, 0, 1)$. To ensure that $u(x)$ is uniquely defined, we demand

$$u_{11}(x) \geq 0, \qquad u_{11}(x) \in \mathbb{R}. \tag{5.21}$$

Without this restriction, $u(x)$ is only defined up to a $U(1)_s$ phase. Since for every space-time point x, $u(x)$ turns $\vec{e}(x)$ into its vacuum field configuration, $u(x)$ can be considered as a new, unique matrix-valued representation of the magnon vector field $\vec{e}(x)$. A detailed construction of $u(x)$ can be found in [46, 63]. Here we simply state the corresponding result, which makes use of the magnon vector field $\vec{e}(x)$ in spherical coordinates

$$\vec{e}(x) = \big(\sin\theta(x)\cos\varphi(x), \sin\theta(x)\sin\varphi(x), \cos\theta(x)\big). \tag{5.22}$$

The field $u(x)$ then takes the form

$$\begin{aligned} u(x) &= \frac{1}{\sqrt{2(1 + e_3(x))}} \begin{pmatrix} 1 + e_3(x) & e_1(x) - ie_2(x) \\ -e_1(x) - ie_2(x) & 1 + e_3(x) \end{pmatrix} \\ &= \begin{pmatrix} \cos(\frac{\theta(x)}{2}) & \sin(\frac{\theta(x)}{2})\exp(-i\varphi(x)) \\ -\sin(\frac{\theta(x)}{2})\exp(i\varphi(x)) & \cos(\frac{\theta(x)}{2}) \end{pmatrix}. \end{aligned} \tag{5.23}$$

We demand that under $SU(2)_s$ the magnon field $u(x)$ obeys

$$u(x)'P(x)'u(x)'^\dagger = u(x)P(x)u(x)^\dagger = \frac{1}{2}(\mathbb{1} + \sigma_3). \tag{5.24}$$

Although $u(x)$ in the form of Eq. (5.23) is now uniquely defined, it is not yet guaranteed that after a global spin rotation $u(x)'$ is still unique. If one assumes $u(x)' = u(x)g^\dagger$ with $g \in SU(2)_s$ to be the correct transformation, it is then possible that $u_{11}(x)' \notin \mathbb{R}_{\geqslant 0}$ because of picking up a possible $U(1)_s$ phase. To eliminate such a possible phase and therefore to guarantee uniqueness, i.e. Eq. (5.21), we define the non-linear, local transformation $h(x)$, which takes the form

$$h(x) = \exp\big(i\alpha(x)\sigma_3\big) = \begin{pmatrix} \exp(i\alpha(x)) & 0 \\ 0 & \exp(-i\alpha(x)) \end{pmatrix} \in U(1)_s. \tag{5.25}$$

To get the correct $SU(2)_s$ transformation behaviour of the diagonalising field, we now have to multiply the assumed transformation law suitably with $h(x)$ to get

$$u(x)' = h(x)u(x)g^\dagger, \qquad u_{11}(x)' \geq 0, \tag{5.26}$$

where $g \in SU(2)_s$ defines $h(x)$ uniquely. With Eq. (5.26) and the fact that diagonal-matrices commute, Eq. (5.24) is satisfied. Due to a non-linear realisation, the global $SU(2)_s$ symmetry g now appears as a local transformation $h(x) \in U(1)_s$[3] except the following case. If the global spin rotation g itself is an element of the unbroken subgroup $U(1)_s$, that is to say $g = \mathrm{diag}\big(\exp(i\beta), \exp(-i\beta)\big) \in U(1)_s$, the local transformation $h(x)$ reduces to $h(x) = g$ and thus becomes linearly and globally realised. Note that the space-time dependence of $h(x)$ originates from the space-time dependence of the magnon field $P(x)$. This magnon field dependence is the characteristic property of the non-linear realisation.

We will now prove that the group structure of the global symmetry group $SU(2)_s$ is correctly transfered to the unbroken subgroup $U(1)_s$ by the corresponding non-linear realisation. This is the case when a composite transformation $g = g_2 g_1 \in SU(2)_s$ leads to a composite transformation $h(x) = h_2(x)h_1(x) \in U(1)_s$, which then represents the $SU(2)_s$ group structure in a local manner in the unbroken subgroup. Let us first perform the global $SU(2)_s$ transformation g_1, i.e.

$$P(x)' = g_1 P(x) g_1^\dagger, \qquad u(x)' = h_1(x)u(x)g_1^\dagger, \tag{5.27}$$

which defines the non-linear transformation $h_1(x)$. Now we perform the second global transformation g_2, which defines the non-linear transformation $h_2(x)$. That is

$$\begin{aligned} P(x)'' &= g_2 P(x)' g_2^\dagger = g_2 g_1 P(x)(g_2 g_1)^\dagger = g P(x) g^\dagger, \\ u(x)'' &= h_2(x)u(x)' g_2^\dagger = h_2(x)h_1(x)u(x)(g_2 g_1)^\dagger = h(x)u(x)g^\dagger. \end{aligned} \tag{5.28}$$

We identify $h(x) = h_2(x)h_1(x) \in U(1)_s$ and thus conclude that indeed the group structure of $SU(2)_s$ is properly inherited to $U(1)_s$ by the non-linear realisation.

As discussed, the rotation symmetry O changes the sign of the $\vec{e}(x)$ field and is therefore a spontaneously broken discrete symmetry. Under O the diagonalising field $u(x)$ transforms as

$$\begin{aligned} {}^O u(x) &= \frac{1}{\sqrt{2(1-e_3(Ox))}} \begin{pmatrix} 1-e_3(Ox) & -e_1(Ox)+ie_2(Ox) \\ e_1(Ox)+ie_2(Ox) & 1-e_3(Ox) \end{pmatrix} \\ &= \begin{pmatrix} \sin(\frac{\theta(Ox)}{2}) & -\cos(\frac{\theta(Ox)}{2})\exp(-i\varphi(Ox)) \\ \cos(\frac{\theta(Ox)}{2})\exp(i\varphi(Ox)) & \sin(\frac{\theta(Ox)}{2}) \end{pmatrix} \\ &= \tau(Ox)u(Ox), \end{aligned} \tag{5.29}$$

[3]Formally this will become explicit when we consider the explicit transformation behaviour of a hole field under a global spin rotation in section 6.2.

with

$$\tau(x) = \frac{1}{\sqrt{e_1(x)^2 + e_2(x)^2}} \begin{pmatrix} 0 & -e_1(x) + ie_2(x) \\ e_1(x) + ie_2(x) & 0 \end{pmatrix} = \begin{pmatrix} 0 & -\exp(-i\varphi(x)) \\ \exp(i\varphi(x)) & 0 \end{pmatrix}. \tag{5.30}$$

Since the transformation matrix $\tau(x)$ depends on a specific configuration of $u(x)$, which itself depends on $P(x)$ (remember $u(x)$ diagonalises $P(x)$), it becomes clear, that also the rotation symmetry O is realised in a non-linear manner and $\tau(x)$ plays the same role as $h(x)$. Under the combined symmetry O' one finds ${}^{O'}u(x) = h(Ox)\,{}^{O}u(x)g^\dagger$ with $g = i\sigma_2$. The local transformation $h(x)$ then takes the form $h(Ox) = (i\sigma_2)\tau(Ox)^\dagger$ such that

$${}^{O'}u(x) = (i\sigma_2)\tau(Ox)^\dagger\tau(Ox)u(Ox)(i\sigma_2)^\dagger = (i\sigma_2)u(Ox)(i\sigma_2)^\dagger = u(Ox)^*. \tag{5.31}$$

The combined symmetry O' is not spontaneously broken and therefore magnon-field-independent or, equivalently, linearly realised. Comparing Eq. (5.31) with Eq. (5.29) again clarifies why we introduced O': The composed transformation O' is easier to handle than the pure rotation symmetry O.

Since time-reversal T is a spontaneously broken discrete symmetry in an antiferromagnet, independent of any specific lattice structure, $u(x)$ again transforms non-linearly under T. One finds

$${}^{T}u(x) = {}^{O}u(O^{-1}Tx) = \tau(Tx)u(Tx). \tag{5.32}$$

On the other hand, the combined time-reversal T' is unbroken and therefore realised in a linear manner, i.e.

$${}^{T'}u(x) = {}^{O'}u(O^{-1}Tx) = u(Tx)^*. \tag{5.33}$$

It remains to list the transformation behaviour of $u(x)$ under the shift symmetry D_i and the reflexion symmetry R which leads to

$$\begin{aligned} {}^{D_i}u(x) &= u(x), \\ {}^{R}u(x) &= u(Rx). \end{aligned} \tag{5.34}$$

In an antiferromagnet on a square lattice the shift symmetry D_i instead of O is spontaneously broken and hence non-linearly realised.

5.2.1 Composite magnon field $v_\mu(x)$

In this section we introduce a matrix-valued $SU(2)_s$ vector field v_μ, whose components couple the magnon to the hole fields in the low-energy effective field theory. As a composite anti-Hermitean field, v_μ consists of the diagonalising field $u(x)$ and therefore contains the necessary information for a further representation of the magnon field. The vector field v_μ is given by

$$v_\mu(x) = u(x)\partial_\mu u(x)^\dagger, \tag{5.35}$$

and transforms under a global $SU(2)_s$ spin rotation as

$$v_\mu(x)' = h(x)u(x)g^\dagger\partial_\mu[gu(x)^\dagger h(x)^\dagger] = h(x)[v_\mu(x) + \partial_\mu]h(x)^\dagger. \tag{5.36}$$

The transformation properties of all the other symmetries of the Hubbard model can be worked out by making use of the already elaborated transformation behaviour of $u(x)$. One finds

$$\begin{aligned}
D_i: \quad & {}^{D_i}v_\mu(x) = v_\mu(x), \\
O: \quad & {}^{O}v_1(x) = \tau(Ox)\tfrac{1}{2}\big(v_1(Ox) + \partial_1 + \sqrt{3}v_2(Ox) + \sqrt{3}\partial_2\big)\tau(Ox)^\dagger, \\
& {}^{O}v_2(x) = \tau(Ox)\tfrac{1}{2}\big(-\sqrt{3}v_1(Ox) - \sqrt{3}\partial_1 + v_2(Ox) + \partial_2\big)\tau(Ox)^\dagger, \\
& {}^{O}v_t(x) = \tau(Ox)(v_t(Ox) + \partial_t)\tau(Ox)^\dagger, \\
O': \quad & {}^{O'}v_1(x) = \tfrac{1}{2}\big(v_1(Ox)^* + \sqrt{3}v_2(Ox)^*\big), \\
& {}^{O'}v_2(x) = \tfrac{1}{2}\big(-\sqrt{3}v_1(Ox)^* + v_2(Ox)^*\big), \\
& {}^{O'}v_t(x) = v_t(Ox)^*, \\
R: \quad & {}^{R}v_1(x) = v_1(Rx), \\
& {}^{R}v_2(x) = -v_2(Rx), \\
& {}^{R}v_t(x) = v_t(Rx), \\
T: \quad & {}^{T}v_i(x) = \tau(Tx)(v_i(Tx) + \partial_i)\tau(Tx)^\dagger, \\
& {}^{T}v_t(x) = -\tau(Tx)(v_t(Tx) + \partial_t)\tau(Tx)^\dagger, \\
T': \quad & {}^{T'}v_i(x) = v_i(Tx)^*, \\
& {}^{T'}v_t(x) = -v_t(Tx)^*.
\end{aligned} \tag{5.37}$$

The composite magnon field v_μ is a 2×2 traceless and anti-Hermitean matrix and can thus be expressed as a linear combination of Pauli matrices σ_a,

$$v_\mu(x) = iv_\mu^a(x)\sigma_a = i\begin{pmatrix} v_\mu^3(x) & v_\mu^+(x) \\ v_\mu^-(x) & -v_\mu^3(x) \end{pmatrix}, \quad a\in\{1,2,3\}, \quad v_\mu^a(x)\in\mathbb{R}, \tag{5.38}$$

where the factor i makes $v_\mu(x)$ anti-Hermitean.[4] The components $v_\mu^a(x)$ of the above decomposition are given by

$$v_\mu^a(x) = \frac{1}{2i}\mathrm{Tr}\left[v_\mu(x)\sigma_a\right]. \tag{5.39}$$

Note, that the components $v_\mu^a(x)$ are not independent degrees of freedom since they are composed of magnon fields. Additionally, we define the fields

$$v_\mu^\pm(x) = v_\mu^1(x) \mp iv_\mu^2(x). \tag{5.40}$$

Let us now investigate how the third component $v_\mu^3(x)$ and the vector fields $v_\mu^\pm(x)$ transform under a global $SU(2)_s$ spin rotation. By means of Eq. (5.25) and Eq. (5.36) one obtains

[4] The Pauli matrices form a basis in the space of traceless and Hermitean 2×2 matrices.

$$\begin{aligned} v_\mu^3(x)' &= v_\mu^3(x) - \partial_\mu \alpha(x), \\ v_\mu^\pm(x)' &= \exp(\pm 2i\alpha(x)) v_\mu^\pm(x). \end{aligned} \tag{5.41}$$

The above transformation laws reveal the "gauge" character under $U(1)_s$, leading to an Abelian $U(1)_s$ gauge field behaviour of $v_\mu^3(x)$. Due to an appropriate phase, the $v_\mu^\pm(x)$ behave as vector fields charged under $U(1)_s$. However, it should be pointed out, that $SU(2)_s$ is not gauged in the standard way. In fact, the "gauge" field behaviour of $v_\mu^3(x)$ stems from the non-linear realisation of $SU(2)_s$.

The transformation properties of $v_\mu^3(x)$ and $v_\mu^\pm(x)$ under the discrete symmetries of the Hubbard model are worked out with the aid of Eq. (5.37) and Eq. (5.38). We obtain

$$\begin{aligned}
D_i: \quad & {}^{D_i}v_\mu^3(x) = v_\mu^3(x), \\
O: \quad & {}^{O}v_1^3(x) = \tfrac{1}{2}\big(- v_1^3(Ox) + \partial_1\varphi(Ox) - \sqrt{3}v_2^3(Ox) + \sqrt{3}\partial_2\varphi(Ox)\big), \\
& {}^{O}v_2^3(x) = \tfrac{1}{2}\big(\sqrt{3}v_1^3(Ox) - \sqrt{3}\partial_1\varphi(Ox) - v_2^3(Ox) + \partial_2\varphi(Ox)\big), \\
& {}^{O}v_t^3(x) = -v_t^3(Ox) + \partial_t\varphi(Ox), \\
O': \quad & {}^{O'}v_1^3(x) = -\tfrac{1}{2}\big(v_1^3(Ox) + \sqrt{3}v_2^3(Ox)\big), \\
& {}^{O'}v_2^3(x) = \tfrac{1}{2}\big(\sqrt{3}v_1^3(Ox) - v_2^3(Ox)\big), \\
& {}^{O'}v_t^3(x) = -v_t^3(Ox), \\
R: \quad & {}^{R}v_1^3(x) = v_1^3(Rx), \\
& {}^{R}v_2^3(x) = -v_2^3(Rx), \\
& {}^{R}v_t^3(x) = v_t^3(Rx), \\
T: \quad & {}^{T}v_i^3(x) = -v_i^3(Tx) + \partial_i\varphi(Tx), \\
& {}^{T}v_t^3(x) = v_t^3(Tx) - \partial_t\varphi(Tx), \\
T': \quad & {}^{T'}v_i^3(x) = -v_i^3(Tx), \\
& {}^{T'}v_t^3(x) = v_t^3(Tx)
\end{aligned} \tag{5.42}$$

and

$$
\begin{aligned}
D_i: \quad & {}^{D_i}v_\mu^\pm(x) = v_\mu^\pm(x), \\
O: \quad & {}^{O}v_1^\pm(x) = -\exp(\mp 2i\varphi(Ox))\tfrac{1}{2}\big(v_1^\mp(Ox) + \sqrt{3}v_2^\mp(Ox)\big), \\
& {}^{O}v_2^\pm(x) = \exp(\mp 2i\varphi(Ox))\tfrac{1}{2}\big(\sqrt{3}v_1^\mp(Ox) - v_2^\mp(Ox)\big), \\
& {}^{O}v_t^\pm(x) = -\exp(\mp 2i\varphi(Ox))v_t^\mp(x), \\
O': \quad & {}^{O'}v_1^\pm(x) = -\tfrac{1}{2}\big(v_1^\mp(Ox) + \sqrt{3}v_2^\mp(Ox)\big), \\
& {}^{O'}v_2^\pm(x) = \tfrac{1}{2}\big(\sqrt{3}v_1^\mp(Ox) - v_2^\mp(Ox)\big), \\
& {}^{O'}v_t^\pm(x) = -v_t^\mp(Ox), \\
R: \quad & {}^{R}v_1^\pm(x) = v_1^\pm(Rx), \\
& {}^{R}v_2^\pm(x) = -v_2^\pm(Rx), \\
& {}^{R}v_t^\pm(x) = v_t^\pm(Rx), \\
T: \quad & {}^{T}v_i^\pm(x) = -\exp(\mp 2i\varphi(Tx))v_i^\mp(Tx), \\
& {}^{T}v_t^\pm(x) = \exp(\mp 2i\varphi(Tx))v_t^\mp(Tx), \\
T': \quad & {}^{T'}v_i^\pm(x) = -v_i^\mp(Tx), \\
& {}^{T'}v_t^\pm(x) = v_t^\mp(Tx).
\end{aligned}
\tag{5.43}
$$

The lowest order magnon action of Eq. (5.9) can now be reformulated in terms of the composite magnon field $v_\mu(x)$. It is given by

$$
S[v_\mu^\pm] = \int d^2x\, dt\; 2\rho_s \left(v_i^+ v_i^- + \frac{1}{c^2} v_t^+ v_t^- \right). \tag{5.44}
$$

At first sight, $v_\mu^+ v_\mu^-$ looks like a mass term of a charged vector field. In fact, containing derivatives acting on $u(x)$, it is the kinetic term of a massless Goldstone boson. The magnon action in Eq. (5.9) and Eq. (5.44) are equivalent, i.e. $S[\vec{e}] = S[v_\mu]$. Using Eq. (5.39) and Eq. (5.23) one can work out

$$
\begin{aligned}
v_\mu^1(x) &= \frac{1}{2}\Big[\sin(\theta(x))\cos(\varphi(x)) + \partial_\mu\theta(x)\sin(\varphi(x)) \Big], \\
v_\mu^2(x) &= \frac{1}{2}\Big[\sin(\theta(x))\sin(\varphi(x)) - \partial_\mu\theta(x)\cos(\varphi(x)) \Big].
\end{aligned}
\tag{5.45}
$$

Plugging Eq. (5.45) into

$$
v_\mu^+ v_\mu^- = (v_\mu^1)^2 + (v_\mu^2)^2 \tag{5.46}
$$

and use Eq. (5.22) one gets

$$
v_\mu^+ v_\mu^- = \frac{1}{4}(\partial_\mu e_1 \partial_\mu e_1 + \partial_\mu e_2 \partial_\mu e_2 + \partial_\mu e_3 \partial_\mu e_3) = \frac{1}{4}\partial_\mu \vec{e} \cdot \partial_\mu \vec{e} \tag{5.47}
$$

and therefore indeed

$$
S[\vec{e}] = S[v_\mu]. \tag{5.48}
$$

Chapter 6

Identification of effective fields for doped holes

In chapter 5 we have discussed the low-energy physics of a pure, i.e. undoped, quantum antiferromagnet. A pure antiferromagnet corresponds to the vacuum or ground state in the framework of the effective field theory. On the level of the Hubbard model, this charge neutral state is realised through a half-filled system. The half-filled state of the Hubbard model is the microscopic analogue of the Dirac sea in a relativistic quantum field theory. An additional fermion in the state with $\mu = 0$ is then denoted as an electron, while a fermion removed from such a state represents a hole. Finally, we are interested in antiferromagnets with a *small* amount of doped holes or, in correspondence to the above picture, removed electrons. The low-energy effective action under construction, until now, consists of the pure magnon sector and is thus an effective field theory for an undoped antiferromagnet. To include the dynamics of holes and, in particular, their interaction through magnon exchange in the effective description, we now derive the correct degrees of freedom for holes. This procedure parallels the derivation of the fields for free Dirac fermions. Additionally, we now include spin and, as an important intermediate step between microscopic and effective theory, we couple the diagonalising magnon field $u(x)$ to the fermion operator C_x of the Hubbard model. It should be emphasised that the operators and fields introduced in the subsequent sections describe combinations of electrons and holes. Therefore we generically denote these objects by *fermion* operators or fields until we finally extract the effective hole fields by analysing mass terms in section 6.5.

6.1 Momentum space pockets for doped holes

The transformation properties of the fields and therefore the final form of the effective Lagrangian depends on where in momentum space low-energy excitations are located. It is therefore indispensable to know where in the Brillouin zone doped fermions occur. Because we intend to construct an effective theory for holes, we focus on the question at which momenta k in the Brillouin zone a single hole has its energy minima. The dispersion relation $E(k)$ for a single hole was simulated using a loop-cluster algorithm for the t-J model in [16]. Fig. 6.1 reveals that the circular shaped hole pockets are located at $(\pm\frac{2\pi}{3a}, \pm\frac{2\pi}{3\sqrt{3}a})$ and $(0, \pm\frac{4\pi}{3\sqrt{3}a})$ in the first Brillouin zone.

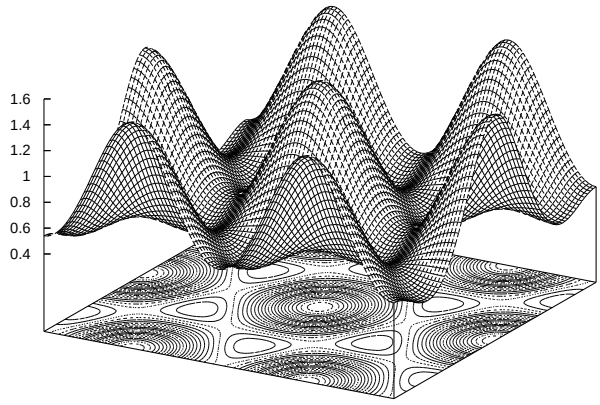

Figure 6.1: *The dispersion relation $E(k)/t$ for a single hole in an antiferromagnet on the honeycomb lattice simulated in the t-J model for $J/t = 2$. [16]*

The position of the hole pockets is thus identical to the position of the Dirac cones in the framework of the effective theory for free fermions discussed in chapter 4. Therefore, doped holes occupy the same pockets α and β as the Dirac fermions do and the corresponding lattice momenta are again given by

$$k^{\alpha} = -k^{\beta} = (0, \frac{4\pi}{3\sqrt{3}a}), \tag{6.1}$$

with their periodic copies in the Brillouin zone. To formally address the final hole fields to k^{α} and k^{β}, we superimpose the same $\{A_1, A_2, A_3\}$ and $\{B_1, B_2, B_3\}$ sublattice structure on the bipartite honeycomb lattice as discussed in section 4.2.1.

6.2 Discrete fermionic lattice operators with sublattice index

To establish an interface between microscopic operators and the final effective fermion fields, we define appropriate fermionic lattice operators by coupling the diagonalising magnon field $u(x)$ of Eq. (5.20) to the 2×2 matrix-valued fermion operator C_x of Eq. ((3.26). Hence, we introduce

$$\Psi_x^X = u(x) C_x, \tag{6.2}$$

with $x \in X$, $X \in \{A_1, A_2, A_3, B_1, B_2, B_3\}$. For fermion operators on even sublattices one then obtains

$$\Psi_x^X = u(x) \begin{pmatrix} c_{x\uparrow} & c_{x\downarrow}^{\dagger} \\ c_{x\downarrow} & -c_{x\uparrow}^{\dagger} \end{pmatrix} = \begin{pmatrix} \psi_{x,+}^X & \psi_{x,-}^{X\dagger} \\ \psi_{x,-}^X & -\psi_{x,+}^{X\dagger} \end{pmatrix}, \quad x \in X, X \in \{A_1, A_2, A_3\}, \tag{6.3}$$

while on odd sublattices Eq. (6.2) is given by

$$\Psi_x^X = u(x) \begin{pmatrix} c_{x\uparrow} & -c_{x\downarrow}^\dagger \\ c_{x\downarrow} & c_{x\uparrow}^\dagger \end{pmatrix} = \begin{pmatrix} \psi_{x,+}^X & -\psi_{x,-}^{X\dagger} \\ \psi_{x,-}^X & \psi_{x,+}^{X\dagger} \end{pmatrix}, \quad x \in X, X \in \{B_1, B_2, B_3\}. \tag{6.4}$$

In the framework of the microscopic theory we have chosen the x_3-axis to be a global spin quantisation axis with $\uparrow$ and $\downarrow$ denoting the corresponding projection of S_x^3. In a system with a spontaneously broken $SU(2)_s$ spin symmetry, however, it is natural to introduce the staggered magnetisation as a new, *local* quantisation axis. The $+(-)$ notation then indicates parallel (anti-parallel) spin alignment with respect to the direction of $\vec{e}(x)$. The operators $\psi_{x,\pm}^X$ still obey canonical anticommutator relations. One should keep in mind, that $u(x)$ in this context is evaluated on discrete lattice sites. The above operators Ψ_x^X not only address the six sublattices in coordinate space but also inherit the transformation properties from the underlying microscopic operators of the Hubbard model. Eq. (6.2) then ensures, that the non-linearly realised $SU(2)_s$ symmetry is implemented on the fermionic lattice operators as a local transformation in the unbroken subgroup $U(1)_s$. This will become clear by means of Eq. (3.29), Eq. (5.26), and Eq. (6.2). We find

$$\Psi_x^{X\prime} = u(x)' C_x' = h(x) u(x) g^\dagger g C_x = h(x) \Psi_x^X, \tag{6.5}$$

with $h(x) \in U(1)_s$. Under $SU(2)_Q$, Eq. (6.2) transforms as

$$\vec{Q} \Psi_x^X = \vec{Q} u(x) \vec{Q} C_x = u(x) C_x \Omega^T = \Psi_x^X \Omega^T. \tag{6.6}$$

Also the discrete symmetries of the Hubbard model are implemented on the above fermionic lattice operators by using the transformation properties of C_x and $u(x)$ derived in section 3.2.6 and 5.2. One finds

$$\begin{aligned} D_i: &\quad {}^{D_i}\Psi_x^X = \Psi_{x+a_i}^{D_i X}, \\ O: &\quad {}^{O}\Psi_x^X = \tau(Ox) \Psi_{Ox}^{OX} \sigma_3, \\ O': &\quad {}^{O'}\Psi_x^X = (i\sigma_2) \Psi_{Ox}^{OX} \sigma_3, \\ R: &\quad {}^{R}\Psi_x^X = \Psi_{Rx}^{RX}. \end{aligned} \tag{6.7}$$

The sublattices $D_i X$, OX, and RX are obtained by shifting, rotating and reflecting sublattice X. Since time-reversal acts as an anti-unitary operator in the microscopic framework, it is not ensured to be correctly inherited by using Eq. (6.2). Thus, we do not yet list T and T'. We will afterwards use well defined time-reversal transformations T and T' on the final effective fermion fields. On the level of the fermionic lattice operators Ψ_x^X, it is not yet necessary to investigate the transformation properties of the components $\psi_{x,\pm}^X$. We will do this in the following chapter, when Ψ_x^X will be treated as a matrix-valued field.

6.3 Fermion fields with a sublattice index

In the final effective theory, doped holes will be described by anticommuting fields, i.e. Grassmann fields, in a Euclidean action. In the context of the effective theory for free fermions, having no $SU(2)_s \to U(1)_s$ symmetry breaking and thus no non-linear realisation, we derived the final fields by replacing the microscopic operators $c_x^{X_i}$ by the continuum Grassmann fields

$\psi^{X_i}(x)$. No interface like Eq. (6.2) was needed. Now, however, we substitute the fermionic lattice operators of Eq. (6.3) and Eq. (6.4) by the matrix-valued continuum fields

$$\begin{aligned}
\Psi^X(x) &= \begin{pmatrix} \psi_+^X(x) & \psi_-^{X\dagger}(x) \\ \psi_-^X(x) & -\psi_+^{X\dagger}(x) \end{pmatrix}, \qquad X \in \{A_1, A_2, A_3\}, \\
\Psi^X(x) &= \begin{pmatrix} \psi_+^X(x) & -\psi_-^{X\dagger}(x) \\ \psi_-^X(x) & \psi_+^{X\dagger}(x) \end{pmatrix}, \qquad X \in \{B_1, B_2, B_3\},
\end{aligned} \tag{6.8}$$

consisting of Grassmann fields $\psi_\pm^X(x)$ instead of lattice operators $\psi_{x,\pm}^X$. Again, the conjugated fields $\psi_\pm^{X\dagger}(x)$ have to be treated as independent of $\psi_\pm^X(x)$. To avoid confusion with relativistic theories, the conjugated fields are not denoted by $\bar{\psi}_\pm^X(x)$. For notational convenience we also introduce

$$\begin{aligned}
\Psi^{X\dagger}(x) &= \begin{pmatrix} \psi_+^{X\dagger}(x) & \psi_-^{X\dagger}(x) \\ \psi_-^X(x) & -\psi_+^X(x) \end{pmatrix}, \qquad X \in \{A_1, A_2, A_3\}, \\
\Psi^{X\dagger}(x) &= \begin{pmatrix} \psi_+^{X\dagger}(x) & \psi_-^{X\dagger}(x) \\ -\psi_-^X(x) & \psi_+^X(x) \end{pmatrix}, \qquad X \in \{B_1, B_2, B_3\},
\end{aligned} \tag{6.9}$$

consisting of the same Grassmann fields as $\Psi^X(x)$. Therefore, $\Psi^{X\dagger}(x)$ depends on $\Psi^X(x)$.

In analogy to section 4.2.3, we postulate, that the matrix-valued fields $\Psi^X(x)$ transform exactly like their operator counterparts Ψ_x^X. This is the most rigorous connection we can establish between the effective and the microscopic theory. This procedure leads to

$$\begin{aligned}
SU(2)_s: \quad & \Psi^X(x)' = h(x)\Psi^X(x), \\
SU(2)_Q: \quad & {}^{\vec{Q}}\Psi^X(x) = \Psi^X(x)\Omega^T, \\
D_i: \quad & {}^{D_i}\Psi^X(x) = \Psi^{D_iX}(x), \\
O: \quad & {}^{O}\Psi^X(x) = \tau(Ox)\Psi^{OX}(Ox)\sigma_3, \\
O': \quad & {}^{O'}\Psi^X(x) = (i\sigma_2)\Psi^{OX}(Ox)\sigma_3, \\
R: \quad & {}^{R}\Psi^X(x) = \Psi^{RX}(Rx), \\
T: \quad & {}^{T}\Psi^X(x) = \tau(Tx)(i\sigma_2)\left[\Psi^{X\dagger}(Tx)^T\right]\sigma_3, \\
& {}^{T}\Psi^{X\dagger}(x) = -\sigma_3\left[\Psi^X(Tx)^T\right](i\sigma_2)^\dagger\tau(Tx)^\dagger, \\
T': \quad & {}^{T'}\Psi^X(x) = -\left[\Psi^{X\dagger}(Tx)^T\right]\sigma_3, \\
& {}^{T'}\Psi^{X\dagger}(x) = \sigma_3\left[\Psi^X(Tx)^T\right].
\end{aligned} \tag{6.10}$$

One recognises the $SU(2)_s \otimes SU(2)_Q$ symmetry behaviour of the matrix-valued fermion fields. Now, the transformation behaviour under time-reversal T and T' are listed. The form of the time-reversal symmetry T for an effective field theory with a non-linearly realised $SU(2)_s$ symmetry can be deduced from the canonical form of time-reversal in the path integral of a non-relativistic theory with a linearly realised spin symmetry. The fermion fields in the two

formulations just differ by a factor $u(x)$. Note, that an upper index T on the left denotes time-reversal, while on the right it denotes transpose. By means of the transformation laws from (6.10) one can now evaluate the transformation properties of the Grassmann-valued components. They transform as

$$\begin{aligned}
SU(2)_s: \quad & \psi_{\pm}^{X}(x)' = \exp(\pm i\alpha(x))\psi_{\pm}^{X}(x), \\
U(1)_Q: \quad & {}^{Q}\psi_{\pm}^{X}(x) = \exp(i\omega)\psi_{\pm}^{X}(x), \\
D_i: \quad & {}^{D_i}\psi_{\pm}^{X}(x) = \psi_{\pm}^{D_i X}(x), \\
O: \quad & {}^{O}\psi_{\pm}^{X}(x) = \mp\exp(\mp i\varphi(Ox))\psi_{\mp}^{OX}(Ox), \\
O': \quad & {}^{O'}\psi_{\pm}^{X}(x) = \pm\psi_{\mp}^{OX}(Ox), \\
R: \quad & {}^{R}\psi_{\pm}^{X}(x) = \psi_{\pm}^{RX}(Rx), \\
T: \quad & {}^{T}\psi_{\pm}^{X}(x) = \exp(\mp i\varphi(Tx))\psi_{\pm}^{X\dagger}(Tx), \\
& {}^{T}\psi_{\pm}^{X\dagger}(x) = -\exp(\pm i\varphi(Tx))\psi_{\pm}^{X}(Tx), \\
T': \quad & {}^{T'}\psi_{\pm}^{X}(x) = -\psi_{\pm}^{X\dagger}(Tx), \\
& {}^{T'}\psi_{\pm}^{X\dagger}(x) = \psi_{\pm}^{X}(Tx).
\end{aligned} \tag{6.11}$$

It should be emphasised, that $SU(2)_Q$ is displayed only on the matrix-valued fermion fields $\Psi^X(x)$. Since the spin as well as the staggered magnetisation gets flipped under time-reversal, the projection of one onto the other remains invariant. It follows that $+$ and $-$ are not interchanged under T and T'.

6.4 Fermion fields with a sublattice and a momentum index

The effective degrees of freedom shall describe fermions located at the α or the β pocket in momentum space. To impose this property on the fermion fields, they need an additional momentum index $f \in \{\alpha, \beta\}$. We achieve this by accomplishing again the discrete Fourier transformation of Eq. (4.20) now with the matrix-valued fields from Eq. (6.8). This leads to the same linear combinations of fields we already derived in the framework of free fermions in section 4.2.2, i.e.

$$\begin{aligned}
\Psi^{A,\alpha}(x) &= \frac{1}{\sqrt{3}}\Big[\exp(i\tfrac{2\pi}{3})\Psi^{A_1}(x) + \Psi^{A_2}(x) + \exp(-i\tfrac{2\pi}{3})\Psi^{A_3}(x)\Big], \\
\Psi^{A,\beta}(x) &= \frac{1}{\sqrt{3}}\Big[\exp(-i\tfrac{2\pi}{3})\Psi^{A_1}(x) + \Psi^{A_2}(x) + \exp(i\tfrac{2\pi}{3})\Psi^{A_3}(x)\Big], \\
\Psi^{B,\alpha}(x) &= \frac{1}{\sqrt{3}}\Big[\exp(i\tfrac{2\pi}{3})\Psi^{B_1}(x) + \Psi^{B_2}(x) + \exp(-i\tfrac{2\pi}{3})\Psi^{B_3}(x)\Big], \\
\Psi^{B,\beta}(x) &= \frac{1}{\sqrt{3}}\Big[\exp(-i\tfrac{2\pi}{3})\Psi^{B_1}(x) + \Psi^{B_2}(x) + \exp(i\tfrac{2\pi}{3})\Psi^{B_3}(x)\Big].
\end{aligned} \tag{6.12}$$

The conjugated matrix-valued field combinations can be deduced by applying a †-operation on Eq. (6.12). However, as already argued, these fields do not represent independent degrees of freedom. Therefore, we do not list them explicitly. Formally, the Fourier transformed matrix-valued fields of Eq. (6.12) can be written as

$$\Psi^{A,f}(x) = \frac{1}{\sqrt{3}} \sum_{n=1}^{3} \exp(-ik^f v_n) \Psi^{A_n}(x) = \begin{pmatrix} \psi_+^{A,f}(x) & \psi_-^{A,f'\dagger}(x) \\ \psi_-^{A,f}(x) & -\psi_+^{A,f'\dagger}(x) \end{pmatrix},$$
$$\Psi^{B,f}(x) = \frac{1}{\sqrt{3}} \sum_{n=1}^{3} \exp(-ik^f w_n) \Psi^{B_n}(x) = \begin{pmatrix} \psi_+^{B,f}(x) & -\psi_-^{B,f'\dagger}(x) \\ \psi_-^{B,f}(x) & \psi_+^{B,f'\dagger}(x) \end{pmatrix}, \tag{6.13}$$

with their conjugated counterparts

$$\Psi^{A,f\dagger}(x) = \begin{pmatrix} \psi_+^{A,f\dagger}(x) & \psi_-^{A,f\dagger}(x) \\ \psi_-^{A,f'}(x) & -\psi_+^{A,f'}(x) \end{pmatrix}, \qquad \Psi^{B,f\dagger}(x) = \begin{pmatrix} \psi_+^{B,f\dagger}(x) & \psi_-^{B,f\dagger}(x) \\ -\psi_-^{B,f'}(x) & \psi_+^{B,f'}(x) \end{pmatrix}. \tag{6.14}$$

The transformation properties of Eq. (6.12) are

$$\begin{aligned}
SU(2)_s: \quad & \Psi^{X,f}(x)' = h(x)\Psi^{X,f}(x), \\
SU(2)_Q: \quad & \vec{Q}\Psi^{X,f}(x) = \Psi^{X,f}(x)\Omega^T, \\
D_i: \quad & {}^{D_i}\Psi^{X,f}(x) = \exp(ik^f a_i)\Psi^{X,f}(x), \\
O: \quad & {}^{O}\Psi^{A,\alpha}(x) = \exp(-i\tfrac{2\pi}{3})\tau(Ox)\Psi^{B,\beta}(Ox)\sigma_3, \\
& {}^{O}\Psi^{A,\beta}(x) = \exp(i\tfrac{2\pi}{3})\tau(Ox)\Psi^{B,\alpha}(Ox)\sigma_3, \\
& {}^{O}\Psi^{B,\alpha}(x) = \exp(i\tfrac{2\pi}{3})\tau(Ox)\Psi^{A,\beta}(Ox)\sigma_3, \\
& {}^{O}\Psi^{B,\beta}(x) = \exp(-i\tfrac{2\pi}{3})\tau(Ox)\Psi^{A,\alpha}(Ox)\sigma_3, \\
O': \quad & {}^{O'}\Psi^{A,\alpha}(x) = \exp(-i\tfrac{2\pi}{3})(i\sigma_2)\Psi^{B,\beta}(Ox)\sigma_3, \\
& {}^{O'}\Psi^{A,\beta}(x) = \exp(i\tfrac{2\pi}{3})(i\sigma_2)\Psi^{B,\alpha}(Ox)\sigma_3, \\
& {}^{O'}\Psi^{B,\alpha}(x) = \exp(i\tfrac{2\pi}{3})(i\sigma_2)\Psi^{A,\beta}(Ox)\sigma_3, \\
& {}^{O'}\Psi^{B,\beta}(x) = \exp(-i\tfrac{2\pi}{3})(i\sigma_2)\Psi^{A,\alpha}(Ox)\sigma_3, \\
R: \quad & {}^{R}\Psi^{X,f}(x) = \Psi^{X,f'}(Rx), \\
T: \quad & {}^{T}\Psi^{X,f}(x) = \tau(Tx)(i\sigma_2)\left[\Psi^{X,f'\dagger}(Tx)^T\right]\sigma_3, \\
& {}^{T}\Psi^{X,f\dagger}(x) = -\sigma_3\left[\Psi^{X,f'}(Tx)^T\right](i\sigma_2)^\dagger\tau(Tx)^\dagger, \\
T': \quad & {}^{T'}\Psi^{X,f}(x) = -\left[\Psi^{X,f'\dagger}(Tx)^T\right]\sigma_3, \\
& {}^{T'}\Psi^{X,f\dagger}(x) = \sigma_3\left[\Psi^{X,f'}(Tx)^T\right].
\end{aligned} \tag{6.15}$$

For the Grassmann-valued components we read off

$$
\begin{aligned}
SU(2)_s: \quad & \psi_{\pm}^{X,f}(x)' = \exp(\pm i\alpha(x))\psi_{\pm}^{X,f}(x), \\
U(1)_Q: \quad & {}^{Q}\psi_{\pm}^{X,f}(x) = \exp(i\omega)\psi_{\pm}^{X,f}(x), \\
D_i: \quad & {}^{D_i}\psi_{\pm}^{X,f}(x) = \exp(ik^f a_i)\psi_{\pm}^{X,f}(x), \\
O: \quad & {}^{O}\psi_{\pm}^{A,\alpha}(x) = \mp\exp(-i\tfrac{2\pi}{3})\exp(\mp i\varphi(Ox))\psi_{\mp}^{B,\beta}(Ox), \\
& {}^{O}\psi_{\pm}^{A,\beta}(x) = \mp\exp(i\tfrac{2\pi}{3})\exp(\mp i\varphi(Ox))\psi_{\mp}^{B,\alpha}(Ox), \\
& {}^{O}\psi_{\pm}^{B,\alpha}(x) = \mp\exp(i\tfrac{2\pi}{3})\exp(\mp i\varphi(Ox))\psi_{\mp}^{A,\beta}(Ox), \\
& {}^{O}\psi_{\pm}^{B,\beta}(x) = \mp\exp(-i\tfrac{2\pi}{3})\exp(\mp i\varphi(Ox))\psi_{\mp}^{A,\alpha}(Ox), \\
O': \quad & {}^{O'}\psi_{\pm}^{A,\alpha}(x) = \pm\exp(-i\tfrac{2\pi}{3})\psi_{\mp}^{B,\beta}(Ox), \\
& {}^{O'}\psi_{\pm}^{A,\beta}(x) = \pm\exp(i\tfrac{2\pi}{3})\psi_{\mp}^{B,\alpha}(Ox), \\
& {}^{O'}\psi_{\pm}^{B,\alpha}(x) = \pm\exp(i\tfrac{2\pi}{3})\psi_{\mp}^{A,\beta}(Ox), \\
& {}^{O'}\psi_{\pm}^{B,\beta}(x) = \pm\exp(-i\tfrac{2\pi}{3})\psi_{\mp}^{A,\alpha}(Ox), \\
R: \quad & {}^{R}\psi_{\pm}^{X,f}(x) = \psi_{\pm}^{X,f'}(Rx), \\
T: \quad & {}^{T}\psi_{\pm}^{X,f}(x) = \exp(\mp i\varphi(Tx))\psi_{\pm}^{X,f'\dagger}(Tx), \\
& {}^{T}\psi_{\pm}^{X,f\dagger}(x) = -\exp(\pm i\varphi(Tx))\psi_{\pm}^{X,f'}(Tx), \\
T': \quad & {}^{T'}\psi_{\pm}^{X,f}(x) = -\psi_{\pm}^{X,f'\dagger}(Tx), \\
& {}^{T'}\psi_{\pm}^{X,f\dagger}(x) = \psi_{\pm}^{X,f'}(Tx).
\end{aligned}
\tag{6.16}
$$

6.5 Identifying the final fields for holes

In this section, we construct the final effective fields, which describe a doped hole in an antiferromagnet. So far, the matrix-valued fermion fields have a well defined transformation property under $SU(2)_Q$. Therefore, up to now, these fields may represent a combination of electrons and holes. To impose this symmetry on the effective Lagrangian would result in a theory containing electrons and holes at the same time. However, such an effective theory is only valid for the Hubbard model at half-filling, where holes and electrons are present simultaneously.[1] On the other hand, in real materials, as well as in the t-J model, either holes or electrons do exist. From this it follows, that also our effective Lagrangian must describe either doped holes or doped electrons. Such a Lagrangian, however, cannot maintain the particle-hole symmetry of $SU(2)_Q$. Only the $U(1)_Q$ fermion number symmetry remains. We decided to construct a low-energy effective field theory for a hole doped antiferromagnet.

To determine the correct low-energy effective degrees of freedom for holes, we first have to construct all possible mass terms invariant under the given symmetries. This procedure can be performed in two different notations: The trace notation, using the matrix-valued fields $\Psi^{X,f}(x)$, or the component notation, using the Grassmann-valued fields $\psi_{\pm}^{X,f}(x)$. Let us briefly discuss the assets and drawbacks of these two methods.[2] The trace notation allows

[1] Remember: For $\mu \neq 0$ the Hubbard Hamiltonian is $SU(2)_Q$ variant.

[2] The pros and cons of the trace- and the component notation are detailed discussed in [64].

us to easily find expressions invariant under $SU(2)_Q$, since this symmetry is only defined on the matrix-valued fermion fields. The main difficulty of the trace notation is, however, to eliminate all linear dependencies in a given class of terms, e.g. mass terms, arising from the fact, that these notation is not unique. The main advantage of the component notation, though, is its uniqueness. After the construction of all invariant expressions in a certain class of terms, no linear dependencies remain. Thus, we first construct all mass terms in component notation to evaluate how many independent expressions must remain using afterwards the trace notation. We found that the class of mass terms consists of two linear independent terms in which the fields are diagonal in all indices. With this knowledge, we then switched to the trace notation, allowing us to implement the $SU(2)_Q$ symmetry. Of course, one still has to ensure that all the found trace terms are linearly independent. The most general mass terms then read

$$\begin{aligned}
&\sum_{f=\alpha,\beta} \frac{1}{2}\,\mathrm{Tr}\big[\mathcal{M}(\Psi^{A,f\dagger}\sigma_3\Psi^{A,f} - \Psi^{B,f\dagger}\sigma_3\Psi^{B,f}) + m(\Psi^{A,f\dagger}\Psi^{A,f}\sigma_3 + \Psi^{B,f\dagger}\Psi^{B,f}\sigma_3)\big] \\
&\quad= \sum_{f=\alpha,\beta} \big[\mathcal{M}\big(\psi_+^{A,f\dagger}\psi_+^{A,f} - \psi_-^{A,f\dagger}\psi_-^{A,f} + \psi_-^{B,f\dagger}\psi_-^{B,f} - \psi_+^{B,f\dagger}\psi_+^{B,f}\big) \\
&\qquad\quad + m\big(\psi_+^{A,f\dagger}\psi_+^{A,f} + \psi_-^{A,f\dagger}\psi_-^{A,f} + \psi_+^{B,f\dagger}\psi_+^{B,f} + \psi_-^{B,f\dagger}\psi_-^{B,f}\big)\big] \\
&\quad= \sum_{f=\alpha,\beta} \Bigg[\big(\psi_+^{A,f\dagger},\, \psi_+^{B,f\dagger}\big)\begin{pmatrix} \mathcal{M}+m & 0 \\ 0 & -\mathcal{M}+m \end{pmatrix}\begin{pmatrix} \psi_+^{A,f} \\ \psi_+^{B,f} \end{pmatrix} \\
&\qquad\quad + \big(\psi_-^{A,f\dagger},\, \psi_-^{B,f\dagger}\big)\begin{pmatrix} -\mathcal{M}+m & 0 \\ 0 & \mathcal{M}+m \end{pmatrix}\begin{pmatrix} \psi_-^{A,f} \\ \psi_-^{B,f} \end{pmatrix}\Bigg].
\end{aligned} \tag{6.17}$$

The term proportional to $\mathcal{M}$ is invariant under $SU(2)_Q$. The expression proportional to m, however, is only invariant under the $U(1)_Q$ fermion number symmetry and therefore breaks $SU(2)_Q$. To identify the correct fields for holes, we have to diagonalise the mass matrices. However, since these matrices are already diagonal, we can directly read off the eigenvalues $\pm\mathcal{M} + m$. For $m = 0$ we have a particle-hole symmetric situation. The eigenvalue $\mathcal{M}$ corresponds to the rest mass of the particles, while the rest mass of the holes corresponds to the eigenvalue $-\mathcal{M}$. The masses are shifted to $\pm\mathcal{M} + m$ when we allow the $SU(2)_Q$ breaking term ($m \neq 0$) and the particle-hole symmetry is currently destroyed. Hole fields now correspond to the lower eigenvalue $-\mathcal{M} + m$ and are identified by the corresponding eigenvectors

$$\psi_+^{B,\alpha}(x), \qquad \psi_+^{B,\beta}(x), \qquad \psi_-^{A,\alpha}(x), \qquad \psi_-^{A,\beta}(x).$$

One can show that indeed the hole fields of Eq. (6.18) and their conjugated counterparts do form a closed set under the various symmetry transformations. We thus simplify the notation since a hole with spin + (−) is always located on sublattice B (A). To avoid redundancy, we therefore drop the sublattice index. The full set of independent low-energy degrees of freedom describing a doped hole in an antiferromagnet on the honeycomb lattice then reads

$$\begin{aligned}
&\psi_+^{\alpha}(x) = \psi_+^{B,\alpha}(x), \quad \psi_+^{\beta}(x) = \psi_+^{B,\beta}(x), \quad \psi_-^{\alpha}(x) = \psi_-^{A,\alpha}(x), \quad \psi_-^{\beta}(x) = \psi_-^{A,\beta}(x), \\
&\psi_+^{\alpha\dagger}(x) = \psi_+^{B,\alpha\dagger}(x), \quad \psi_+^{\beta\dagger}(x) = \psi_+^{B,\beta\dagger}(x), \quad \psi_-^{\alpha\dagger}(x) = \psi_-^{A,\alpha\dagger}(x), \quad \psi_-^{\beta\dagger}(x) = \psi_-^{A,\beta\dagger}(x).
\end{aligned} \tag{6.18}$$

Under the symmetries of the Hubbard model these fields transform as

$$
\begin{aligned}
SU(2)_s: \quad & \psi_\pm^f(x)' = \exp(\pm i\alpha(x))\psi_\pm^f(x), \\
U(1)_Q: \quad & {}^Q\psi_\pm^f(x) = \exp(i\omega)\psi_\pm^f(x), \\
D_i: \quad & {}^{D_i}\psi_\pm^f(x) = \exp(ik^f a_i)\psi_\pm^f(x), \\
O: \quad & {}^O\psi_\pm^\alpha(x) = \mp\exp(\pm i\tfrac{2\pi}{3} \mp i\varphi(Ox))\psi_\mp^\beta(Ox), \\
& {}^O\psi_\pm^\beta(x) = \mp\exp(\mp i\tfrac{2\pi}{3} \mp i\varphi(Ox))\psi_\mp^\alpha(Ox), \\
O': \quad & {}^{O'}\psi_\pm^\alpha(x) = \pm\exp(\pm i\tfrac{2\pi}{3})\psi_\mp^\beta(Ox), \\
& {}^{O'}\psi_\pm^\beta(x) = \pm\exp(\mp i\tfrac{2\pi}{3})\psi_\mp^\alpha(Ox), \\
R: \quad & {}^R\psi_\pm^f(x) = \psi_\pm^{f'}(Rx), \\
T: \quad & {}^T\psi_\pm^f(x) = \exp(\mp i\varphi(Tx))\psi_\pm^{f'\dagger}(Tx), \\
& {}^T\psi_\pm^{f\dagger}(x) = -\exp(\pm i\varphi(Tx))\psi_\pm^{f'}(Tx), \\
T': \quad & {}^{T'}\psi_\pm^f(x) = -\psi_\pm^{f'\dagger}(Tx), \\
& {}^{T'}\psi_\pm^{f\dagger}(x) = \psi_\pm^{f'}(Tx).
\end{aligned}
\tag{6.19}
$$

In analogy to BχPT, the $SU(2)_s$ symmetry is realised as a local transformation in the subgroup $U(1)_s$.

In order to extract the final hole fields, we have eliminated the electrons from the theory and at the same time broken the particle-hole symmetry of $SU(2)_Q$. Thus, the effective Lagrangian will solely be invariant under the $U(1)_Q$ fermion number symmetry. Since $SU(2)_Q$ is then no longer a symmetry of our Lagrangian, we need not search for terms in trace notation. To extract low energy degrees of freedom describing doped electrons demands the same procedure as we now applied for the holes. One first has to determine where in the Brillouin zone doped electrons occur. Afterwards, one performs the appropriate discrete Fourier transformation to end up with matrix-valued fermion fields with sublattice and momentum indices now addressing the electron pockets. The final electron fields are then identified by the eigenvectors corresponding to the upper eigenvalue $+\mathcal{M} + m$.

Even though $SU(2)_Q$ is now no longer a symmetry of the effective theory to be constructed, the current chapter has shown that this symmetry is of central importance to identify the correct fields for doped holes.

Chapter 7

Low-energy effective field theory for magnons and holes

In analogy to χPT, we have constructed the leading order effective action for magnons in section 5.1. After constructing the relevant degrees of freedom and their transformation laws under the various symmetries of the microscopic models, we now additionally present the leading order terms of a systematic low-energy effective field theory for doped holes. Including holes in our effective description now corresponds to BχPT in QCD. The effective Euclidean action in Eq. (5.9) is then extended to

$$S\left[\psi_{\pm}^{f\dagger}, \psi_{\pm}^{f}, \vec{e}\right] = \int d^2x \; dt \; \sum_{n_\psi} \mathcal{L}_{n_\psi}. \tag{7.1}$$

The theory is now completely well-defined by the partition function

$$\mathcal{Z} = \int \mathcal{D}\psi_{\pm}^{f\dagger} \mathcal{D}\psi_{\pm}^{f} \mathcal{D}\vec{e} \; \exp\left(-S\left[\psi_{\pm}^{f\dagger}, \psi_{\pm}^{f}, \vec{e}\right]\right). \tag{7.2}$$

Remember, that n_ψ denotes the number of hole fields a given term in the Lagrangian $\mathcal{L}_{n_\psi}$ contains. In section 5.1, we have already argued that in an antiferromagnet at low energy $E \propto p$ for magnons. It follows from the t-J model simulation in [16] that holes have a non-relativistic dispersion relation, i.e. $E \propto p^2$, close to the energy minimum. Therefore one temporal derivative counts as two spatial derivatives. Up to $\mathcal{O}(p^2)$ in the derivative expansion, we thus only allow terms including at most one temporal or two spatial derivatives. Due to the non-linear realisation of the $SU(2)_s$ spin symmetry, the magnon fields are coupled to the hole fields through $v_\mu^3(x)$ and $v_\mu^\pm(x)$. Since $v_\mu(x) = u(x)\partial_\mu u(x)^\dagger$, both components $v_\mu^3(x)$ and $v_\mu^\pm(x)$ contain a ∂_μ derivative which must be counted too.

If one intends to do loop-calculations within the effective Lagrangian framework, a reliable power counting scheme is needed. This would guarantee a finite number of terms contributing to each order in perturbation theory. A power counting scheme becomes essential as soon as the magnon and the hole sector are mixed, i.e. hole fields are coupled to magnon fields. Due to the different dispersion relations of magnons and holes, it is then not a priori determined to which order in the derivative expansion a mixed term with $v_t^\pm$ or v_t^3 belongs to. Consider e.g. the expression $\partial_t \psi_{\pm}^{f\dagger} v_t^3 \psi_{\pm}^{f}$. At first sight, this term is of $\mathcal{O}(p^3)$ in the derivative expansion. The time derivative acting on the hole field is of $\mathcal{O}(p^2)$ and the time derivative acting on the

magnon field in v_t^3 is of $\mathcal{O}(p)$. However, we are free to let the time derivative from v_t^3 act on $\psi_\pm^f$ by partial integration. In this case, $\partial_t \psi_\pm^{f\dagger} v_t^3 \psi_\pm^f$ suddenly is of $\mathcal{O}(p^4)$. To determine the order of a certain term, we conventionally act with *all* derivatives on the hole fields. The power counting scheme in BχPT for $B = 1$, the analogue of doping one hole into the antiferromagnet, has been developed in [65]. In the pure magnon (pion) sector ($B = 0$) a reliable power counting was developed by J. Gasser and H. Leutwyler in [66]. For $B \geq 2$ a general power counting scheme is still missing. Recent developments can be found in [67]. The absence of a correct power counting method in the effective field theory for magnons and holes, however, does not affect the calculations for the spiral phases.

7.1 Effective action for magnons and holes

In Eq. (5.9) we established the leading order effective Lagrangian in the pure magnon sector

$$\mathcal{L}_0 = \frac{\rho_s}{2}\left(\partial_i \vec{e}\cdot\partial_i \vec{e} + \frac{1}{c^2}\partial_t \vec{e}\cdot\partial_t \vec{e}\right). \tag{7.3}$$

We are now using the final hole fields and their conjugated counterparts of Eq. (6.18) to construct the hole sector ($n_\psi \geqslant 2$) of the above effective action. As discussed in section 4.3, each terms consists of as many $\psi_\pm^{X,f\dagger}(x)$ as $\psi_\pm^{X,f}(x)$ fields. Otherwise, uncompensated phase factors would remain after applying a $U(1)_Q$ transformation. The Lagrangian with two hole fields up to $\mathcal{O}(p^2)$ in the derivative expansion takes the form

$$\begin{aligned}\mathcal{L}_2 = \sum_{\substack{f=\alpha,\beta\\ s=+,-}} \Big[& M\psi_s^{f\dagger}\psi_s^f + \psi_s^{f\dagger} D_t \psi_s^f + \frac{1}{2M'} D_i\,\psi_s^{f\dagger} D_i \psi_s^f \\ & + \Lambda \psi_s^{f\dagger}(is v_1^s + \sigma_f v_2^s)\psi_{-s}^f + iK\big[(D_1 + is\sigma_f D_2)\psi_s^{f\dagger}(v_1^s + is\sigma_f v_2^s)\psi_{-s}^f \\ & \quad - (v_1^s + is\sigma_f v_2^s)\psi_s^{f\dagger}(D_1 + is\sigma_f D_2)\psi_{-s}^f\big] \\ & + \sigma_f L \psi_s^{f\dagger}\epsilon_{ij} f_{ij}^3 \psi_s^f + N_1 \psi_s^{f\dagger} v_i^s v_i^{-s}\psi_s^f \\ & + is\sigma_f N_2\big(\psi_s^{f\dagger} v_1^s v_2^{-s}\psi_s^f - \psi_s^{f\dagger} v_2^s v_1^{-s}\psi_s^f\big)\Big]. \end{aligned} \tag{7.4}$$

We have introduced the field strength tensor of the composite Abelian "gauge" field which is defined by

$$f_{ij}^3(x) = \partial_i v_j^3(x) - \partial_j v_i^3(x). \tag{7.5}$$

Again

$$\sigma_f = \begin{cases} 1 & f = \alpha \\ -1 & f = \beta \end{cases}, \tag{7.6}$$

and the covariant derivatives in Eq. (7.4) are given by

$$
\begin{aligned}
D_t\psi^f_\pm(x) &= \left[\partial_t \pm iv^3_t(x) - \mu\right]\psi^f_\pm(x),\\
D_i\psi^f_\pm(x) &= \left[\partial_i \pm iv^3_i(x)\right]\psi^f_\pm(x)\\
D_t\psi^{f\dagger}_\pm(x) &= \left[\partial_t \mp iv^3_t(x) - \mu\right]\psi^{f\dagger}_\pm(x),\\
D_i\psi^{f\dagger}_\pm(x) &= \left[\partial_i \mp iv^3_i(x)\right]\psi^{f\dagger}_\pm(x).
\end{aligned}
\tag{7.7}
$$

The chemical potential μ enters the covariant time-derivative like an imaginary constant vector potential for the fermion number symmetry $U(1)_Q$. It should be pointed out, that these covariant derivatives are introduced due to the non-linear realisation of the $SU(2)_s$ spin symmetry. They are not there as a result of a canonical $SU(2)$ gauge procedure. Being low-energy constants, M and M' denote the rest and the kinetic mass of a hole. Since our effective theory is a non-relativistic theory, in general, M and M' are not equal. In [16], a simulation on the honeycomb lattice with 3456 spins and $J/t = 2.0$ results in $M' = 4.1(1)/ta^2$ for the kinetic mass. The term proportional to $1/2M'$ describes the propagation of a free hole with lattice momenta in the α or β pocket as well as magnon exchange processes between two holes. In section 6.1 of [55] it is shown that $v^\pm_\mu$ contributes to a single magnon exchange between two holes while v^3_μ contributes to a two-magnon exchange. The expressions proportional to the low-energy coupling constants Λ and K both describe magnon exchange interactions but are not of the same order in the derivative expansion. Since $v^\pm_i$ contributes only one spatial derivative, the Λ-term is the leading hole-one-magnon exchange contribution to $\mathcal{L}_2$. The K-term contains two spatial derivatives and is therefore of $\mathcal{O}(p^2)$. The parameters L, N_1 and N_2 are low-energy couplings for hole-two-magnon exchanges. The appropriate terms are of $\mathcal{O}(p^2)$. All low-energy constants in Eq. (7.4) are real-valued and, due to the factor i in front of K and N_2, $\mathcal{L}_2$ leads to a Hermitean Hamiltonian. It is straightforward to show that terms of the form $\psi^{f\dagger}_\pm D_i\psi^f_\pm$ add up to zero under O'. Also the effective Lagrangian containing magnons *and* holes is only valid for energy values small compared to ρ_s.

There exists no L-term in the effective $\mathcal{L}_2$ for holes on the square lattice. Using the symmetry transformations of the hole fields on the square lattice, we have proved that such a term is forbidden by D'_i, R, and T'.

The dispersion relation for a single free hole up to $\mathcal{O}(p^2)$ can be derived from $\mathcal{L}_2$ and is given by

$$
E^f(p) = M + \frac{p_i^2}{2M'} + \mathcal{O}(p^4), \tag{7.8}
$$

which is the canonical dispersion relation for a free, non-relativistic particle.[1] Note that $p = (p_1, p_2)$ is defined relative to the center of the hole pockets. Eq. (7.8) confirms that the two pockets α and β indeed show up circular shape which is in agreement with the simulation of the t-J model discussed in section 6.1.

Furthermore, we constructed the leading order of $\mathcal{L}_4$. This contribution to the Lagrangian consists of terms describing short-ranged contact interactions between holes. Since we are

[1] A derivation of the dispersion relation in the framework of the spiral phases can be found in appendix A.

more interested in the long-range interaction physics, we restrict ourselves to terms with four hole fields and no derivatives. The leading order of $\mathcal{L}_4$ is then given by

$$\mathcal{L}_4 = \sum_{s=+,-} \Big\{ \frac{G_1}{2} (\psi_s^{\alpha\dagger}\psi_s^{\alpha}\psi_{-s}^{\alpha\dagger}\psi_{-s}^{\alpha} + \psi_s^{\beta\dagger}\psi_s^{\beta}\psi_{-s}^{\beta\dagger}\psi_{-s}^{\beta}) + G_2 \psi_s^{\alpha\dagger}\psi_s^{\alpha}\psi_s^{\beta\dagger}\psi_s^{\beta} + G_3 \psi_s^{\alpha\dagger}\psi_s^{\alpha}\psi_{-s}^{\beta\dagger}\psi_{-s}^{\beta} \Big\}. \tag{7.9}$$

The low-energy fermion coupling constants G_1, G_2, and G_3 again are real-valued. As a consequence of the Pauli principle, all terms with two identical hole fields vanish. Therefore an expression like $\propto \sum_{s=+,-} \left(\psi_s^{\alpha\dagger}\psi_s^{\alpha}\psi_s^{\alpha\dagger}\psi_s^{\alpha} + \psi_s^{\beta\dagger}\psi_s^{\beta}\psi_s^{\beta\dagger}\psi_s^{\beta}\right)$, although invariant under all symmetries, does not enter the Lagrangian. Furthermore, the Pauli principle sets an upper bound to the value of n_ψ. Since there are eight different hole fields, $n_\psi \leq 8$ in terms without derivatives, otherwise these terms are zero.

7.2 Accidental symmetries

Accidental symmetries are symmetries only present in some order of the effective Lagrangian because these symmetries are not shared by the underlying microscopic models. The following two accidental global symmetries are present just in some leading order terms of the effective action and are thus broken explicitly at higher orders in the derivative expansion.

7.2.1 Galilean boost symmetry

Real materials emerge from a dynamical formation of their crystal lattice. Due to this process, translation and Galilean invariance are spontaneously broken. The corresponding Goldstone bosons are known as phonons. It is expected that the formation of Cooper pairs in the HTSC regime can not be understood by taking into account only phonons. Therefore, these Goldstone bosons are not included in our effective field theory. In fact, the underlying Hubbard and t-J model do not describe phonons since they are based on a rigid lattice structure imposed by hand. This leads to an explicitly broken Galilean symmetry on the level of the microscopic models. Nevertheless, for $c \to \infty$ and without the term proportional to iK in $\mathcal{L}_2$, Eq. (7.3), Eq. (7.4), and Eq. (7.9) feature an accidental Galilean boost symmetry. This symmetry acts on the magnon and hole fields as

$$\begin{aligned}
G: \quad {}^{G}P(x) &= P(Gx), \qquad Gx = (x_1 - v_1 t, x_2 - v_2 t, t), \\
{}^{G}\psi_{\pm}^{f}(x) &= \exp(-p_i^f x_i + \omega^f t)\psi_{\pm}^{f}(Gx), \\
{}^{G}\psi_{\pm}^{f\dagger}(x) &= \exp(p_i^f x_i - \omega^f t)\psi_{\pm}^{f\dagger}(Gx), \\
{}^{G}v_i^3(x) &= v_i^3(Gx), \\
{}^{G}v_t^3(x) &= v_t^3(Gx) - v_i v_i^3(Gx), \\
{}^{G}v_i^{\pm}(x) &= v_i^{\pm}(Gx), \\
{}^{G}v_t^{\pm}(x) &= v_t^{\pm}(Gx) - v_i v_i^{\pm}(Gx).
\end{aligned} \tag{7.10}$$

The invariance only holds under the conditions

$$p_1^f = M' v_1, \qquad p_2^f = M' v_2, \quad \text{and} \quad \omega^f = \frac{(p_i^f)^2}{2M'}. \tag{7.11}$$

The Galilean boost velocity v can be derived alternatively by means of the hole dispersion relation in Eq. (7.8) and $v_i = dE^f/dp_i^f$. Although the Galilean boost symmetry is explicitly broken at higher orders of the derivative expansion, this symmetry has physical implications. Without a loss of generality, the leading one-magnon exchange between two holes can be investigated in their rest frame.[2]

7.2.2 Continuous $O(\gamma)$ rotation symmetry

Except the term proportional to iK, $\mathcal{L}_2$ of Eq. (7.4) as well as $\mathcal{L}_4$ of Eq. (7.9) are invariant under a continuous spatial rotation by an angle γ. We denote this accidental symmetry by $O(\gamma)$. The involved fields transform under $O(\gamma)$ as

$$\begin{aligned}
&{}^{O(\gamma)}\psi_{\pm}^f(x) = \exp(is\sigma_f \tfrac{\gamma}{2})\psi_{\pm}^f(O(\gamma)x),\\
&{}^{O(\gamma)}v_1(x) = \cos\gamma\ v_1(O(\gamma)x) + \sin\gamma\ v_2(O(\gamma)x),\\
&{}^{O(\gamma)}v_2(x) = -\sin\gamma\ v_1(O(\gamma)x) + \cos\gamma\ v_2(O(\gamma)x)
\end{aligned} \tag{7.12}$$

with

$$O(\gamma)x = O(\gamma)(x_1, x_2, t) = (\cos\gamma\ x_1 - \sin\gamma\ x_2, \sin\gamma\ x_1 + \cos\gamma\ x_2, t). \tag{7.13}$$

Here, v_i denotes the composite magnon field. This symmetry is not present in the Λ-term of the square lattice. The $O(\gamma)$ invariance has some interesting implications for the spiral phases we will discuss in chapter 8.

[2] Magnon induced two-hole bound states are discussed in [39].

Part II

Spiral phases

Chapter 8

Spiral phases of a lightly hole-doped antiferromagnet on the honeycomb lattice

In this chapter we consider an antiferromagnet with a homogeneously distributed, small amount of doped holes. A homogeneous hole density can be achieved, when the composite magnon vector field $v_i(x)$ constitutes a constant magnon background field for the doped fermions. For simplicity, we restrict ourselves to time-independent variations, i.e. $v_t(x) = 0$. Such a uniform background field, however, does not restrict the local staggered magnetisation $\vec{e}(x)$ to a constant configuration. Moreover, it has been proven in [36, 37] that the most general configuration of $\vec{e}(x)$ in a homogeneously doped antiferromagnet is a spiral. A spiral is characterised as a helical spin state with the staggered magnetisation vector rotating in the (x_1, x_2)-plane. With the same methods as for the square lattice, we now investigate spiral phases in a hole-doped antiferromagnet on the honeycomb lattice, however, we will not include 4-fermion terms in our discussions. In addition to the following calculations, the influence of the 4-fermion contact interaction terms onto spiral phases has been considered in [17] by using first order perturbation theory. It will be interesting to see that possible spirals do not have a preferred spatial propagation direction. This feature stems from the accidental continuous $O(\gamma)$ symmetry in the leading order of the corresponding effective Lagrangian for the honeycomb lattice and is therefore not present in the square lattice case.

We start by introducing a composite magnon vector field which is constant up to a local $U(1)_s$ "gauge" transformation. We will then show that an undoped antiferromagnet leads to a homogeneous phase of the staggered magnetisation. This proves that doping is indeed a necessary ingredient for a possible spiral configuration. Afterwards, the energy of a single hole in an antiferromagnet is derived from the appropriate fermionic Hamiltonian. A variational calculation then allows us to investigate potential spiral phases depending on the low-energy constants of the effective field theory.

8.1 Spirals within a constant composite magnon vector field $v_i(x)'$

Let us first specify what we mean by a constant magnon background field. Due to the non-linear realisation of $SU(2)_s$, the effective Lagrangian for magnons and holes exhibits invariance under a local $U(1)_s$ "gauge" transformation. We therefore make use of this "gauge" freedom by setting the $v_i(x)$ to constants up to a "gauge" transformation $\alpha(x)$. Using Eq. (5.23), Eq. (5.39), and the transformation laws of $v_\mu^3(x)$ and $v_\mu^\pm(x)$ in Eq. (5.41) we thus have

$$\begin{aligned} v_i^3(x)' &= v_i^3(x) - \partial_i\alpha(x) = \sin^2\left(\frac{\theta(x)}{2}\right)\partial_i\varphi(x) - \partial_i\alpha(x) = c_i^3, \\ v_i^\pm(x)' &= v_i^\pm(x)\exp(\pm 2i\alpha(x)) \\ &= \frac{1}{2}\big[\sin\theta(x)\partial_i\varphi(x) \pm i\partial_i\theta(x)\big]\exp(\mp i(\varphi(x) - 2\alpha(x))) = c_i^\pm, \end{aligned} \tag{8.1}$$

with c_i^3 and $c_i^\pm$ indicating the constant magnon background field. The quantities c_i^3 and $c_i^\pm$ are also denoted as spiral parameters. We now restrict our further investigations to a particular class of spiral configurations parameterised by

$$\theta(x) = \theta_0, \quad \varphi(x) = k_i x_i. \tag{8.2}$$

From Eq. (8.1) we thus identify

$$v_t(x) = 0, \quad v_i^3(x) = k_i \sin^2\left(\frac{\theta_0}{2}\right), \quad v_i^\pm(x) = \frac{k_i}{2}\sin\theta_0\exp(\mp i k_i x_i). \tag{8.3}$$

To achieve

$$c_i^+ = c_i^- = c_i \in \mathbb{R}, \tag{8.4}$$

we choose the gauge transformation $\alpha(x)$ to be

$$\alpha(x) = \frac{1}{2}\varphi(x) = \frac{1}{2}k_i x_i. \tag{8.5}$$

By the use of Eq. (8.5) one then obtains

$$\begin{aligned} &v_t(x)' = 0, \quad v_i^3(x)' = v_i^3(x) - \partial_i\alpha(x) = k_i(\sin^2\left(\frac{\theta_0}{2}\right) - \frac{1}{2}) = c_i^3, \\ &v_i^\pm(x)' = v_i^\pm(x)\exp(\pm 2i\alpha(x)) = \frac{k_i}{2}\sin\theta_0 = c_i, \end{aligned} \tag{8.6}$$

and therefore the condition of Eq. (8.4) is satisfied. Remember that $\vec{e}(x) \in S^2$ and hence the direction of the staggered magnetisation vector is determined by the two angles $\theta(x)$ and $\varphi(x)$. The above choice of a constant $\theta(x)$ ensures a spiral plane always parallel to the equatorial plane of S^2. The vector $k = (k_1, k_2)$ defines the direction along which the spiral is oriented. According to [36, 37], the wave-number or spiral pitch is given by

$$|k| = 2\sqrt{c_i^3 c_i^3 + c_i c_i} = \frac{2\pi}{\lambda}, \quad \text{with} \quad \frac{c_i}{c_i^3} = a, \quad a \in \mathbb{R}. \tag{8.7}$$

Eq. (8.7) determines the velocity of the spiral and the wavelength λ of a spiral is given by the spatial distance between two equally oriented staggered magnetisation vectors $\vec{e}(x)$. A system is said to be in a homogeneous phase when $k_i = c_i = 0$. The above constraint $c_i/c_i^3 = a$ then implies $c_i^3 = 0$ and therefore the spiral pitch vanishes.

8.2 Homogeneous phase in the undoped antiferromagnet

Since we do not allow any variation in time, the leading order in the energy density of the pure magnon sector ϵ_m is given by the first term of $\mathcal{L}_0$ in Eq. (5.9). Including the above treatments, ϵ_m takes the form

$$\epsilon_m = \frac{\rho_s}{2}\partial_i\vec{e}(x)\cdot\partial_i\vec{e}(x) = 2\rho_s v_i^+(x)v_i^-(x) = 2\rho_s(c_1^2 + c_2^2) = \frac{\rho_s}{2}(k_1^2 + k_2^2)\sin^2\theta_0. \tag{8.8}$$

A minimisation of ϵ_m with respect to the spiral parameters c_i leads to $c_i = 0$ and therefore to a vanishing spiral pitch k, i.e. $\varphi(x) = 0$. The staggered magnetisation vector $\vec{e}(x)$ thus points homogeneously in one direction in S^2 determined by the angle θ_0. This result implies that a spiral phase of $\vec{e}(x)$ indeed must be induced by doping. A homogeneous magnon field configuration in *coordinate* space is depicted in Fig. 8.1.

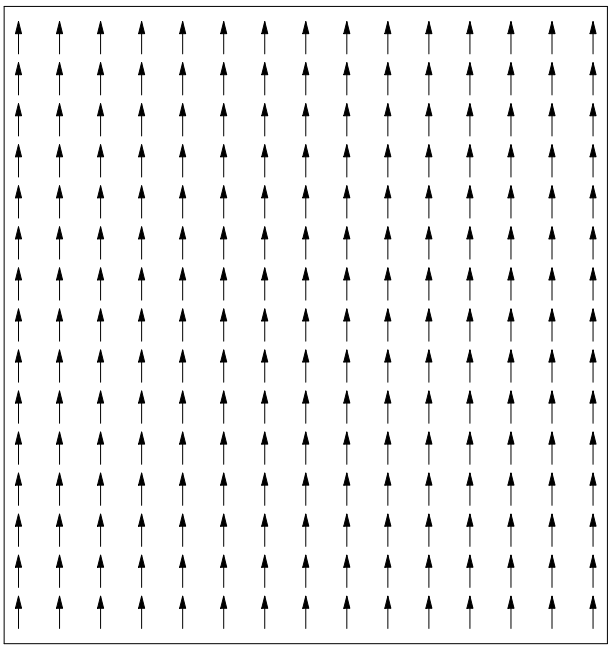

Figure 8.1: *The homogeneous phase with a constant $\vec{e}(x)$ in coordinate space.*

8.3 Homogeneous versus spiral phase in a hole-doped antiferromagnet

In order to investigate homogeneous or spiral phases of $\vec{e}(x)$ in an antiferromagnet with uniformly doped holes, we proceed according to the subsequent variational calculation scheme:

1. We calculate the energy of a single doped hole.
2. The energy density of all the holes doped into the system ϵ_h is minimised, while the total density of holes n is kept fixed. Hence, we have to solve a variational problem with constraints. As usual, this will be done by means of a Lagrange multiplier. During this procedure the spiral parameters remain unaffected.
3. The total energy density of the system ϵ is then minimised by a variation with respect to $|c| = \sqrt{c_1^2 + c_2^2}$.

Even though the most general configuration of the staggered magnetisation $\vec{e}(x)$, assuming a constant magnon background field, is proven to be a spiral, it is energetically not always the most favorable. Moreover, the values of the low-energy constants ρ_s, M', and Λ will determine whether $\vec{e}(x)$ will be in a homogeneous or a spiral phase.

8.3.1 Fermionic contribution to the energy

In order to compute the energy of a single hole, we have to derive the fermionic Hamiltonian H, acting as an operator in a Hilbert space, from the classical Lagrangian $\mathcal{L}_2$. In this thesis we neglect the 4-fermion couplings and we only involve the hole-one-magnon exchange term proportional to Λ which is of $\mathcal{O}(p)$ in the derivative expansion. The terms proportional to K, L, N_1, and N_2 are of $\mathcal{O}(p^2)$ and thus negligible. To derive the fermionic Hamiltonian from the leading order of $\mathcal{L}_2$, we disregard all terms with a time-derivative, and we replace the Grassmann fields by the creation and annihilation operators $\Psi_s^{f\dagger}$ and Ψ_s^f with flavour $f \in \{\alpha, \beta\}$ and spin $s \in \{+, -\}$. These fermion operators obey standard anticommutation relations. The appropriate Hamiltonian is then given by

$$H = \int d^2x \sum_{\substack{f=\alpha,\beta \\ s=+,-}} \left[M\Psi_s^{f\dagger}\Psi_s^f + \frac{1}{2M'} D_i\Psi_s^{f\dagger} D_i\Psi_s^f + \Lambda\Psi_s^{f\dagger}(isv_1^s + \sigma_f v_2^s)\Psi_{-s}^f \right], \quad (8.9)$$

with the spatial covariant derivatives

$$\begin{aligned} D_i\Psi_\pm^f(x) &= \left[\partial_i \pm iv_i^3(x)\right] \Psi_\pm^f(x), \\ D_i\Psi_\pm^{f\dagger}(x) &= \left[\partial_i \mp iv_i^3(x)\right] \Psi_\pm^{f\dagger}(x). \end{aligned} \quad (8.10)$$

Again, $\sigma_\alpha = 1$ and $\sigma_\beta = -1$. The Hamiltonian of Eq. (8.9) and therefore the energy of a doped hole is invariant under time-independent, local $U(1)_s$ "gauge" transformations

$$\begin{aligned} \Psi_\pm^f(x)' &= \exp(\pm i\alpha(x))\Psi_\pm^f(x), \\ v_i^3(x)' &= v_i^3(x) - \partial_i\alpha(x), \\ v_i^\pm(x)' &= v_i^\pm(x)\exp(\pm 2i\alpha(x)). \end{aligned} \quad (8.11)$$

We are thus allowed to choose $\alpha(x)$ according to Eq. (8.5) obtaining a constant magnon background field for the doped holes, i.e.

$$v_i^3(x)' = c_i^3, \qquad v_i^{\pm}(x)' = c_i, \qquad c_i^3, c_i \in \mathbb{R}. \tag{8.12}$$

It is important to state once again that the local $U(1)_s$ symmetry is not a regular gauge transformation. In fact, the non-linear realisation of the global $SU(2)_s$ symmetry leads to the local gauge behaviour of $U(1)_s$. In general, it is therefore not true that every local transformation $\alpha(x)$ corresponds to a global spin rotation of $SU(2)_s$. However, since the energy of a hole is a physical quantity, and therefore a gauge invariant quantity, we are in this case completely free in our choice of $\alpha(x)$ even though the corresponding choice may not represent an $SU(2)_s$ spin rotation. We make use of this freedom in Eq. (8.5). The gauge freedom, however, is restricted as soon as we consider gauge variant quantities. In this case, $\alpha(x)$ *must* correspond to a global $SU(2)_s$ spin rotation.

In appendix A we diagonalise the Hamiltonian by transforming Eq. (8.9) into momentum space. The transformed Hamiltonian can afterwards be considered separately for $f = \alpha$ and $f = \beta$ since the Λ-term does not mix the flavours. On the other hand, the direction of the spin s gets flipped under magnon exchange. The Hamiltonian for a single hole with momentum $p = (p_1, p_2)$ is given by

$$H^f(p) = \begin{pmatrix} M + \frac{(p_i - c_i^3)^2}{2M'} & \Lambda(ic_1 + \sigma_f c_2) \\ \Lambda(-ic_1 + \sigma_f c_2) & M + \frac{(p_i + c_i^3)^2}{2M'} \end{pmatrix}. \tag{8.13}$$

Diagonalising $H^f(p)$ leads to the energy eigenvalues

$$E_{\pm}^f(p) = M + \frac{p_i^2 + (c_i^3)^2}{2M'} \pm \sqrt{\left(\frac{p_i c_i^3}{M'}\right)^2 + \Lambda^2 |c|^2}. \tag{8.14}$$

In contrast to the energy eigenvalues derived in the square lattice case, the above $E_{\pm}^f$ relation is independent of the flavour index f. Nevertheless, we keep f as an index to be aware of involving two flavours in our calculations. Note, that the indices $\pm$ of $E_{\pm}^f$ no longer indicate the projection of the spin onto the staggered magnetisation vector because the eigenvectors corresponding to $E_{\pm}^f$ are linear combinations of hole fields with different spin orientations. The index $+(-)$ now refers to a state with higher(lower) energy. Eq. (8.14) has a minimum at $p = (0, 0)$ for which

$$E_{\pm}^f(0) = M + \frac{(c_i^3)^2}{2M'} \pm |\Lambda||c|. \tag{8.15}$$

Because ϵ_m is independent of c_i^3, we determine c_1^3 and c_2^3 by minimising $E_-^f(0)$. This leads to $c_1^3 = c_2^3 = 0$. By investigating the corresponding Hesse-matrix and $M' > 0$, we showed that Eq. (8.14) indeed has a local minimum at $(p_1, p_2, c_i^3) = (0, 0, 0)$. Eq. (8.14) then simplifies to

$$E_{\pm}^f(p) = M + \frac{p_i^2}{2M'} \pm |\Lambda||c|. \tag{8.16}$$

By a possible field redefinition one can always achieve $\Lambda > 0$ and therefore $|\Lambda| = \Lambda$. Eq. (8.6) with $c_i^3 = 0$ leads to $\sin^2(\frac{\theta_0}{2}) = \frac{1}{2}$. This implies $\theta_0 = \pm\frac{\pi}{2}$ and therefore it is energetically most

favoured that $\vec{e}(x)$ rotates in the equatorial plane of S^2.

Let us now point out an essential difference regarding possible spiral phases between the honeycomb and the square lattice. The above energy eigenvalues depend on $|c|$. The wave number of the spiral with $c_i^3 = 0$ is given by $|k| = 2|c|$. Thus, potential spiral configurations of $\vec{e}(x)$ will solely depend on the norm of k and therefore do not prefer any particular spatial direction. This effect stems from the accidental continuous $O(\gamma)$ symmetry of the Λ-term discussed in section 7.2.2. One should bear in mind that this symmetry is only a feature of the leading terms in the effective action for holes and is explicitly broken at higher orders in the derivative expansion. It is therefore expected that a spiral gets a preferred propagation direction once one includes higher order terms. The Λ-term in the leading order effective Lagrangian for holes on the square lattice does not exhibit the $O(\gamma)$ symmetry. Hence, the energy eigenvalues do not just depend on $|c|$ but on c_1 and c_2. From this it follows that in the case of a square lattice a spiral is oriented along a specific direction.

It follows from Eq. (8.16) that filled hole pockets $P_\pm^f$ are circles defined by

$$\frac{p_i^2}{2M'} = T_\pm^f, \tag{8.17}$$

where $T_\pm^f$ denotes the kinetic energy of a hole in the pocket $P_\pm^f$ at the Fermi surface. The Fermi radius is then given by

$$|p| = \sqrt{2M'T_\pm^f}. \tag{8.18}$$

In the first Brillouin zone, the circular shape of a hole pocket results from collecting the three pieces of a circular area at each equivalent point together. The hole density in a certain pocket $n_\pm^f$ is given by the corresponding occupied area in momentum space

$$n_\pm^f = \frac{1}{(2\pi)^2}\int_{P_\pm^f} d^2p = \frac{1}{2\pi}M'T_\pm^f, \tag{8.19}$$

and the kinetic energy density of a filled pocket is determined by

$$t_\pm^f = \frac{1}{(2\pi)^2}\int_{P_\pm^f} d^2p\ \frac{p_i^2}{2M'} = \frac{1}{4\pi}M'{T_\pm^f}^2. \tag{8.20}$$

The total density of holes including all pockets reads

$$n = n_+^\alpha + n_-^\alpha + n_+^\beta + n_-^\beta = \frac{1}{2\pi}M'(T_+^\alpha + T_-^\alpha + T_+^\beta + T_-^\beta), \tag{8.21}$$

and the total energy density of the holes is

$$\epsilon_h = \epsilon_+^\alpha + \epsilon_-^\alpha + \epsilon_+^\beta + \epsilon_-^\beta, \tag{8.22}$$

with

$$\epsilon_\pm^f = \frac{1}{(2\pi)^2}\int_{P_\pm^f} d^2p\ E_\pm^f(p) = (M \pm \Lambda|c|)n_\pm^f + t_\pm^f. \tag{8.23}$$

The kinetic energy of a hole, i.e. the parameter $T_{\pm}^{f}$, determines the filling of the various pockets. According to step two in the variational calculation scheme we now minimise ϵ_h by varying $T_{\pm}^{f}$, while we keep n fix. We therefore introduce

$$S \equiv \epsilon_h - \mu n, \tag{8.24}$$

with μ being a Lagrange multiplier which fixes the density of the holes. The variation demands

$$\frac{\partial S}{\partial T_{\pm}^{f}} = \frac{1}{2\pi} M'(M \pm \Lambda|c| + T_{\pm}^{f} - \mu) = 0. \tag{8.25}$$

The constraint of a fixed hole density will be incorporated as a further equation. Together with the system of equations in Eq. (8.25), the parameters $T_{\pm}^{f}$ and μ can then be related to the low-energy constants M, M', and Λ as well as $|c|$ and n. Afterwards, the relations for $T_{\pm}^{f}$ are plugged into the expression for the total energy density of the system ϵ. According to step three in our scheme, we then minimise the total energy density by varying with respect to $|c|$. Once the minimum is found, we are left with an expression which depends only on the fermion density and the low-energy constants. It is then determined by the values of ρ_s, M', and Λ which configuration of the staggered magnetisation $\vec{e}(x)$ is energetically favourable and how many pockets are filled. Remember, that we always consider a small amount of doped holes. Let us now populate the different pockets with holes.

8.3.2 Four populated hole pockets

In this subsection we populate all four hole pockets $P_{\pm}^{f}$. Eq. (8.25) and the constraint of a fixed n then leads to

$$\mu = M + \frac{\pi n}{2M'}, \qquad T_{\pm}^{f} = \frac{\pi n}{2M'} \mp \Lambda|c|. \tag{8.26}$$

In that case the total energy density of the system is given by

$$\begin{aligned} \epsilon &= \epsilon_0 + \epsilon_m + \epsilon_h \\ &= \epsilon_0 + 2\rho_s|c|^2 + \epsilon_+^{\alpha} + \epsilon_-^{\alpha} + \epsilon_+^{\beta} + \epsilon_-^{\beta} \\ &= \epsilon_0 + 2\rho_s|c|^2 + Mn + \frac{\pi n^2}{4M'} - \frac{1}{\pi} M'\Lambda^2|c|^2 \\ &= \left(2\rho_s - \frac{1}{\pi} M'\Lambda^2\right)|c|^2 + \epsilon_0 + Mn + \frac{\pi n^2}{4M'}. \end{aligned} \tag{8.27}$$

Here ϵ_0 denotes the energy density of an undoped antiferromagnet. Under the restriction $2\pi\rho_s > M'\Lambda^2$, the parabola of Eq. (8.27) has a minimum for $|c| = 0$. The energy density is bounded from below and the configuration of the staggered magnetisation is homogeneous. Therefore, in the (x_1, x_2)-plane, we have a constant unit-vector field for $\vec{e}(x)$, which corresponds to the situation in Fig. 8.1. Each of these vectors points in the same direction in the equatorial plane of S^2. The minimised energy density with four populated hole pockets then takes the form

$$\epsilon_4 = \epsilon_0 + Mn + \frac{\pi n^2}{4M'}. \tag{8.28}$$

With the constraint $2\pi\rho_s < M'\Lambda^2$, however, the parabola of the energy density has a maximum for $|c| = 0$ and is therefore not bounded from below. Since the energy density in this case has no minimum, $|c|$ seems to grow to infinity. According to Eq. (8.26), this would lead to the physically meaningless situation of a negative kinetic energy $T_+^f < 0$, i.e. a negatively filled f_+- pocket. Moreover, a continuously growing $|c|$ would induce an arbitrarily small λ and thus the $\vec{e}(x)$ vector becomes a fast rotating object. However, once the wavelength enters the range of a few lattice spacings, the effective field theory approach is not valid any more because short distances are associated with high energies. What actually happens for $2\pi\rho_s < M'\Lambda^2$ is that the system empties both hole pockets with energy index $+$. Nevertheless, for completeness, we will now discuss the case where three hole pockets are occupied.

8.3.3 Three populated hole pockets

In this subsection we discuss the case of three filled hole pockets. In addition to the pockets with E_-^α and E_-^β, the pocket with the higher energy E_+^α is populated. Since $E_\pm^f$ is in fact independent of f, one could also choose to fill the β_+-pocket. The total density of holes is then given by

$$n = n_+^\alpha + n_-^\alpha + n_-^\beta = \frac{1}{2\pi} M'(T_+^\alpha + T_-^\alpha + T_-^\beta), \tag{8.29}$$

and the contribution of the holes to ϵ reads

$$\epsilon_h = \epsilon_+^\alpha + \epsilon_-^\alpha + \epsilon_-^\beta. \tag{8.30}$$

According to Eq. (8.25), the variation yields

$$\mu = M + \frac{2\pi n}{3M'} - \frac{\Lambda}{3}|c|, \qquad T_+^\alpha = \frac{2\pi n}{3M'} - \frac{4\Lambda}{3}|c|, \qquad T_-^\alpha = T_-^\beta = \frac{2\pi n}{3M'} + \frac{2\Lambda}{3}|c|, \tag{8.31}$$

and the total energy density can be derived as

$$\begin{aligned} \epsilon &= \epsilon_0 + \epsilon_m + \epsilon_h = \epsilon_0 + 2\rho_s|c|^2 + \epsilon_+^\alpha + \epsilon_-^\alpha + \epsilon_-^\beta \\ &= \epsilon_0 + 2\rho_s|c|^2 + \left(M - \frac{\Lambda}{3}|c|\right) n + \frac{\pi n^2}{3M'} - \frac{2}{3\pi} M'\Lambda^2|c|^2 \\ &= \left(2\rho_s - \frac{2}{3\pi} M'\Lambda^2\right)|c|^2 - \frac{\Lambda n}{3}|c| + \epsilon_0 + Mn + \frac{\pi n^2}{3M'}. \end{aligned} \tag{8.32}$$

Under the constraint $3\pi\rho_s > M'\Lambda^2$, the parabola of ϵ is bounded from below and the energy density is minimised for

$$|c| = \frac{\pi}{4} \frac{\Lambda n}{3\pi\rho_s - M'\Lambda^2}. \tag{8.33}$$

Hence, the staggered magnetisation $\vec{e}(x)$ picks up a spiral phase with wave number

$$|k| = 2|c| = \frac{\pi}{2} \frac{\Lambda n}{3\pi\rho_s - M'\Lambda^2}. \tag{8.34}$$

A spiral phase of $\vec{e}(x)$ is depicted in Fig. 8.2. The minimised energy density with three populated hole pockets then reads

$$\epsilon_3 = \epsilon_0 + Mn + \frac{\pi}{3M'}\left(1 - \frac{1}{8}\frac{M'\Lambda^2}{3\pi\rho_s - M'\Lambda^2}\right)n^2. \tag{8.35}$$

Because

$$\epsilon_3 - \epsilon_4 = \frac{n^2\pi(\Lambda^2 M' - 2\pi\rho_s)}{8M'(\Lambda^2 M' - 3\pi\rho_s)} > 0, \tag{8.36}$$

under the condition $2\pi\rho_s > M'\Lambda^2$, the spiraling phase of $\vec{e}(x)$ in the three pocket case is energetically less favourable than the homogeneous phase due to four filled hole pockets. For $2\pi\rho_s < M'\Lambda^2$, however, $T_+^\alpha < 0$ which again represents an unphysical situation. In reality, the α_+-pocket gets completely emptied.

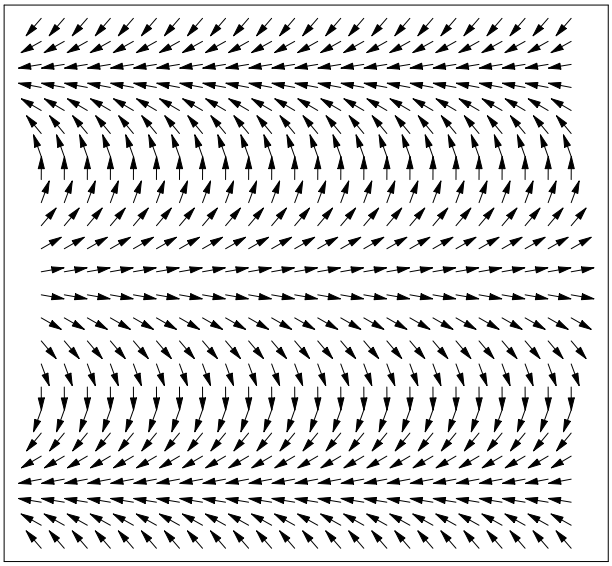

Figure 8.2: *The staggered magnetisation $\vec{e}(x)$ in a spiral phase with helical structure.*

8.3.4 Two populated hole pockets

Under the condition $2\pi\rho_s < M'\Lambda^2$ the system completely empties both pockets with higher energies. Therefore, we now investigate the case when the two pockets with E_-^α and E_-^β are filled with holes. The corresponding hole density reads

$$n = n_-^\alpha + n_-^\beta = \frac{1}{2\pi}M'(T_-^\alpha + T_-^\beta), \tag{8.37}$$

and the contribution to the total energy takes the form

$$\epsilon_h = \epsilon_-^\alpha + \epsilon_-^\beta. \tag{8.38}$$

Varying with respect to T_-^f and including the constraint of a fixed n leads to

$$\mu = M + \frac{\pi n}{M'} - \Lambda|c|, \qquad T_-^\alpha = T_-^\beta = \frac{\pi n}{M'}. \tag{8.39}$$

The total energy density then reads

$$\begin{aligned} \epsilon &= \epsilon_0 + \epsilon_m + \epsilon_h = \epsilon_0 + 2\rho_s|c|^2 + \epsilon_-^\alpha + \epsilon_-^\beta \\ &= \epsilon_0 + 2\rho_s|c|^2 + (M - \Lambda|c|)\, n + \frac{\pi n^2}{2M'} \\ &= 2\rho_s|c|^2 - \Lambda n|c| + \epsilon_0 + Mn + \frac{\pi n^2}{2M'}. \end{aligned} \tag{8.40}$$

Since $\rho_s > 0$, the parabola of ϵ is bounded from below without any restriction on the low-energy constants. Eq. (8.40) is minimised at

$$|c| = \frac{\Lambda}{4\rho_s} n. \tag{8.41}$$

Again, the staggered magnetisation is in a spiral phase with spiral pitch

$$|k| = 2|c| = \frac{\Lambda}{2\rho_s} n. \tag{8.42}$$

Using Eq. (8.41), the minimised total energy takes the form

$$\epsilon_2 = \epsilon_0 + Mn + \left(\frac{\pi}{2M'} - \frac{\Lambda^2}{8\rho_s}\right) n^2. \tag{8.43}$$

For $2\pi\rho_s > M'\Lambda^2$, four filled pockets lead to a homogeneous phase of $\vec{e}(x)$. This phase is more stable than the spiral phase from the two-pocket case since

$$\epsilon_2 - \epsilon_4 = \frac{n^2}{8M'\rho_s} \left(2\pi\rho_s - \Lambda^2 M'\right) > 0, \tag{8.44}$$

with $2\pi\rho_s > M'\Lambda^2$. In contrast to the three- and the four-pocket situations, which become physically meaningless for $2\pi\rho_s < M'\Lambda^2$, the spiral phase of the two-pocket case still makes sense under this condition.

8.3.5 One populated hole pocket

Finally, we consider the case where the pocket with energy states E_-^α is filled with holes. Alternatively one could also populate the β_--pocket. The density is given by

$$n = n_-^\alpha = \frac{1}{2\pi} M' T_-^\alpha, \tag{8.45}$$

and the contribution to ϵ simply reduces to

$$\epsilon_h = \epsilon_-^\alpha. \tag{8.46}$$

The variation leads to

$$\mu = M + \frac{2\pi n}{M'} - \Lambda|c|, \qquad T_-^\alpha = \frac{2\pi n}{M'}. \tag{8.47}$$

The total energy density then takes the form

$$\begin{aligned}\epsilon &= \epsilon_0 + \epsilon_m + \epsilon_h = \epsilon_0 + 2\rho_s|c|^2 + \epsilon_-^\alpha \\ &= \epsilon_0 + 2\rho_s|c|^2 + (M - \Lambda|c|)\, n + \frac{\pi n^2}{M'} \\ &= 2\rho_s|c|^2 - \Lambda n|c| + \epsilon_0 + Mn + \frac{\pi n^2}{M'}. \end{aligned} \tag{8.48}$$

Like in the two-pocket case, the parabola is bounded from below because $\rho_s > 0$. The total energy density ϵ is minimised at

$$|c| = \frac{\Lambda}{4\rho_s} n. \tag{8.49}$$

Thus, the staggered magnetisation picks up a spiral phase with wave number

$$|k| = 2|c| = \frac{\Lambda}{2\rho_s} n. \tag{8.50}$$

The minimised energy is given by

$$\epsilon_1 = \epsilon_0 + Mn + \left(\frac{\pi}{M'} - \frac{\Lambda^2}{8\rho_s}\right) n^2. \tag{8.51}$$

Since

$$\epsilon_1 - \epsilon_2 = \frac{\pi n^2}{2M'} > 0, \tag{8.52}$$

the spiral due to one filled pocket is always energetically less favourable than the spiral in the two-pocket case.

Chapter 9

Conclusions and outlook

In close analogy to baryon chiral perturbation theory, we have constructed a systematic low-energy effective field theory for magnons and holes in an antiferromagnet on the honeycomb lattice. Apart from basic properties of field theories such as locality, unitarity and causality, the key ingredients of an effective field theory are symmetries. Therefore, we have started this thesis by investigating the symmetry properties of the underlying honeycomb lattice which, in contrast to the square lattice, belongs to the family of non-Bravais lattices. In general, an effective field theory describes the low-energy physics of an underlying microscopic model. In this thesis, it is assumed that the Hubbard model serves as a reliable microscopic theory describing antiferromagnetism. Because the final effective Lagrangian for magnons and holes must inherit the symmetries of the Hubbard Hamiltonian, a symmetry analysis, now incorporating the microscopic model, has been worked out in chapter 3. A symmetry of the Hubbard model at half-filling, which plays a particular role in the identification of the final effective hole fields, is the so-called pseudo-spin symmetry $SU(2)_Q$. This symmetry is a non-Abelian extension of the $U(1)_Q$ fermion number symmetry and relates the particle and the hole sector in a symmetric way. The $SU(2)_Q$ symmetry, however, is in fact not present in real materials. Before discussing the particular role of $SU(2)_Q$ in the context of the identification procedure of the final hole fields, we will first review the investigation of the weakly coupled Hubbard model.

Motivated by graphene, a two-dimensional, semi-metallic graphite monolayer consisting of carbon atoms on a honeycomb lattice, we have investigated the weak coupling limit of the Hubbard model at half-filling by additionally allowing a next-to-nearest neighbour hopping parameter $t' \neq 0$. For a Coulomb repulsion $U = 0$, the corresponding Hamiltonian has been diagonalised analytically. By expanding the corresponding dispersion relations, we have confirmed that the low-energy excitations of graphene are indeed free, massless relativistic Dirac fermions occurring in the vicinity of the six Dirac points in the Brillouin zone. Interestingly, although breaking the particle-hole symmetry of $SU(2)_Q$, non-zero values of t' did not destroy the Dirac cones and, as a conclusion, the Dirac fermions remain massless for all t and t'. The fermion velocity $v_F = \frac{3ta}{2}$ has been derived and with the aid of some specific unitary transformations, we have shown the equivalence between the quantum mechanical Dirac Hamiltonian for a massless particle and the half-filled Hubbard Hamiltonian for $t' = 0$ and $U = 0$ at low energies. By addressing effective fields to the same pockets as in the theory for magnons and holes, we have identified the correct low-energy degrees of freedom

and their symmetry behaviour to construct an effective field theory for free Dirac fermions. According to the prediction of the microscopic theory, the resulting leading order effective Lagrangian indeed contains no mass terms. Once again, the effective field theory approach has thus demonstrated its power. However, to bring our low-energy description closer to real graphene, one additionally has to include spin and contact interaction terms including more than two fermion fields. To conclude, we have shown that the effective Lagrangian $\mathcal{L}_2^{free}$ is equal to the Euclidean metric Dirac Lagrangian in $(2+1)$-dimensions for a free and massless particle.

Quantum antiferromagnets exhibit a spontaneous $SU(2)_s \to U(1)_s$ symmetry breakdown. In the case of an undoped antiferromagnet, the low-energy physics is therefore dominated by magnons, two linearly independent massless Goldstone boson excitations resulting from spontaneous symmetry breaking. We have constructed the leading order effective action for magnons in an antiferromagnet on the honeycomb lattice, which is fully determined by the two low-energy constants c and ρ_s. It turned out, that the corresponding Lagrangian is equal to the effective Lagrangian in the pure magnon sector derived for the square lattice. In order to couple doped holes to the magnons, the global $SU(2)_s$ spin symmetry is afterwards realised non-linearly as a *local* symmetry in the unbroken subgroup $U(1)_s$. A non-trivial step is the identification of the low-energy degrees of freedom that describe doped holes. We have established an interface between microscopic and effective field theory by introducing a discrete fermionic lattice operator with sublattice index $\Psi_x^X = u(x)C_x$. This step guarantees that the non-linearly realised $SU(2)_s$ symmetry is implemented on the effective hole fields as a local $U(1)_s$ symmetry. Moreover, Ψ_x^X is able to address the new sublattice structure which has been imposed on the honeycomb lattice to properly address the fermion fields to the hole pockets at lattice momenta $k^\alpha = -k^\beta = (0, \pm 4\pi/(3\sqrt{3}a))$ in the first Brillouin zone. Until now, the fermion fields may consist of a combination of electrons and holes. As a next step, in order to describe doped holes with the effective Lagrangian, we therefore have broken the $SU(2)_Q$ symmetry by the identification of the final hole fields. This has been done by diagonalising mass matrices containing $SU(2)_Q$-variant and $SU(2)_Q$-invariant terms. The hole fields have then been identified as the eigenvectors corresponding to the lower eigenvalue. Once the symmetry properties of the final hole fields are worked out, it is straightforward to construct the leading order effective Lagrangian. In chapter 7 we have presented the effective Lagrangian with two hole fields up to $\mathcal{O}(p^2)$ in the derivative expansion as well as the leading order effective Lagrangian containing four hole fields and no derivatives. The latter describes short-ranged contact interactions between holes. Each term in the Lagrangian is multiplied with a low-energy constant, which depends on material properties. The leading order effective action then enters the corresponding Euclidean path-integral.

In the second part of this thesis, the low-energy effective field theory for magnons and holes has served as an instrument to investigate possible spiral phases of the staggered magnetisation $\vec{e}(x)$ in an antiferromagnet on the honeycomb lattice with a small amount of homogeneously doped holes. To achieve a constant magnon background field, and hence a homogeneous hole density, we have restricted ourselves to a composite magnon vector field $v_i(x)$, which is constant up to a local $U(1)_s$ "gauge" transformation. Under this condition, the proof in [36, 37] predicts a spiral to be the most general configuration of $\vec{e}(x)$. A minimisation of the magnonic contribution to the total energy density has revealed that doping is a necessary condition for a potential spiral phase of $\vec{e}(x)$. To derive the dispersion relation of a single hole $E_\pm^f$ in the

pocket $P_{\pm}^{f}$ ($f \in \{\alpha, \beta\}$), we have diagonalised the $U(1)_s$ transformed fermionic Hamiltonian neglecting the vertices K, L, N_1, and N_2. By means of a variational calculation with constraints, we have afterwards calculated an expression for the total energy density of a doped antiferromagnet which depends on the low-energy constants ρ_s, M', and Λ. The values of these constants then determine whether a homogeneous or a spiral phase of $\vec{e}(x)$ is energetically favoured, and which pockets are filled with holes. We have found that for $2\pi\rho_s > M'\Lambda^2$ the staggered magnetisation $\vec{e}(x)$ is in a homogeneous phase and all four pockets are filled. On the other hand, for $2\pi\rho_s < M'\Lambda^2$, the staggered magnetisation $\vec{e}(x)$ is in a spiral phase and the two pockets with lower energy values E_{-}^{α} and E_{-}^{β} are filled with holes. We have seen that possible spiral phases only depend on the wave number $|k|$ and are therefore independent of any particular spatial direction. This is due to the accidental $O(\gamma)$ symmetry of the involved Λ-term from $\mathcal{L}_2$. The $O(\gamma)$ symmetry is not present in the Λ-term of $\mathcal{L}_2$ for holes on the square lattice. As a result, spiral configurations of $\vec{e}(x)$ show a preferred spatial propagation direction. However, higher order terms in the effective Lagrangian explicitly break the $O(\gamma)$ symmetry.

To conclude this thesis, let us outline two possible future projects in the framework of low-energy effective field theories for doped antiferromagnets:

Real antiferromagnets are in general not clean systems. They may contain irregularities, e.g. missing sites, in their lattice structure. In addition, also doped holes or electrons can be the source of such impurities. The doped entities then locate themselves on the impurities, which may be the origin for a phase separation between antiferromagnetism and superconductivity. To bring the effective description closer to reality, one therefore could additionally incorporate impurities in an effective field theory for holes and electrons. It will then be interesting to investigate interaction processes between impurities and electrons or holes.

Another future task could be the construction of a systematic low-energy effective field theory for antiferromagnets with an underlying geometrically frustrated lattice, e.g. the triangular or the kagome lattice. The fact that these materials are frustrated, leads to a lack of unbiased numerical results in the single-fermion sector. Even at half-filling, simulations of microscopic models on such lattice structures are afflicted by a severe sign-problem. It is therefore difficult to determine the exact position of the fermion pockets in momentum space by simulating the microscopic Hamiltonian. Eventually, in addition, experimental results must be considered too in order to find out where in momentum space doped electrons or holes have their energy minima. After the pockets are located, the necessary effective degrees of freedom and their symmetry properties can be worked out to finally construct the effective action in the same manner as for the square and the honeycomb lattice.

In this thesis we have layed the groundwork for potential future studies in these directions.

Acknowledgments

First of all I wish to express my gratitude to Professor Uwe-Jens Wiese for opening the door towards the beauty of theoretical physics. Without his explanations and advice this thesis never could have been written. Professor Wiese is able to create a working atmosphere where we, making our first steps in research, feel both challenged and at the same time comfortable.

I am greatly indebted to my fellow Marcel Wirz for the unique collaboration not only during the time of this thesis. It was the pure pleasure for me to share many extraordinary moments of new insights with him as well as struggling together with unsolved problems. Looking at a hexagon will always remind me of our intense discussions or even disputes. Our successful liaison physique now comes to an end but I am glad to know that from now on he can devote himself to his real passion: Mathematics. Perhaps, from time to time, we can search together for a unitary transformation of something. Thanks!

To start a thesis is always accompanied with many unknowns. One can therefore be just grateful to have such experienced specialists at ones side as Dr. Florian Kämpfer, Dr. Fu-Jiung Jiang, Dr. Christoph Brügger, Professor Christoph Hofmann, and Urs Gerber. Especially Florian and Fu-Jiung spent so much time on patiently answering our questions. Only in such a helpful atmosphere we were able to unlock the terra incognita of magnons and holes.

I would also like to thank Peter Kienholz and David "Dave" Baumgartner for sharing the office with me. Dave, whose lively character is an essential ingredient of the pleasant working atmosphere in the famous B-Floor, I would like to thank for awakening the race driver in me. The author wishes to express further thanks to Stefan "Stibu" Lanz, Christoph "Schübi" Schüpbach, Lorenzo Mercolli, and Christine Bolliger for answering questions concerning Latex, quantum field theory, or simply playing music together in the "Marcel Steffen Hochzeitskappelle". I would like to thank Ruth Bestgen, Esther Fiechter, Ottilia Hänni, and Kathrin Weyeneth for taking care of administration issues.

Special thanks are dedicated to my parents and especially my mother. Without her support in many regards my studies would not have been possible.

There are situations in physics where words are not the appropriate language to really capture the fundamentals of nature. However, there are also moments besides physics, where words can not truly express the thing-in-itself. Eva, it rests such a lot of unspeakable when I say thank you for being with me during the last years.

Appendix A

Construction of the fermionic Hamiltonian in momentum space

In this appendix, a detailed construction of the single hole Hamiltonian $H^f(p)$ in Eq. (8.13) is presented. Throughout the following calculation, we use the notation

$$x = (\vec{x}, t) = (x_1, x_2, t), \qquad p = (\vec{p}, E(\vec{p})) = (p_1, p_2, E(\vec{p})). \tag{A.1}$$

We start with the fermionic Hamiltonian H of Eq. (8.9)

$$H = \int d^2x \sum_{\substack{f=\alpha,\beta \\ s=+,-}} \Big[M\Psi_s^{f\dagger}\Psi_s^f + \frac{1}{2M'} D_i\Psi_s^{f\dagger} D_i\Psi_s^f + \Lambda\Psi_s^{f\dagger}(isv_1^s + \sigma_f v_2^s)\Psi_{-s}^f \Big]. \tag{A.2}$$

In order to get

$$v_i^3(x)' = c_i^3, \qquad v_i^{\pm}(x)' = c_i, \qquad c_i^3, c_i \in \mathbb{R}, \tag{A.3}$$

we now perform a time-independent, local $U(1)_s$ gauge transformation on H leading to

$$H' = \int d^2x \sum_{\substack{f=\alpha,\beta \\ s=+,-}} \Big[M\Psi_s^{f\dagger'}\Psi_s^{f'} + \frac{1}{2M'} D_i\Psi_s^{f\dagger'} D_i\Psi_s^{f'} + \Lambda\Psi_s^{f\dagger'}(isc_1 + \sigma_f c_2)\Psi_{-s}^{f'} \Big], \tag{A.4}$$

with the covariant derivatives

$$\begin{aligned} D_i\Psi_s^{f'}(x) &= \left[\partial_i + isc_i^3\right]\Psi_s^{f'}(x), \\ D_i\Psi_s^{f\dagger'}(x) &= \left[\partial_i - isc_i^3\right]\Psi_s^{f\dagger'}(x). \end{aligned} \tag{A.5}$$

For notational convenience, we neglect the primes in the subsequent considerations. The Fourier decomposition of the fermion operators $\Psi_s^f(x)$ and $\Psi_s^{f\dagger}(x)$ is defined as

$$\begin{aligned} \Psi_s^f(x) &= \frac{1}{(2\pi)^2}\int d^2p\ \widetilde{\Psi}_s^f(\vec{p},t)\exp(-i\vec{p}\cdot\vec{x}) = \frac{1}{(2\pi)^2}\int d^2p\ \widetilde{\Psi}_s^f\exp(-i\vec{p}\cdot\vec{x}), \\ \Psi_s^{f\dagger}(x) &= \frac{1}{(2\pi)^2}\int d^2p\ \widetilde{\Psi}_s^{f\dagger}(\vec{p},t)\exp(i\vec{p}\cdot\vec{x}) = \frac{1}{(2\pi)^2}\int d^2p\ \widetilde{\Psi}_s^{f\dagger}\exp(i\vec{p}\cdot\vec{x}). \end{aligned} \tag{A.6}$$

The covariant derivative acts on the operator Ψ_s^f as

$$\begin{aligned} D_i\Psi_s^f &= \partial_i\Psi_s^f + isc_i^3\Psi_s^f \\ &= \partial_i\frac{1}{(2\pi)^2}\int d^2p\ \widetilde{\Psi}_s^f \exp(-i\vec{p}\cdot\vec{x}) + isc_i^3\frac{1}{(2\pi)^2}\int d^2p\ \widetilde{\Psi}_s^f \exp(-i\vec{p}\cdot\vec{x}) \\ &= \frac{1}{(2\pi)^2}\int d^2p\ (-ip_i)\widetilde{\Psi}_s^f \exp(-i\vec{p}\cdot\vec{x}) + isc_i^3\frac{1}{(2\pi)^2}\int d^2p\ \widetilde{\Psi}_s^f \exp(-i\vec{p}\cdot\vec{x}) \\ &= \frac{1}{(2\pi)^2}\int d^2p\ (-ip_i + isc_i^3)\widetilde{\Psi}_s^f \exp(-i\vec{p}\cdot\vec{x}). \end{aligned} \tag{A.7}$$

Performing a similar calculation for $\Psi_s^{f\dagger}$ yields

$$D_i\Psi_s^{f\dagger} = \frac{1}{(2\pi)^2}\int d^2p\ (ip_i - isc_i^3)\widetilde{\Psi}_s^{f\dagger}\exp(i\vec{p}\cdot\vec{x}). \tag{A.8}$$

Because we do not include 4-fermion contact interaction terms, H is diagonal in the flavour index f. The above Hamiltonian can therefore be separated for each flavour α and β. By means of the Eqs. (A.6), (A.7), and (A.8) the Hamiltonian for a flavour f then reads

$$\begin{aligned} H^f = \frac{1}{(2\pi)^4}\int d^2x\int d^2p\int d^2p'\sum_{s=+,-}\exp(i(\vec{p}-\vec{p}\,')\vec{x}) \\ \times\Big\{\Big[M\widetilde{\Psi}_s^{f\dagger}\widetilde{\Psi}_s^f + \frac{1}{2M'}\widetilde{\Psi}_s^{f\dagger}(ip_i - isc_i^3)(-ip_i' + isc_i^3)\widetilde{\Psi}_s^f \\ + \Lambda\widetilde{\Psi}_s^{f\dagger}(isc_1 + \sigma_f c_2)\widetilde{\Psi}_{-s}^f\Big]\Big\}. \end{aligned} \tag{A.9}$$

After using

$$\frac{1}{(2\pi)^2}\int d^2x\ \exp(i(\vec{p}-\vec{p}\,')\vec{x}) = \delta^{(2)}(\vec{p}-\vec{p}\,'), \tag{A.10}$$

we perform the integration over p' to obtain

$$\begin{aligned} H^f &= \frac{1}{(2\pi)^2}\int d^2p\sum_{s=+,-}\Big[M\widetilde{\Psi}_s^{f\dagger}\widetilde{\Psi}_s^f + \frac{1}{2M'}\widetilde{\Psi}_s^{f\dagger}(p_i - sc_i^3)^2\widetilde{\Psi}_s^f + \Lambda\widetilde{\Psi}_s^{f\dagger}(isc_1+\sigma_f c_2)\widetilde{\Psi}_{-s}^f\Big] \\ &= \frac{1}{(2\pi)^2}\int d^2p\ \Big[M\widetilde{\Psi}_+^{f\dagger}\widetilde{\Psi}_+^f + \frac{1}{2M'}\widetilde{\Psi}_+^{f\dagger}(p_i - c_i^3)^2\widetilde{\Psi}_+^f + \Lambda\widetilde{\Psi}_+^{f\dagger}(ic_1+\sigma_f c_2)\widetilde{\Psi}_-^f \\ &\qquad + M\widetilde{\Psi}_-^{f\dagger}\widetilde{\Psi}_-^f + \frac{1}{2M'}\widetilde{\Psi}_-^{f\dagger}(p_i + c_i^3)^2\widetilde{\Psi}_-^f + \Lambda\widetilde{\Psi}_-^{f\dagger}(-ic_1+\sigma_f c_2)\widetilde{\Psi}_+^f\Big]. \end{aligned} \tag{A.11}$$

We now rewrite H^f in spinor notation to identify $H^f(\vec{p})$. One gets

$$H^f = \frac{1}{(2\pi)^2}\int d^2p\ \left[\left(\widetilde{\Psi}_+^{f\dagger},\widetilde{\Psi}_-^{f\dagger}\right)H^f(\vec{p})\begin{pmatrix}\widetilde{\Psi}_+^f\\ \widetilde{\Psi}_-^f\end{pmatrix}\right], \tag{A.12}$$

with

$$H^f(\vec{p}) = \begin{pmatrix} M + \frac{(p_i - c_i^3)^2}{2M'} & \Lambda(ic_1 + \sigma_f c_2) \\ \Lambda(-ic_1 + \sigma_f c_2) & M + \frac{(p_i + c_i^3)^2}{2M'} \end{pmatrix}. \tag{A.13}$$

Up to notational conventions in the argument, $H^f(\vec{p})$ is equal to the Hamiltonian in Eq. (8.13). One should keep in mind, that $\widetilde{\Psi}_s^f = \widetilde{\Psi}_s^f(\vec{p}, t)$ is still a $U(1)_s$ gauge transformed field. A diagonalisation of H^f leads to the energy eigenvalues of Eq. (8.14)

$$E_\pm^f(\vec{p}) = M + \frac{p_i^2 + (c_i^3)^2}{2M'} \pm \sqrt{\left(\frac{p_i c_i^3}{M'}\right)^2 + \Lambda^2 |c|^2}. \tag{A.14}$$

Bibliography

[1] J. C. Bednorz and K. A. Müller, Z. Phys. B64 (1986) 189.

[2] P. W. Anderson, Science 235 (1987) 1196.

[3] H. Takahashi *et al.*, Nature 453 (2008) 376.

[4] A. Damascelli, Z. Hussain, and Z.-X. Shen, Rev. Mod. Phys. 75 (2003) 473.

[5] K. Takada, H. Sakurai, E. Takayama-Muromachi, F. Izumi, R. Dilanian, and T. Sasaki, Nature (London) 422 (2003) 53.

[6] S. Weinberg, Physica 96 A (1979) 327.

[7] J. Gasser and H. Leutwyler, Nucl. Phys. B250 (1985) 465.

[8] C. G. Callan, S. Coleman, J. Wess, and B. Zumino, Phys. Rev. 177 (1969) 2247.

[9] H. Georgi, Weak Interactions and Modern Particle Theory, Benjamin-Cummings Publishing Company, 1984.

[10] J. Gasser, M. E. Sainio, and A. Svarc, Nucl. Phys. B307 (1988) 779.

[11] E. Jenkins and A. Manohar, Phys. Lett. B255 (1991) 558.

[12] V. Bernard, N. Kaiser, J. Kambor, and U.-G. Meissner, Nucl. Phys. B388 (1992) 315.

[13] T. Becher and H. Leutwyler, Eur. Phys. J. C9 (1999) 643.

[14] C. Brügger, F. Kämpfer, M. Pepe, and U.-J. Wiese, Phys. Rev. B74 (2006) 224432.

[15] C. Brügger, C. Hofmann, F. Kämpfer, M. Moser, M. Pepe, and U.-J. Wiese, Phys. Rev. B75 (2007) 214405.

[16] F. - J. Jiang, F. Kämpfer, M. Nyfeler, and U. -J. Wiese, arXiv: 0807. 2977v1 [cond-mat. str-el] (2008).

[17] F. - J. Jiang, F. Kämpfer, C. P. Hofmann, and U. -J. Wiese, arXiv: 0809. 4998v1 [cond-mat. str-el] (2008).

[18] B. I. Shraiman and E. D. Siggia, Phys. Rev. Lett. 60 (1988) 740; Phys. Rev. Lett. 61 (1988) 467; Phys. Rev. Lett. 62 (1989) 1564; Phys. Rev. B46 (1992) 8305.

[19] C. L. Kane, P. A. Lee, and N. Read, Phys. Rev. B39 (1989) 6880.

[20] C. L. Kane, P. A. Lee, T. K. Ng, B. Chakraborty, and N. Read, Phys. Rev. B41 (1990) 2653.

[21] B. Chakraborty, N. Read, C. Kane, and P. A. Lee, Phys. Rev. B42 (1990) 4819.

[22] A. Auerbach and B. E. Larson, Phys. Rev. B43 (1991) 7800.

[23] S. Sarker, C. Jayaprakash, H. R. Krishnamurthy, and W. Wenzel, Phys. Rev. B43 (1991) 8775.

[24] R. Eder, Phys. Rev. B43 (1991) 10706.

[25] E. Arrigoni and G. C. Strinati, Phys. Rev. B44 (1991) 7455.

[26] J. Igarashi and P. Fulde, Phys. Rev. B45 (1992) 10419.

[27] R. Frésard and P. Wölfle, J. Phys.: Condens. Matter 4 (1992) 3625.

[28] G. C. Psaltakis and N. Papanicolaou, Phys. Rev. B48 (1993) 456.

[29] H. Mori and M. Hamada, Phys. Rev. B48 (1993) 6242.

[30] A. V. Chubukov and K. A. Musaelian, Phys. Rev. B51 (1995) 12605.

[31] C. Zhou and H. J. Schulz, Phys. Rev. B52 (1995) R11557.

[32] A. V. Chubukov and D. K. Morr, Phys. Rev. B57 (1998) 5298.

[33] N. Karchev, Phys. Rev. B57 (1998) 10913.

[34] L. O. Manuel and H. A. Ceccatto, Phys. Rev. B61 (2000) 3470.

[35] O. P. Sushkov and V. N. Kotov, Phys. Rev. B70 (2004) 024503.

[36] C. Brügger, C. P. Hofmann, F. Kämpfer, M. Pepe, and U.-J. Wiese, Phys. Rev. B75 (2007) 014421.

[37] C. Brügger, Spiral Phases of Doped Antiferromagnets from a Systematic Low-Energy Effective Field Theory, PhD Thesis, University of Bern (2008).

[38] D. Baumgartner, Spiral Phases in Doped Antiferromagnets, Master Thesis, University of Bern (2008).

[39] M. Wirz, Two-Hole Bound States from an Effective Field Theory for Magnons and Holes in an Antiferromagnet on the Honeycomb Lattice, Master Thesis, University of Bern (2009).

[40] C. Brügger, F. Kämpfer, M. Pepe, and U.-J. Wiese, Eur. Phys. J. B53 (2006) 433.

[41] N. W. Ashcroft, N. D. Mermin, Solid State Physics, Holt, Rinehart and Winston, (1976).

[42] H. Tasaki, arXiv: cond-mat/9512169v4 [cond-mat.str-el] (1997).

[43] J. Hubbard, Proc. Roy. Soc. London A, 276 (1963) 238; M. C. Gutzwiler, Phys. Rev. Lett. 10 (1963) 159; J. Kanamori, Progr. Theor. Phys. 30 (1993) 275.

[44] E. Fradkin, Field Theories of condensed matter systems, Addison-Wesley publishing company, Redwood City, (1991).

[45] R. Marshall, Proc. Roy. Soc. London A, 232 (1955) 48.

[46] F. Kämpfer, Effective Field Theory for Charge Carriers in an Antiferromagnet, Master Thesis, University of Bern (2005).

[47] S. Zhang, Phys. Rev. Lett. 65 (1990) 120.

[48] C. N. Yang and S. Zhang, Mod. Phys. Lett. B4 (1990) 759.

[49] A. H. Castro Neto, F. Guinea, N. M. R. Peres, K. S. Novoselov, and A. K. Geim, arXiv: 0709. 1163v2 [cond-mat. other] (2008).

[50] I. F. Herbut, Phys. Rev. Lett. 97 (2006) 146401.

[51] R. Roldán, M. P. López-Sancho, and F. Guinea, Phys. B77, (2008), 115410.

[52] T. Paiva *et al.*, Phys. Rev. B 72 (2005) 085123.

[53] P. R. Wallace, Phys. Rev. 71 (1947) 622.

[54] J. Goldstone, Nuovo Cimento 19 (1961); J. Goldstone, A. Salam, and S. Weinberg, Phys. Rev. 127 (1962) 965.

[55] F. Kämpfer, Two-hole and two-electron bound states from a systematic low-energy effective field theory for magnons and charge carriers in an antiferromagnet, PhD Thesis, University of Bern (2007).

[56] P. Hasenfratz and F. Niedermayer, Phys. Lett. B268 (1991) 231.

[57] S. Chakravarty, B. I. Halperin, and D. R. Nelson, Phys. Rev. B39 (1989) 2344.

[58] U. Gerber, C. P. Hofmann, F. -J. Jiang, M. Nyfeler, and U. -J. Wiese, arXiv: 0901. 0445v1 [cond-mat. str-el] (2009).

[59] N. D. Mermin, and H. Wagner, Phys. Rev. Lett. 17 (1966) 1133.

[60] P. C. Hohenberg, Phys. Rev. 158 (1967) 383.

[61] S. Coleman, Commun. Math. Phys. 31 (1973) 259.

[62] S. Coleman, J. Wess, and B. Zumino, Phys. Rev. 177 (1969) 2239.

[63] F. Kämpfer, M. Moser, and U.-J. Wiese, Nucl. Phys. B729 (2005) 317.

[64] M. Moser, Effective field theory for charge carriers in an antiferromagnet, PhD Thesis, University of Bern (2006).

[65] T. Becher, and H. Leutwyler, Eur. Phys. J. C9 (1999) 147.

[66] J. Gasser, and H. Leutwyler, Nucl. Phys. B250 (1985) 465.

[67] S. R. Beane, D. B. Kaplan, and A. V. Vuorinen, arXiv: 0812. 3938v2 [nucl-th] (2008).

Erklärung

gemäss Art. 28 Abs. 2 RSL 05

Name/Vorname:	Bessire Bänz
Matrikelnummer:	04-107-991
Studiengang:	Physik
	Bachelor ☐ Master ☒ Dissertation ☐
Titel der Arbeit:	Spiral phases from a systematic low-energy effective field theory for magnons and holes in an antiferromagnet on the honeycomb lattice
Leiter der Arbeit:	Prof. Dr. Uwe-Jens Wiese

Ich erkläre hiermit, dass ich diese Arbeit selbständig verfasst und keine anderen als die angegebenen Quellen benutzt habe. Alle Stellen, die wörtlich oder sinngemäss aus Quellen entnommen wurden, habe ich als solche gekennzeichnet. Mir ist bekannt, dass andernfalls der Senat gemäss Artikel 36 Absatz 1 Buchstabe o des Gesetzes vom 5. September 1996 über die Universität zum Entzug des auf Grund dieser Arbeit verliehenen Titels berechtigt ist.

Bern, den 16. März 2009